The Joint IPWG/GEWEX Precipitation Assessment

June 2021

Bibliographic information

This report should be cited as:

Roca, R., Z.S. Haddad, F.F. Akimoto, L. Alexander, A. Behrangi, G. Huffman, S. Kato, C. Kidd, P.E. Kirstetter, T. Kubota, C. Kummerow, T.S. L'Ecuyer, V. Levizzani, V. Maggioni, C. Massari, H. Masunaga, M. Schröder, F.J. Tapiador, F.J. Turk and N. Utsumi, 2021: The Joint IPWG/GEWEX Precipitation Assessment. WCRP Report 2/2021, World Climate Research Programme (WCRP): Geneva, Switzerland, 125 pp.

Contact information

All enquiries regarding this report should be directed to wcrp@wmo.int or:

World Climate Research Programme
c/o World Meteorological Organization
7 bis, Avenue de la Paix
Case Postale 2300
CH-1211 Geneva 2
Switzerland

Cover image credit

"Rain-day" by Flickr user Anatol C

Copyright notice

Authorship and publisher's notice

This report was authored by members of the International Precipitation Working Group (IPWG) and the Global Energy and Water Exchanges (GEWEX) Data and Analysis Panel (GDAP).

List of authors
Ziad S. Haddad, Francis J. Turk, Nobuyuki Utsumi, Pierre-Emmanuel Kirstetter, Chris Kidd, Viviana Maggioni, Rémy Roca, Seiji Kato, Tristan L'Ecuyer, Francisco J. Tapiador, Vincenzo Levizzani, Hirohiko Masunaga, Fumie F. Akimoto, Takuji Kubota, Chris Kummerow, Marc Schröder, Hirohiko Masunaga, Lisa Alexander, George Huffman, Christian Massari and Ali Behrangi

The IPWG focuses the scientific community on operational and research satellite-based quantitative precipitation measurement issues and challenges. It provides a forum for operational and research users of satellite precipitation measurements to exchange information on methods for measuring precipitation and the impact of space borne precipitation measurements in numerical weather and hydrometeorological prediction and climate studies.

GDAP was organized to bring together theoretical and experimental insights into the radiative interactions and climate feedbacks associated with cloud processes. The central question that governs the GDAP mission is: "how sensitive is the Earth's climate to changes in radiative and other forcings?"

WCRP is co-sponsored by the World Meteorological Organization (WMO), the Intergovernmental Oceanographic Commission (IOC) of UNESCO and the International Science Council (ISC), see www.wmo.int, www.ioc-unesco.org and council.science.

Foreword

This report is a result of an interesting journey that originated in discussions between Rémy Roca, chair of Global Energy and Water Exchanges (GEWEX) Data and Analysis Panel (GDAP), and Ziad Haddad, chair of International Precipitation Working Group (IPWG), during visits to Toulouse and to Pasadena as well as during many of the various workshops and conferences dedicated to precipitation. It culminated in the present report built from contributions by more than 20 scientists from all over the world. The first written draft was completed immediately following an open meeting for interested contributors that took place on a Saturday morning in a public library in the heights of San Diego (Haddad and Roca, 21 October 2017). From this initial plan, many objectives were successfully achieved without modification, while a few required maturation before we were able to include them in the completed assessment, all of this in spite of the ongoing pandemic. The current report completes the GEWEX assessment portfolio and follows the previous IPWG assessment by 10+ years (Gruber and Levizzani, 2008). Hopefully it is the first of a more frequent and regular series of precipitation assessments.

Rémy Roca, Toulouse, 7 October 2020; Ziad S. Haddad, Pasadena, 7 October 2020

Contents

1. Assessment of the Sub-Daily Global Satellite Precipitation Products

1.1. Intrinsic uncertainty in the sub-daily satellite products at their native resolutions

Ziad S. Haddad[1], Francis J. Turk[1], Nobuyuki Utsumi[2] and Pierre-Emmanuel Kirstetter[3]

[1]Jet Propulsion Laboratory, California Institute of Technology, Pasadena, CA, USA

[2]Nagamori Institute of Actuators, Kyoto University of Advanced Science, Kyoto, Japan

[3]University of Oklahoma, Norman, OK, USA

1.1.1. Background

For many hydrological and weather forecasting applications, an important quantity is the amount of precipitation that falls on the Earth's surface over a given time interval, i.e., the surface precipitation rate. However, no satellite instrument is unambiguously sensitive to the instantaneous precipitation rate at the Earth's surface. A vertically profiling radar such as the Dual-Frequency Precipitation Radar (DPR) onboard the joint National Aeronautics and Space Administration (NASA) and Japanese Aerospace Exploration Agency (JAXA) Global Precipitation Measurement (GPM) mission satellite (Hou et al., 2014) is directly sensitive to rain in the near-surface layers of the atmosphere unaffected by surface ground clutter, but its measurements are affected by attenuation due to the condensed water in the higher layers of the cloud. Furthermore, the DPR instrument scan swath is typically too narrow (240 km) to provide substantial global coverage at sub-weekly scales. Passive microwave (MW) radiometers do have more substantial coverage owing to their wider swath (between 800 and 2500 km). These measurements are less directly sensitive to surface rain, with more direct sensitivity to the condensed water in the cloud. The height of the "peak" sensitivity increases as the radiometer channel wavelength decreases, up to infrared (IR) radiometers, which are directly sensitive only to the condensed water at the very top of the cloud (Haddad et al., 2017). IR radiometers are now carried by all meteorological geostationary satellites, providing global coverage with very frequent temporal sampling (at least every 30 minutes or better).

Therefore, the algorithms that generate today's global satellite precipitation products attempt to capitalize on the different strengths of these three types of instrument (radar, passive MW radiometers and frequent-refresh IR radiometers). These algorithms rely upon the reasonable sensitivity of the microwave radiometers, sharpened by reference to the precipitation radars, and enlist the help of IR to interpolate the microwave estimates to the often-long intervals of time between consecutive passive MW observations. These "revisit gaps" can be 5 hours in the tropical latitudes (Kidd et al., 2018a). As a result, one expects three broad sources of uncertainty in the products: a detection-related uncertainty that results from the possible confusion in the interpretation of the passive MW or IR observations between surface rain and cloud-column condensation; an estimation uncertainty that results from the quantitative conversion of the passive MW or IR observations into surface-rain amounts; and an interpolation issue stemming from the ambiguous use of frequent-but-indirectly-sensitive IR information to fill the revisit gaps.

To illustrate this general approach, Figure 1.1.1 depicts an *idealized* set of observations collected from four passive MW satellite overpasses over a given location during a 12-hour period. The data from each passive MW satellite measurement provide an estimate of the

surface precipitation (blue arrows). In this example, the satellites are equally spaced in their observing times, leaving 3-hour revisit gaps. By combining and merging these data with higher time resolution geostationary satellite data, the desired high spatial and temporal resolution precipitation products are produced (denoted by the red arrows). The errors resulting from the combination of all of the processing steps mentioned above are aggregated into the final high-resolution products that are provided to data users. Most often, the error analysis is carried out on the products that are produced at the end of this process, which represents an accumulated error. The purpose of this section is to provide insight to product users on the nature of the error introduced by the various steps. The remainder of this section is devoted to the discussion of these error components in more detail.
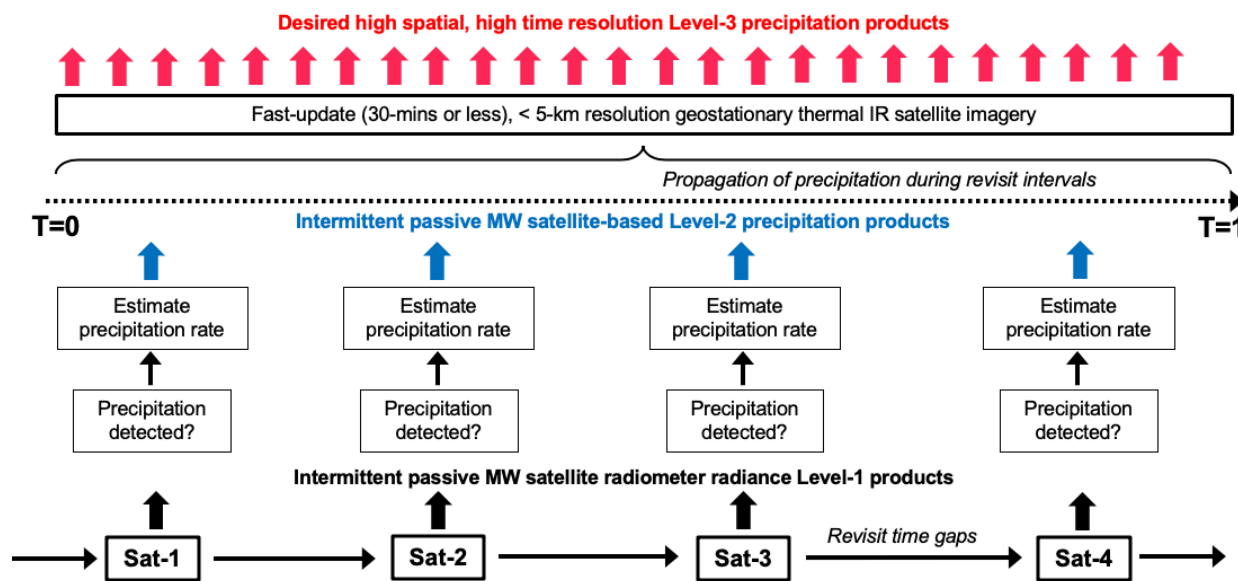
Figure 1.1.1. Idealized depiction showing how intermittent passive MW satellite-based precipitation data (blue arrows) are generated from a limited set of satellite overpasses, and used to produce a high spatial and temporal resolution (red arrows) satellite precipitation product

1.1.2. Satellite precipitation measurements

For the past two decades, the centerpieces of satellite precipitation measurements from space are the GPM core spacecraft (2014–present) and its predecessor, the Tropical Rainfall Measuring Mission (TRMM) (1997–2014) (Kummerow et al., 2000). Only these two spacecraft have a scanning precipitation radar instrument. TRMM and GPM's passive MW radiometers observe precipitation across scan swaths that are much wider (800 km) than the respective radar swath, and indeed the radar measurements are used as benchmarks, available over the common narrow swath, to guide the estimation of surface rain from the passive MW radiometers alone outside the common swath. Yet the swath of each passive MW radiometer is still not wide enough to allow global coverage on sub-daily time scales (i.e. revisit periods of less than 24 hours, let alone three or less as in the example of Figure 1.1.1). That is why the estimates at sub-daily scales require the aggregation of estimates from all available passive MW radiometers. Table 1 of Kidd et al. (2018a) lists the characteristics of the current GPM passive MW radiometers [GPM microwave imager (GMI), Special Sensor Microwave Imager/Sounder (SSMIS), Advanced Microwave Scanning Radiometer 2 (AMSR-2), Microwave Humidity Sounder (MHS) and Advanced Technology Microwave Sounder (ATMS)].

Many of these passive MW radiometers are carried by operational weather satellites, which orbit in sun-synchronous patterns and produce observations near fixed local solar times (so their observations can be efficiently assimilated into numerical weather prediction systems). Others, like GPM, TRMM and the Megha-Tropiques (M-T) satellite built by the Indian Space Research Organization (ISRO) and the French Centre National d'Etudes Spatiales (CNES), orbit in non-sun-synchronous orbits whose local observing times change from day to day, in 30–60-day cycles (depending upon latitude) (Roca et al., 2015; Negri et al., 2002). In contrast to the idealized depiction of Figure 1.1.1, Figure 1.1.2 shows a more realistic set of passive MW observations from the current (2020) GPM-era constellation, whose revisits, unlike Figure 1.1.1, are not evenly spaced in time. Moreover, these consist of different types of radiometers with different channels, resolutions and sensitivities. Therefore, the detection and estimation errors shown in Figure 1.1.1 are different for each sensor.
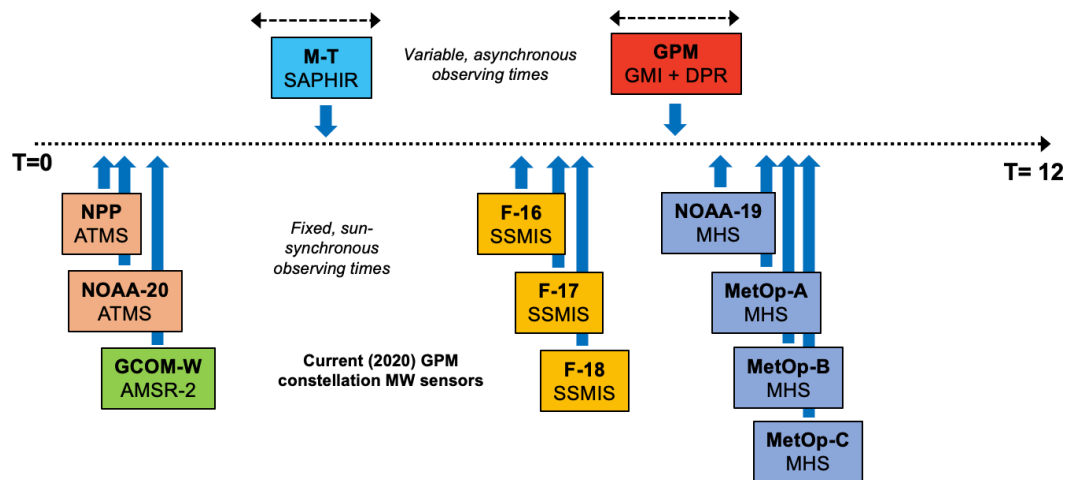
Figure 1.1.2. Depiction of the different passive MW satellites and their capabilities, observing times and revisit intervals during a typical 12-hour period, from the current (2020) GPM constellation era (contrast to idealized Figure 1.1.1)

The sensitivity of the passive MW radiometers is different for different radiometers and for different cloud types. These radiometers measure the net upwelling radiation from the Earth's surface through the atmosphere, in different frequency bands. The upwelling radiation comes primarily from the surface, and is modulated by the constituents of the atmosphere: the gases absorb (and therefore emit), and the hydrometeors (rain drops and the varieties of ice, snow, graupel, etc.) absorb/emit and also scatter the upwelling radiation, mostly out of the beam. This explains why the passive MW radiometers are not specifically sensitive to the precipitation in any single height layer of the cloud, let alone the surface layer. The radars, on the other hand, do not have this limitation, and do enable the estimation of vertical precipitation profiles. That is the justification for the multi-channel passive MW retrieval techniques which use a reference set of nearly-coincident nearly-simultaneous radar measurements (compiled offline, pairing passive MW measurements with the underlying precipitation rates as retrieved from the coincident simultaneous radar measurements), to produce instantaneous surface-rain estimates. These data can indeed be used to spread or "transfer" the DPR/Precipitation Radar (PR) radar structure information to each of the constellation radiometers (e.g., Turk et al., 2018; Kidd et al. 2018a; Petty and Li, 2013), so that each "Level-1" radiometer pixel can be assigned a "Level-2" estimate of the surface precipitation rate. The coincidence reference dataset can be used to retrieve any quantity that can be retrieved from the precipitation radar's measurements, with varying amounts of uncertainty that can be quantified from the reference data themselves, if the reference data are sufficiently extensive to be representative of global precipitation. Fortunately, both GPM and TRMM have asynchronous orbits so that, throughout the course of

a year, they do provide a very large number of near-coincident observations with each of the constellation radiometer satellites.

Lastly, the collection of Level-2 passive MW precipitation products is incorporated into global products covering a time interval, posted at a fixed grid resolution that can be near or finer than the scale of some of the Level-2 products that were used. These are termed "Level-3" products, which provide accumulated precipitation estimates at scales as fine as 30-minute refresh cycles, and 0.1° gridded resolution. For the remainder of this section, the focus is on the Level-3 products that incorporate the Level-2 passive MW precipitation products and high-resolution, fast-refresh cycle geostationary-satellite infrared (IR) observations to cover what would otherwise be lengthy revisit gaps from the Level-2 passive MW precipitation alone.

The next subsection attempts to quantify the order of magnitude of the uncertainties in the Level-3 products separately for each of the three sources of uncertainty. Examples of current widely-used global Level-3 precipitation products of this type include the Integrated Multi-Satellite Retrievals for GPM (IMERG) (Huffman et al., 2018); the Global Satellite Mapping of Precipitation (GSMaP) (Ushio et al., 2009), the National Oceanic and Atmospheric Administration (NOAA) Climate Prediction Center Morphing Technique (CMORPH) (Joyce and Xie, 2011), the Precipitation Estimation from Remotely Sensed Information using Artificial Neural Networks (PERSIANN) (Hsu et al., 1997), and the Self-Calibrating Multivariate Precipitation Retrieval (SCaMPR) (Kuligowski et al., 2013). A description and an intercomparison of many current global precipitation datasets from stations and satellites can be found in Sun et al. (2018). Because they are published at such relatively high spatial and temporal resolution, it is important to give an objective assessment of the uncertainty in these values at their reported resolution.

1.1.3. Intrinsic uncertainty of the Level-3 merged products

Early evaluation initiatives of a number of research Level-3 products were fostered by the International Precipitation Working Group (IPWG) (Ebert et al., 2007; Turk et al., 2008 and references within; see also 1.3 below). More recently in the post-GPM era, more detailed Level-3 evaluation efforts have been reported. A detailed list of these evaluation efforts would be lengthy (and likely incomplete); for reference, we refer to several recently-published studies (Maranan et al., 2020; Le Coz et al., 2020; Chen et al., 2019; Tan et al., 2016; Maggioni et al., 2014) and references within each of these. These studies generally proceed by comparing the values that are reported by a given product with other precipitation estimates. In contrast, in this subsection we review the uncertainties due to the sources of error in the successive steps in the estimation process. Indeed, the Level-3 uncertainty is the result of the accumulated uncertainty in the different steps of the estimation process, which for the purposes here are assumed to start with the Level-2 precipitation products themselves.

There are three main sources of uncertainty: 1) the uncertainty introduced in the precipitation detection by the Level-2 passive MW algorithms (either by omission, if no precipitation is detected so that the retrieval algorithm is not run and the precipitation is assumed to be zero when in fact precipitation was present, or by processing the passive measurements through the retrieval process when in reality there was no rain at the surface); 2) for the detected pixels, the uncertainty introduced by the instantaneous retrieval algorithms; and 3) the uncertainty introduced by the revisit-gap mitigation, i.e. the propagation in time from one Level-2 passive MW precipitation estimate to the next (i.e. from the Level-2 passive MW precipitation at time-1, to the passive MW precipitation at time-2).

4

In the following subsections, the Level-3 propagation-based methods common to operationally-produced precipitation products – IMERG, CMORPH, and GSMaP – are used as examples in the discussion of the third error component (use of IR data to fill passive MW revisit gaps). Products other than these three use different approaches to bring passive MW information to bear on IR data, including self-calibration (as in the case of SCaMPR) or artificial neural networks (as in the case of PERSIANN). The fundamental source of uncertainty in these mostly IR-based products is discussed in 1.1.3.5.

1.1.3.1. Detection errors
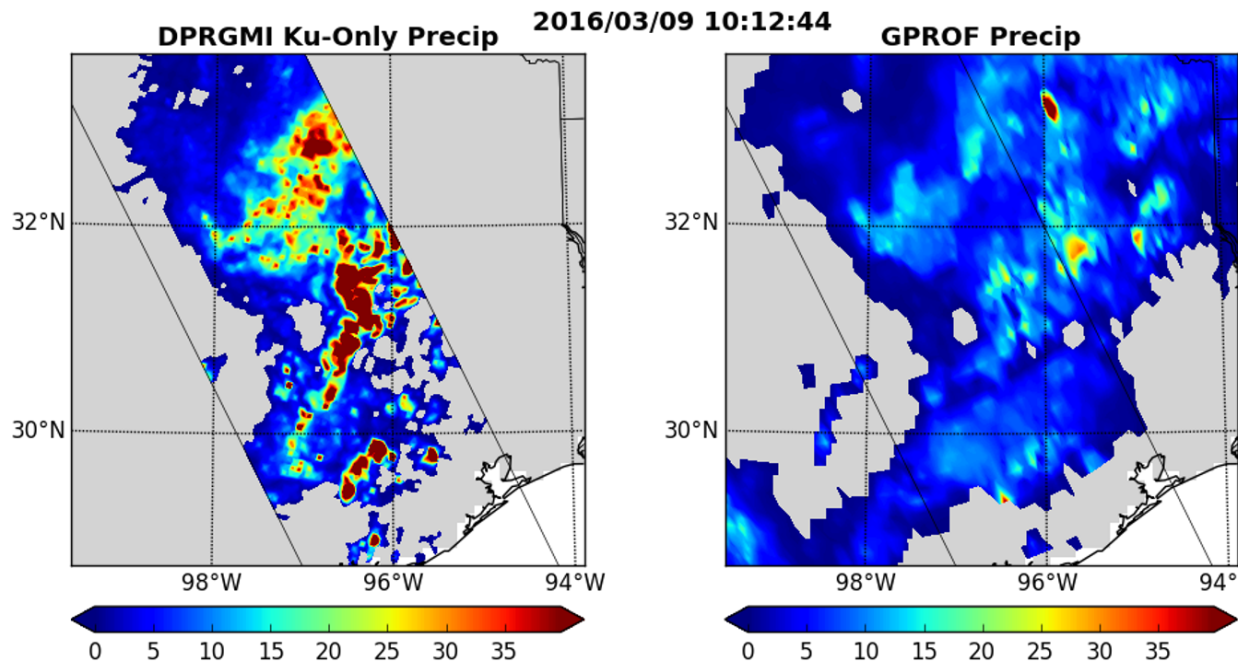
Figure 1.1.3. Side-by-side comparison of the precipitation estimate produced by the GPM combined DPR+GMI (CORRA) product (left panel), and the corresponding GMI-only (GPROF) estimate (right panel).

Establishing the minimum detectable precipitation rate for the Level-2 passive MW algorithms is not a straightforward proposition. The issue is illustrated in Figure 1.1.3, showing a typical pair of instantaneous retrievals, one made by the GMI radiometer algorithm (Goddard Profiling Algorithm, GPROF) (Kummerow et al., 2015) and one by the GPM combined sensor (DPR+GMI) radar radiometer algorithm (Combined Ku Radar-Radiometer Algorithm, CORRA) (Grecu et al., 2016). The substantial areas where the GMI algorithm detects surface precipitation > 0 mm/hr while the CORRA algorithm reports 0 mm/hr surface rain could indicate a greater (if indirect) sensitivity of GMI to lower precipitation rates than the radar, or they could be false alarms where passive MW retrievals were made over a precipitation-free column. In these discrepancies, the radiometer-retrieved rates are never greater than a few mm/hr, yet they do cover a significant area. The reverse can happen too (in the case illustrated, most notably in the area around 29N 96.5W), though this "failure to detect" by the instantaneous passive MW radiometer retrieval algorithms is less common.

Using a research passive MW precipitation profiling method (emissivity principal components, EPC) (Turk et al., 2018) based on the microwave surface emissivity, Utsumi et al. (2020) showed that the probability of detection (POD) over ocean surfaces exceeded 0.7 and was fairly consistent across the five algorithms tested and the choice of precipitation threshold. Over land, POD can drop below 0.6 for vegetated surfaces or coasts (Turk et al., 2018). Similar POD

scores were noted across passive MW sensors (You et al., 2020). Chen et al. (2019) performed a similar experiment and concluded that the conically-scanning imagers generally outperformed the cross-track scanning sounders.

1.1.3.2. Errors inherent to the instantaneous passive MW retrievals

Compared to the Level-3 products, relatively few independent validation studies of Level-2 passive MW constellation products have been done. A comparison of the areas with larger surface rain rates in Figure 1.1.3 illustrates the intrinsic uncertainty in the Level-2 instantaneous retrievals from passive MW measurements. Note how the substantial areas with rain rates higher than 30 mm/hr in the benchmark combined radar+radiometer retrievals are not matched by comparable estimates in the passive-MW-only retrievals. This subsection discusses these uncertainties and their order of magnitude.

Early (SSMI era) passive MW precipitation approaches were based upon mostly statistical methods (Grody et al., 1991) that matched brightness temperature (TB) combinations to observed near-surface reference precipitation estimates made by rain gauges or by rain-gauge-trained ground radars. As such, these methods were tuned to the characteristics of the limited-domain input radar data used. The spatial and temporal variability in the precipitation microphysics and the nature of the weather conditions and surface conditions were not accounted for. The retrievals also failed to provide any physical estimate of the error in the precipitation rate. More recent passive MW Level-2 precipitation data products are more physically-based and account for the error inherent to the passive MW precipitation scheme itself. These include, but are not limited to, GPROF (Kummerow et al., 2015), surface emissivity-based methods (Turk et al., 2018), PRPS (Kidd et al., 2018b), k-nearest neighbor (Takbiri et al., 2019), TB "pseudo channel" schemes (Petty and Li, 2013), MIRS (Boukabara et al., 2011), the JAXA GSMaP scheme (Aonashi et al., 2009) and 1DVAR snowfall (Meng et al., 2017). Often, these methods apply data reduction to the input TB data to isolate the precipitation signal from the naturally-occurring variability in the input TB signal. Provided the collection of *a-priori* data used (in one way or another) is sufficiently representative of the conditions being sampled by the passive MW-based satellites, Bayesian-based methods provide a means to determine the error associated with the mean precipitation estimate.

In the merging algorithms that incorporate the Level-2 passive MW precipitation products and high-resolution, fast-refresh cycle geostationary satellite-based infrared (IR) observations, currently only one of these passive MW algorithms is used. For example, the IMERG Level-3 dataset relies upon passive MW precipitation produced by the GPROF algorithm (Kummerow et al., 2015), and the GSMaP product uses the JAXA passive MW algorithm (Aonashi et al., 2009). Therefore, only the error associated with this single passive MW precipitation technique affects the downstream Level-3 processing.

In reality, each of the passive MW precipitation methods makes different assumptions on many variable processes, such as the form of the particle size distribution, its spatial uniformity or inhomogeneity, etc. For GPM, the core satellite DPR-based precipitation algorithm has four main precipitation products, a DPR-only and a combined DPR+GMI algorithm (CORRA) (Grecu et al., 2016), each with a Normal Scan (NS, or Ku-band only) and a Matched Scan (MS, or Ku+Ka-band) variant, for a total of four reported instantaneous estimates. Each of these retrieval algorithms make various simplifying assumptions to invert the measured radar reflectivity profiles into hydrometeor precipitation profiles. For example, the drop size distribution models used in the DPR algorithms are largely based on measurements from the tropics (Seto et al., 2013), which may not be applicable across the variety of weather systems encountered in the GPM coverage area. The drop size distribution models are selected based

on predefined precipitation types that are imperfectly identified from features in the radar reflectivity profiles. Another source of variability arises from the assumptions used to handle the variable surface radar surface cross section and (for CORRA) the surface emissivity variability (Munchak et al., 2016; Munchak et al., 2020). The multiple sources of uncertainty carry over into the passive MW-only precipitation profile estimates from each constellation MW radiometer.
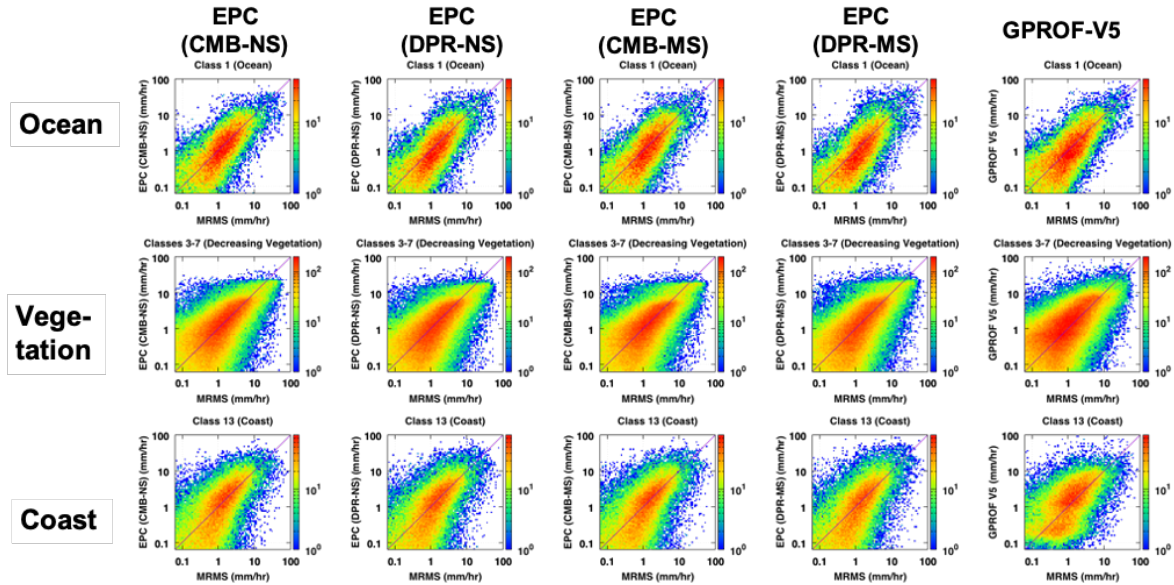
Figure 1.1.4. Comparison of five different instantaneous microwave retrievals versus the benchmark ground gauge-radar based Ground Validation Multi-Radar/Multi-Sensor estimates (horizontal axis; see section 1.2). From left, the EPC algorithm based on the GPM combined radar+radiometer algorithm (CORRA) Normal Scan (NS; Ku-band only) precipitation product, the EPC algorithm based on the GPM radar-only algorithm (DPR) Ku-band only precipitation product, the EPC algorithm based on the CORRA Matched Scan (MS; Ku+Ka-band) precipitation product, the EPC algorithm based on the GPM radar-only algorithm (DPR) Ku+Ka-band) precipitation product, and the Version 5 GPROF algorithm. The rows indicate data is from ocean, vegetated and coastal surface classes. Note the log-log scaling of each panel.
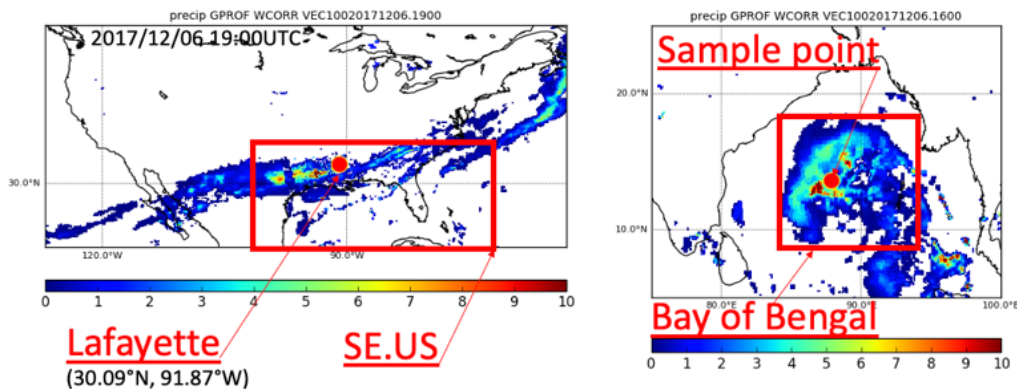
Figure 1.1.5. Maps showing the two locations of the case studies summarized in 1.1.3.2 and 1.1.3.3.

Currently, there is no consistent way to account for the range of uncertainty introduced in these instantaneous estimates, as they are used to make the passive MW constellation estimates,

and ultimately the Level-3 products including IMERG, GSMaP, CMORPH and others. However, one can estimate the magnitude of this uncertainty by comparing instantaneous retrievals to a common reference. Figure 1.1.4 shows a comparison of five different instantaneous GMI microwave retrievals (5 columns) relative to pixel-matched precipitation products derived from the benchmark U.S. ground radar-gauge Ground Validation Multi-Radar/Multi-Sensor (GV-MRMS) (Kirstetter et al., 2012, 2018b) products (horizontal axis; see Section 1.2), illustrating the uncertainty in any individual estimate to be above 100%. Since passive MW measurements are sensitive to the emission from the surface, the validation is separated by the underlying surface classification (ocean, vegetation, coastal), corresponding to each row. A common reference also makes it possible to diagnose and propagate the uncertainty to the Level-3 products (see Figure 1.1.12). Kidd et al. (2018a) used multi-radar multi-sensor (MRMS) to validate the GPROF algorithm across sensors.
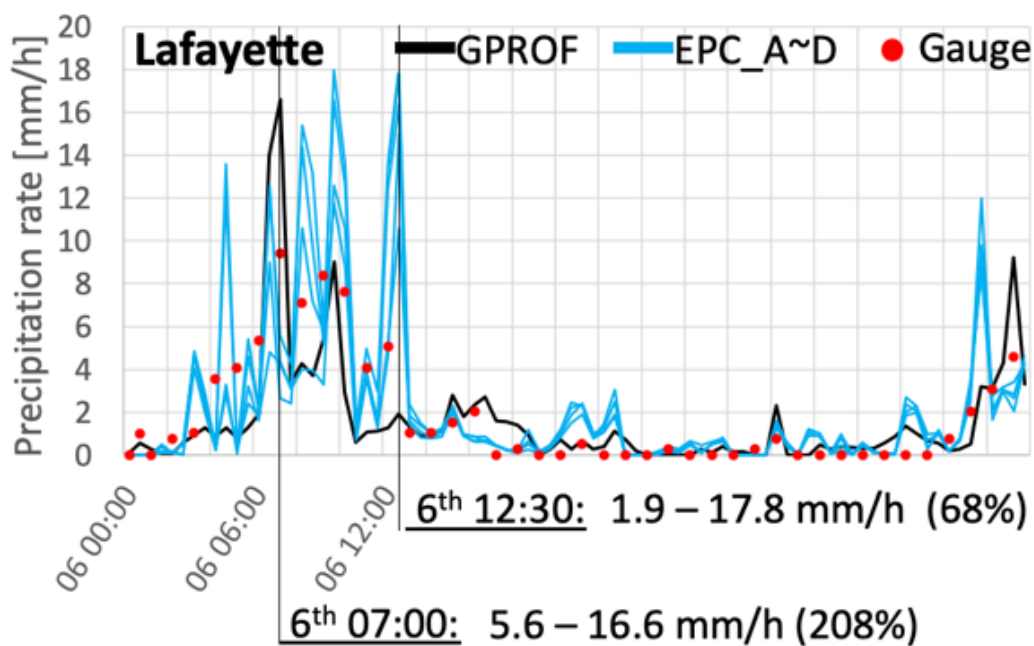
Figure 1.1.6. Time series of the five instantaneous passive microwave retrievals in Figure 1.1.4 for a specific 0.1-degree resolution element near Lafayette, LA (see Figure 1.1.4) on the ground, for a 42-hour period (0 UTC on 6 December 2017 through 18 UTC on December 7). The spread of the estimates is shown (up to 200% at times) as well as the discrepancy between the detection according to the satellite instrument and the lack of rain detected by the gauges at several times. This is most notable at 20 and 22 UTC on the 6th, at 12 and 13 UTC on the 7th.

While Figure 1.1.4 shows overall "bulk" comparisons of many individual per-pixel retrievals, the differences between each of the passive MW products at a specific pixel or "point" are more variable and can vary from location to location. To highlight an individual point location, Figure 1.1.6 shows the range of the five passive MW precipitation products from Figure 1.1.4 for a 42-hour period. The time series is from a specific 0.1-degree grid box point (the posted resolution of many Level-3 precipitation products) shown in Figure 1.1.5. In this example, the spread of the estimates is shown (up to 200% at times) as well as the discrepancy between the detection according to the satellite instrument and the lack of rain detected by the gauges at several times.

8

1.1.3.3. Errors introduced by revisit-gap mitigation

During the revisit gap between any two successive passive MW precipitation datasets, the precipitation is evolving. In Level-3 products such as CMORPH, GSMaP and IMERG, the precipitation evolution between successive passive MW precipitation datasets is accounted for by filtering/"morphing" methods. This process requires the use of ancillary data that is sampled frequently during the revisit gaps, to infer sufficient information to evolve the precipitation at one end of the temporal gap time-1 to the other time-2 (time-1 and time-2 being the observation times of the two passive MW satellites at the two ends of the revisit gap). This is done variously by tracking radiometrically cold IR cloud top patterns between successive 30-min imagery, or by tracking the motion of the precipitable water vapor patterns from global model reanalysis fields (Tan et al., 2019), or by tracking the motion of the IR-derived surface-precipitation fields, or using an empirically-derived filter based on these combined data. In effect, a several-degree box size is used to track the frequently-sampled data features from one time to the next, and to estimate the evolution of surface precipitation along these tracks.
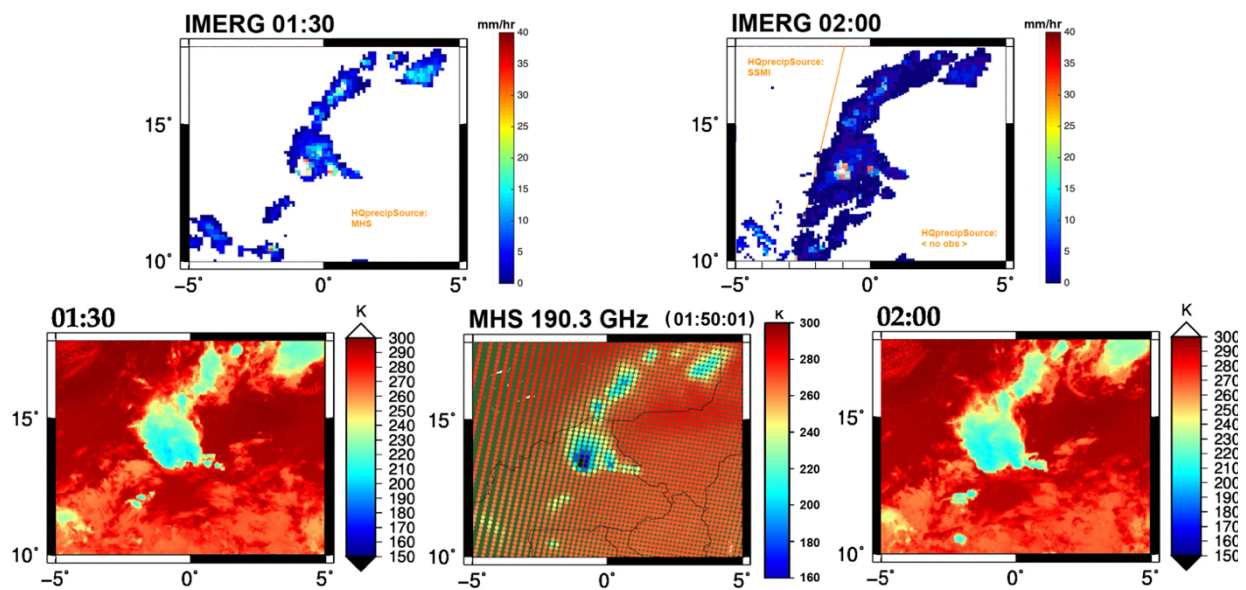
Figure 1.1.7. The top row shows the IMERG estimates of surface rain on 24 July 2014 at 0130 Z and 0200Z over a convective storm in West Africa, with marked differences between the rain fields at the two consecutive times despite the striking similarity of the geostationary IR observations at these times shown in the bottom row, along with the passive MW brightness temperatures measured by the MHS radiometer at 0150Z (Haddad et al., 2017).

Figure 1.1.7 illustrates the result in the case of a mesoscale convective system that developed over West Africa early on the morning of 24 July 2014. The surface rain estimated by the finest-resolution (30-min) IMERG product at 0130 Z is quite different from that at 0200 Z, in spite of the fact that the geostationary IR temperatures are quite similar at both times (lower panels). At 0130 UTC, the HQ precipitation source was from an MHS sounder. At 0200 UTC, the most-recent passive MW source was from the SSMIS (left side of the orange line) but only to the left of the orange line, with no passive MW data available in this 30-minute time on the right side of the line (where the storm was located). The main difference in the precipitation estimates is the large amount of low precipitation rates that appear at 0200 all around the storm as it was delineated at 0130, almost entirely due to the fact that between 0130 to 0200 there was a passive MW observation, by MHS at 0150Z, but between 0200 and 0230 the only MW observation was by SSMIS and missed this storm entirely, so that the estimates at 0200 are

strongly affected by revisit-gap mitigation. In this case, the precipitation at 0200 covers an area that is almost double that at 0130, the excess consisting entirely of rain rates below 2 mm/hr.
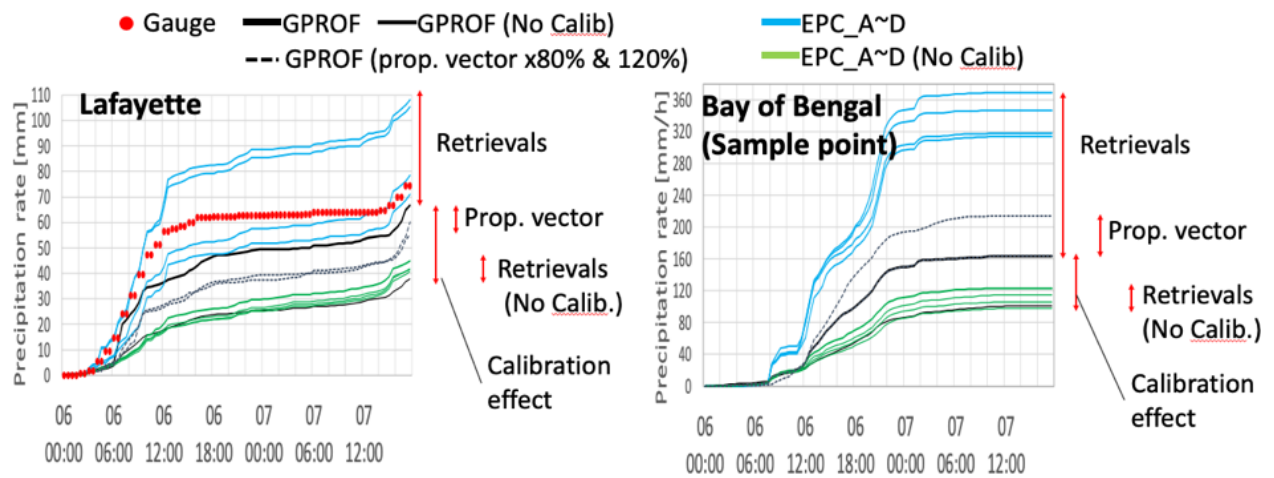
Figure 1.1.8. Accumulated precipitation for the same morphed products shown in Figure 1.1.6, for the Lafayette location (left) and the Bay of Bengal location (right). The comparison shows the result of using different passive MW precipitation products in the generation of the Level-3 merged satellite product, showing spreads that can grow to a factor of three at the end of the 42-hour period.

A more systematic evaluation of the cumulative effect of the interpolation was performed using IMERG as the evaluation medium. To that end, the IMERG technique was adapted into a "test mode" (IMERG-T) (Utsumi et al., 2018), where instead of feeding the IMERG process with the passive MW precipitation data from the GPROF algorithm, it can be fed with other, different passive MW precipitation retrievals. Figure 1.1.8 shows the same case as Figure 1.1.6, but in this example the accumulated precipitation is shown. The accumulated precipitation from the Bay of Bengal area in Figure 1.1.5 is also shown, as a side comparison. IMERG-T was run separately for each of the four passive MW algorithms in Figure 1.1.4. This was done with (blue lines) and without (green lines) the calibration step that is used in IMERG to assure that the histograms of the GPROF-GMI passive MW precipitation match the histograms of each of the other constellation sensors. The "spread" amongst the ten products (four EPC and GPROF, each with a calibrated and uncalibrated version) is shown by the red vertical line "Retrievals". Figure 1.1.8 shows the net effect at a "pointwise" scale, which is the scale at which many Level-3 product users actually use and interpret these data for their analyses. While it shows only two locations, it does highlight the expected variability at the 0.1-degree scale. Other Level-3 product users may spatially average these native 0.1-degree, 30-minute data further, for example, into common 1-degree daily grid boxes (discussed in section 2 below) or 5-day pentads.
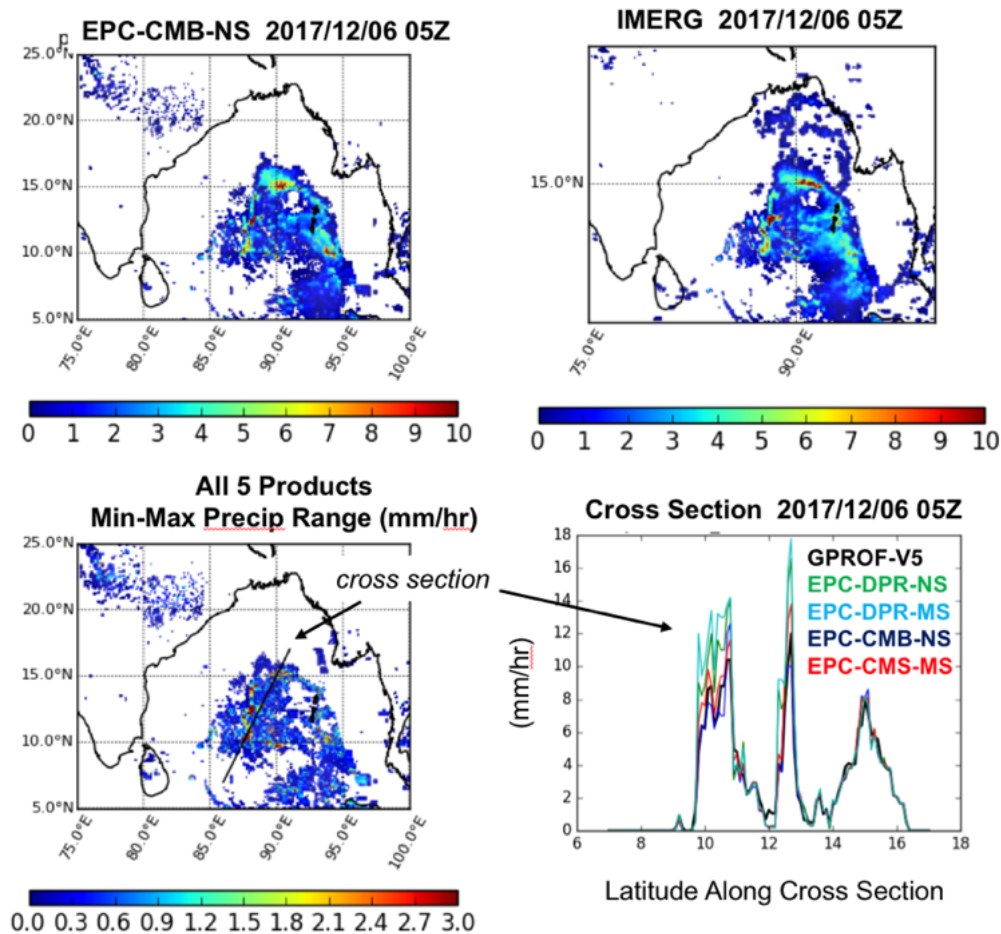
Figure 1.1.9. (**Top right**) Final IMERG precipitation product for the 30-minute interval ending at 05 UTC on 6 December 2017, showing an area in the Indian Ocean. (**Top left**) Corresponding image, except using the EPC CORRA-NS retrieval for each constellation radiometer (except MHS), to carry out the morphing procedure in IMERG-T. (**Lower left**) The ensemble spread (range of maximum-minus-minimum, in mm hr^{-1}) that results when each of the four EPC-based retrievals are fed through the IMERG-T morphing. (**Bottom right**) Final precipitation estimates along the cross-section line shown in the lower right panel for each of the four EPC-based retrievals. IMERG, which morphs using only GPROF precipitation, is shown in the black line.

In Figure 1.1.9, the official IMERG precipitation data valid at 0500 UTC on 6 December 2017 is shown in the upper right panel. This represents the average rain rate in the 30 minutes between 0430-0500 UTC. The collection of passive MW precipitation data products that feed into this IMERG estimate come from different satellite overpasses. Depending upon the orbit characteristics, some pixels in this area may have had a more recent "refresh" from a passive MW satellite than others. In this example, the passive MW precipitation products from the EPC products are based on the DPR+GMI combined Ku-band only product (Grecu et al., 2016). While the overall pattern of the precipitation is similar in the top two panels, there are small scale differences at the 0.1-degree level reported for the IMERG product.

This same process was repeated with the other three radar algorithms, each of whose passive MW precipitation data products were fed into the IMERG processing. The resultant ensemble spread expresses the overall range of variability in the final products considering that all of these factors are processed though IMERG. The lower left panel shows the range (maximum minus minimum) of values produced by the members of this ensemble.

To highlight the difference, the bottom right panel of Figure 1.1.9 shows the final precipitation estimates along the cross-section line shown in the lower right panel (IMERG, which morphs using only GPROF precipitation, is shown for comparison, in the black line), for each of the four EPC-based retrievals. The individual colors each represent the output when each of the four EPC-based estimates are used in the IMERG-T morphing procedure. Note the difference in some of the heaviest precipitation locations can be as much as 40% higher, but only slightly lower, than the IMERG product. *This ensemble analysis expresses the range of precipitation, considering each of the DPR-based precipitation estimates processed through each constellation radiometer, and processed through IMERG.*
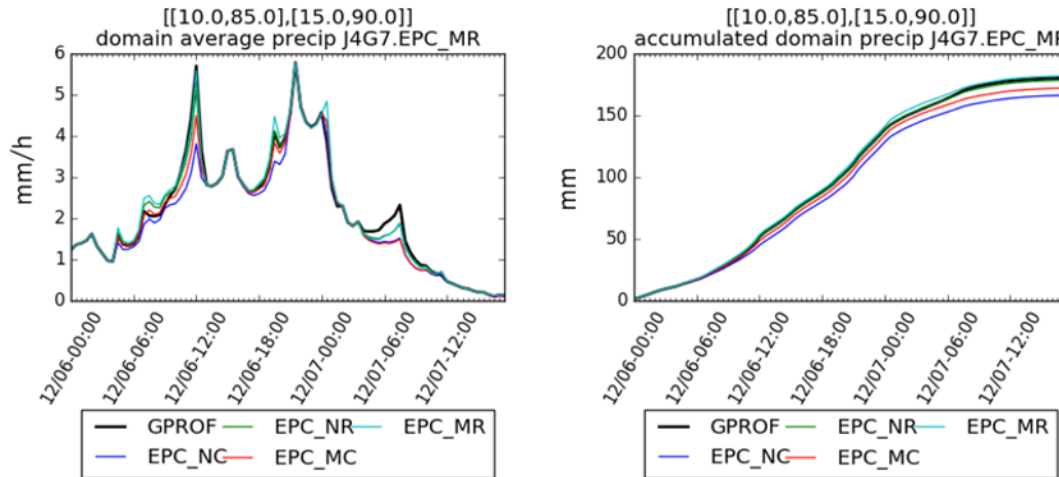
Figure 1.1.10. Analysis of the 36-hour period from 0 UTC on 6 December 2017 to 12 UTC on 7 December 2017, where the domain is a 5° x 5° box in the Bay of Bengal. (**Left**) Domain-average IMERG precipitation product at each 30-minute time step. (**Right**) Accumulated precipitation. The domain-integrated accumulation at the end of the 36-hour period varies between 160 and 188 mm, a span of about 16% of the ensemble mean.

While Figure 1.1.9 highlights differences at the instantaneous (single overpass) scale, Figure 1.1.10 illustrates the cumulative effect of these same ambiguities when averaged over a 5° x 5° domain and over the 36-hour duration of the storm. As expected, spatial and temporal averaging of the native fine-scale data reduces the instantaneous pointwise errors illustrated in Figure 1.1.9, but the uncertainty does not shrink to zero. Using a one-minute updating rain gauge network over Korea, Turk et al. (2009) examined the performance of the NRL-Blend fast-update precipitation product across telescoping space-time averaging scales. The space-time root mean square (RMS) error, mean bias, and correlation matrices were computed using various time windows for the gauge averaging, centered about the satellite observation time (this is necessary since the satellite measurement responds to the precipitation before it has fallen to the ground, where the gauges measure). For ±10 minute rain gauge time windows (Figure 1.1.11), a correlation of 0.6 was achieved at 0.1-degree spatial scale by averaging over 3 days; coarsening the spatial scale to 1.8 degrees produced the same correlation by averaging over one hour. Finer than approximately 24-hours and 1-degree time and space scales, respectively, a rapid decay of the error statistics was obtained by trading off either spatial or time resolution.
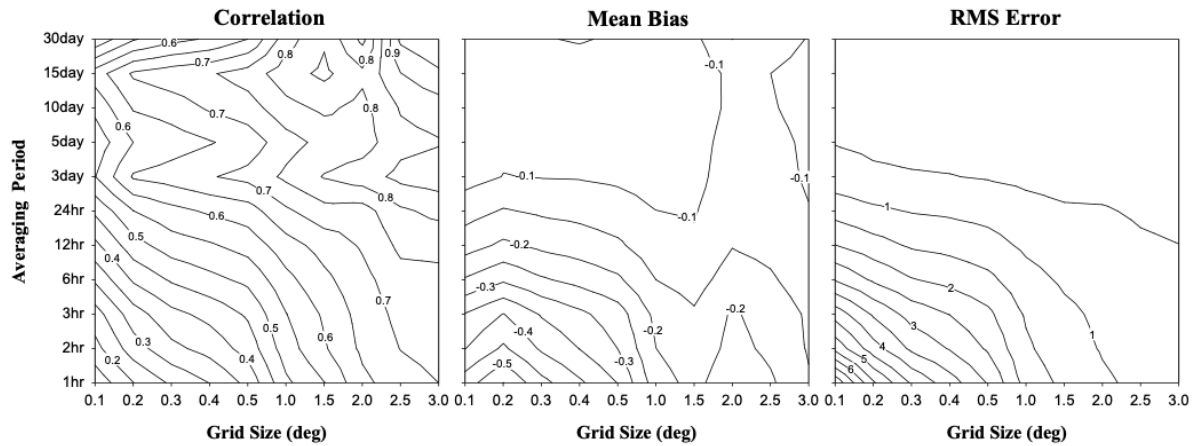
Figure 1.1.11. Space-time contour plots of the correlation coefficient, root mean square error and mean bias for the rain gauge network time window average of ±10 minutes, centered about the time of the GMS satellite observation of Korea. The abscissa and ordinate of each contour plot denotes the spatial and temporal scales, respectively, used to average the rain gauge data and the NRL-blended satellite technique estimated rain (figure adapted from Turk et al., 2009).

1.1.3.4. Sensitivity to IR observations: Uncertainty in quantitative estimation and in interpolation during revisit gaps
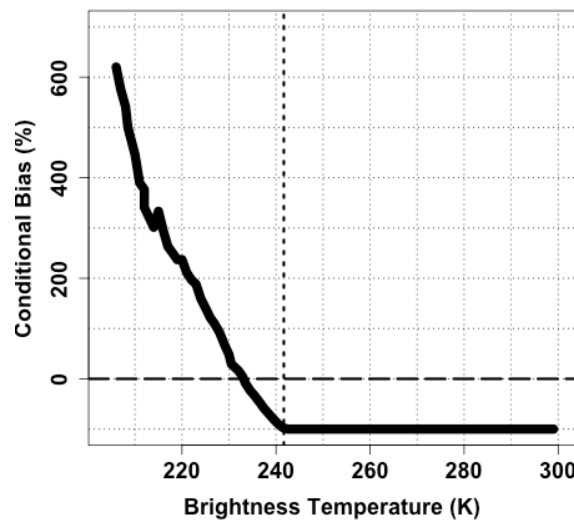
Figure 1.1.12. Relative bias in percentage between the PERSIANN-CCS precipitation estimates relative to the reference GV-MRMS as a function of the IR brightness temperature. This intrinsic bias results from the algorithm assumption that deeper clouds, represented by colder brightness temperatures, produce more surface rain. The conditional bias is a decreasing function of the brightness temperature following the redistribution assigning higher precipitation rates to colder brightness temperatures. The –100% bias above 242 K relates to missed precipitation that also results from the assumption (adapted from Kirstetter et al., 2018a).

Starting in the 1980s, when passive MW data was unavailable or scarce (routine SSMI data began in 1987), but geostationary IR measurements were routinely available hourly, the idea to use instantaneous IR radiances to estimate instantaneous surface rain was proposed and implemented. This was justified by the fact that, in convective storms, deeper clouds tend to produce more surface rain than shallower clouds (Arkin and Meissner, 1987; Huffman et al.,

13

1997). However, a cold IR temperature indicates a high cloud, which is not the same as a deep cloud. Even statistically, TRMM has established that the deepest clouds are not the ones that produce the highest surface rain rates (Hamada and Takayabu, 2016). The ambiguities are even greater away from the tropics, where the rain amounts produced by storms do not have a monotonic relation with the height of the cloud. IR radiances provide indirect information on the occurrence and magnitude of precipitation at the surface. Depending on the cloud type and life cycle, a given IR brightness temperature can be associated with various rain rates, since not all clouds produce precipitation or produce it at the same rate. IMERG combines IR-based Precipitation Estimation from Remotely Sensed Information using Artificial Neural Networks-Cloud Classification System (PERSIANN-CCS: Hong et al., 2004) and retrievals from passive MW estimates. As discussed earlier for passive MW estimates, the uncertainty associated with each PERSIANN-CCS retrieval is critically lacking for optimally merging PERSIANN-CCS outputs with passive MW precipitation and quantifying the propagation of this uncertainty into the final IMERG estimates. Kirstetter et al. (2018b) investigate this question with GV-MRMS over the U.S. over two summers of 2014–2015. They estimate that the PERSIANN-CCS intrinsic uncertainty, arising from assuming that deeper clouds produce more surface rain, can be described as a conditional bias typically ranging from –100% to +600% with the observed brightness temperatures (Fig. 4 in Kirstetter et al., 2018a, reproduced here in Figure 1.1.12). The volume of precipitation that is missed or erroneously detected is substantial (more than 50%), and the quantitative variability of correctly-detected precipitation is not well reproduced.

That is why the idea of using the frequently-available IR measurements to make instantaneous estimates of the underlying surface rain evolved to give rise to the less problematic concept of using them to guide the revisit-gap evolution estimation instead (Joyce et al., 2004, and references within). In this IR-based filtering, the features that are tracked represent cloud top patterns (IR cloud temperatures), rather than the actual evolution in time of the near-surface precipitation itself. The actual precipitation may be evolving faster or slower in space and intensity, in ways that are not easily approximated by locally linear tracking. For example, the precipitation at the surface may be moving slower or faster than the motion inferred from the upper cloud regions, or in extreme cases (where upper/lower vertical shear exists), moving in a different direction. To mitigate, certain algorithms such as CMORPH locally adjust the morphing tracking speed, based on comparisons with precipitation tracked from ground radars (Joyce and Xie, 2011). These discrepancies are a source of uncertainty in the Level-3 precipitation processing.

Using the IMERG-T analysis described above, Figure 1.1.13 illustrates the magnitude of the revisit-gap evolution speed uncertainty. The specific analysis quantifies the effect of artificially slowing down (or speeding up) the motion by 20, 30 or 50%. The difference in the final precipitation field is shown relative to the original precipitation. In this example, the largest differences are observed for the cases where the motion field was slowed down relative to what the IR-based tracking alone provides.

The "spread" at a given point due to the propagation vector variability was already illustrated in Figure 1.1.8 (highlighted by the vertical red arrow labeled "Prop. vector") for each of the two 0.1-degree gridbox locations of Figure 1.1.5. In this example, the most noticeable effect occurs when the motion vectors were slowed down.
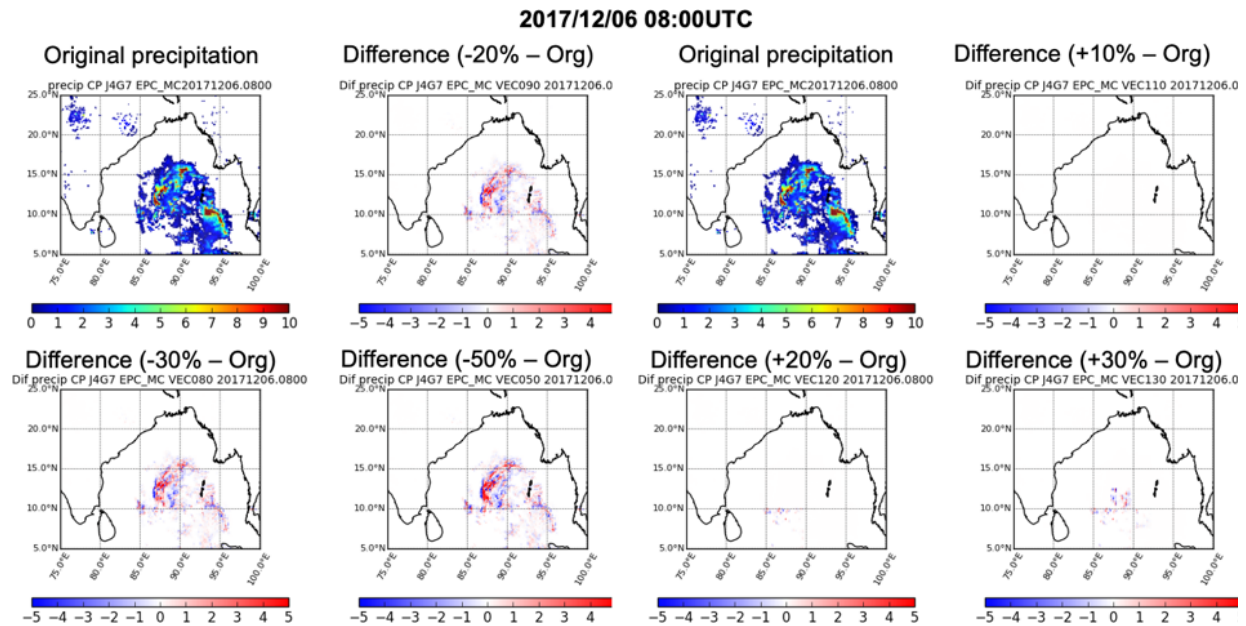
Figure 1.1.13. Left four panels: Net effect when the motion vector is slowed down by 20, 30 and 50% of its original value (upper left panel). **Right four panels**: Same, in the case when the motion vector is sped up by 20, 30 and 50% of its original value.

1.1.4. Summary of the assessment of intrinsic uncertainty

The Level-3 "sub-daily global merged satellite precipitation products" are typically reported on a fixed rectangular latitude-longitude grid at high spatial and temporal resolution (respectively 0.1° and ~0.5 hour). This subsection specifically concerned the uncertainties in these products at their reported resolution. These include the satellite precipitation products listed in Table 1.1.1, and are the building blocks for further coarser-resolution products included in later subsections.

The discussion above summarized the uncertainties that are inherent in the retrieval and processing steps that are used to produce the Level-3 estimates. These include the detection error, the passive MW and IR estimation errors, and the error incurred when using frequent IR information to fill long revisit gaps between passive MW estimates.

By themselves, passive MW observations alone are not capable of perfect detection. There is always an ambiguity between the passive MW TB and the particular atmospheric state that gives rise to these same TBs. For example, very light rainfall over ocean has a similar TB structure as a large amount of non-precipitating cloud water. For lack of a perfect benchmark reference, the exact sensitivity of a passive MW radiometer is challenging to determine.

The uncertainties in the passive MW estimates (second error above) originate from the limited sensitivity of the set of radiometer channels to the desired near-surface precipitation. As the signal that is measured by a passive MW or IR observation originates predominantly from the tops of the clouds, none of the instantaneous-level observations produced from these same sensors are directly and unambiguously sensitive to the underlying near-surface precipitation. Establishment of an absolute error is challenging since a common reference dataset is not globally available. Ground radars are an appropriate source of independent validation, but only cover specific continental land areas–and carry uncertainties of their own.

The majority of passive MW precipitation data is tied to specific local observing times by virtue of the operational nature of the host satellite platform. Only the GPM (and M-T) satellites currently orbit in a non-sun-synchronous orbit pattern capable of sampling (within its latitude coverage). This leads to lengthy gaps in satellite revisit, which are filled in with precipitation estimates created from geostationary-based IR observations. Currently this process is done via weighting of a priori prescribed uncertainties from the individual passive MW observations, with no regard for error in the speed or direction of the motion vectors used to transport the precipitation structure from one time period to the next. Few studies have been done in this regard, which warrant further study.

This section has quantified the order of magnitude of the uncertainty that *has to be expected* in today's merged satellite precipitation products at their native relatively-high (spatial and temporal) resolution, and which therefore exists as the current mutual ambiguity to be expected between the different Level-3 products. The following sections will describe, in more detail, independent validation of the uncertainty attributed to several of the precipitation datasets identified in this section, which includes the use of gauges and ground radars as an independent source.

Table 1.1.1. Global satellite precipitation products evaluated

Product	Resolutions	Advantages	Disadvantages (in addition to possible local bias)
Level-3 MiRS	When aggregated by user: no finer than single-instrument resolution (20–40 km) When pre-aggregated: daily	- Reasonably good sensitivity - Instantaneous estimate for every MW-constellation obs - Same approach over land or water	Snapshots every ~80 minutes on average Revisit time could stretch to 3 hours
Level-3 GPROF	When aggregated by user: no finer than single-instrument resolution (20–40 km) When pre-aggregated: 0.5°/hourly ("3G68" product)	- Reasonably good sensitivity - Instantaneous estimate for every MW-constellation obs - Estimates calibrated by the reference GPM radiometer	Snapshots every ~80 minutes on average Revisit time could stretch to 3 hours
Level-3 GPM radar/combined	When aggregated by user: 5 km When pre-aggregated: 0.25°/daily	- High direct sensitivity to surface rain - High spatial resolution (~5 km)	Revisit time calculated in days

HOAPS	When aggregated by user: no finer than single-instrument resolution When pre-aggregated: 0.5°/6-hourly	Conically-scanning MW radiometers only	Ocean only
CMORPH	8 km/30 minutes (and various other pre-aggregated versions)	- Frequent temporal reporting (~30 mins) - Good spatial resolution (~25 km) - Uses MiRS for instantaneous MW estimates - Uses advection scheme from IR in between MW overpasses	Persistence of any misdetection/amplification of estimation uncertainty
GSMaP	0.1°/hourly (and various other pre-aggregated versions)	- Frequent temporal reporting (~30 mins) - Good spatial resolution (0.1°) - Uses GSMaP_mwLUT for instantaneous MW estimates - Uses change in IR to adjust MW-estimated rain	Persistence of any misdetection/amplification of estimation uncertainty
IMERG rt	0.1°/half-hourly	- Frequent temporal reporting (~30 mins) - Good spatial resolution - Uses GPROF for instantaneous MW estimates - Uses advection scheme from IR in between MW passes - Available within about 5 hours of obs	Persistence of any misdetection/amplification of estimation uncertainty
IMERG late	0.1°/ half-hourly	- Frequent temporal reporting (~30 mins) - Good spatial resolution - Uses GPROF for instantaneous MW estimates - Available within a few weeks of obs	Persistence of any misdetection/amplification of estimation uncertainty
IMERG science	0.1°/ half-hourly	- Frequent temporal reporting (~30 mins) - Good spatial resolution - Uses GPROF for instantaneous MW estimates	Persistence of any misdetection/amplification of estimation uncertainty

		- Available 3 months after obs	
PERSIANN	0.04°/ half-hourly (PERSIANN-CCS)	- Long record back to ~ 1979 - NN approach accounts for regional variability	Mainly IR based – highly Indirect and non-monotone sensitivity to surface rain

Table 1.1.1. Listing of global satellite precipitation products with spatial resolution finer than 0.5 degrees and temporal resolution finer than 6-hourly, that have been evaluated by the IPWG validation subgroup

1.1.5. Recommendations

Recommendation 1.1.1: Encourage the a priori quantification of the uncertainty that should be expected in a given product, given the errors in the input and the uncertainties introduced by the product generation.

In the absence of an undisputed reference truth, the physical validation of an estimation method is very useful in putting bounds on the uncertainty that can be expected, given the author's knowledge of the simplifying assumptions that were made to produce the estimates.

Recommendation 1.1.2: Encourage precipitation product providers to provide uncertainty estimates for each space/time scale of the final precipitation product.

Current global fine-resolution (< 0.1° horizontal, < daily temporal) satellite precipitation products are not mere aggregates of instantaneous satellite estimates. They rely on complex detection, estimation and filtering steps to produce a regularly-gridded product whose individual estimates carry quite a bit of uncertainty. These uncertainties vary from product to product, and consist of a mixture of misdetections and estimation errors that are compounded by revisit-gap-filling procedures that introduce additional uncertainty. Nevertheless, if these uncertainties are considered by the user, the passive MW-based products carry far less uncertainty than those based on geostationary IR alone or on rain gauges.

1.1.6. References

Aonashi, K., J. Awaka, M. Hirose, T. Kozu, T. Kubota, G. Liu, S. Shige, S. Kida, S. Seto and N. Takahashi, 2009: GSMaP passive microwave precipitation retrieval algorithm: Algorithm description and validation. *Journal of the Meteorological Society of Japan*, 87A, 119–136, https://doi.org/10.2151/jmsj.87A.119.

Arkin, P.A., and B.N. Meisner, 1987: The relationship between large-scale convective rainfall and cold cloud over the western hemisphere during 1982–84. *Monthly Weather Review*, 115, 51–74, https://doi.org/10.1175/1520-0493(1987)115%3C0051:TRBLSC%3E2.0.CO;2.

Boukabara, S.A., K. Garrett, W. Chen, F. Iturbide-Sanchez, C. Grassotti, C. Kongoli, R. Chen, Q. Liu, B. Yan and F. Weng, 2011: MiRS: An All-Weather 1DVAR Satellite Data Assimilation and Retrieval System. *IEEE Transactions on Geoscience and Remote Sensing*, 49, 3249–3272, https://doi.org/10.1109/TGRS.2011.2158438.

Chen, H., B. Yong, J.J. Gourley, J. Liu, L. Ren, W. Wang, Y. Hong and J. Zhang, 2019: Impact of the crucial geographic and climatic factors on the input source errors of GPM-based global

satellite precipitation estimates. *Journal of Hydrology*, 575, 1–16, https://doi.org/10.1016/j.jhydrol.2019.05.020.

Ebert, E.E., J.E. Janowiak and C. Kidd, 2007: Comparison of near-real-time precipitation estimates from satellite observations and numerical models. *Bulletin of the American Meteorological Society*, 88, 47–64, https://doi.org/10.1175/BAMS-88-1-47.

Grecu, M., W.S. Olson, S.J. Munchak, S. Ringerud, L. Liao, Z.S. Haddad, B.L. Kelley and S.F. Mclaughlin, 2016: The GPM combined algorithm. *Journal of Atmospheric and Oceanic Technology*, 33, 2225–2245, https://doi.org/10.1175/JTECH-D-16-0019.1.

Grody, N.C., 1991: Classification of snow cover and precipitation using the Special Sensor Microwave Imager. *Journal of Geophysical Research*, 96, 7423–7435, https://doi.org/10.1029/91JD00045.

Haddad, Z.S., R.C. Sawaya, S. Kacimi, O.O. Sy, F.J. Turk and J. Steward, 2017: Interpreting millimeter-wave radiances over tropical convective clouds. *Journal of Geophysical Research: Atmospheres*, 122, 1650–1664, https://doi.org/10.1002/2016JD025923.

Hamada, A., and Y.N. Takayabu, 2016: Improvements in Detection of Light Precipitation with the Global Precipitation Measurement Dual-Frequency Precipitation Radar (GPM DPR). *Journal of Atmospheric and Oceanic Technology*, 33, 653–667, https://doi.org/10.1175/JTECH-D-15-0097.1.

Hong, Y., K.-L. Hsu, S. Sorooshian and X. Gao, 2004: Precipitation Estimation from Remotely Sensed Imagery Using an Artificial Neural Network Cloud Classification System. *Journal of Applied Meteorology and Climatology*, 43, 1834–1853, https://doi.org/10.1175/JAM2173.1.

Hou, A.Y., R.K. Kakar, S. Neeck, A.A. Azarbarzin, C.D. Kummerow, M. Kojima, R. Oki, K. Nakamura and T. Iguchi, 2014: The Global Precipitation Measurement mission. *Bulletin of the American Meteorological Society*, 95, 701–722, https://doi.org/10.1175/BAMS-D-13-00164.1.

Hsu, K., X. Gao, S. Sorooshian and H.V. Gupta, 1997: Precipitation Estimation from Remotely Sensed Information Using Artificial Neural Networks. *Journal of Applied Meteorology and Climatology*, 36, 1176–1190, https://doi.org/10.1175/1520-0450(1997)036<1176:PEFRSI>2.0.CO;2.

Huffman, G.J., R.F. Adler, P. Arkin, A. Chang, R. Ferraro, A. Gruber, J. Janowiak, A. McNab, B. Rudolf and U. Schneider, 1997: The Global Precipitation Climatology Project (GPCP) combined precipitation dataset. *Bulletin of the American Meteorological Society*, 78, 5–20, https://doi.org/10.1175/1520-0477(1997)078%3C0005:TGPCPG%3E2.0.CO;2.

Huffman, G.J., D.T. Bolvin, D. Braithwaite, K. Hsu, R. Joyce, C. Kidd, E.J. Nelkin, S. Sorooshian, J. Tan and P. Xie, 2018: *IMERG Algorithm Theoretical Basis Document*, https://pmm.nasa.gov/sites/default/files/document_files/IMERG_ATBD_V5.2_0.pdf.

Joyce, R.J., J.E. Janowiak, P.A. Arkin and P. Xie, 2004: CMORPH: A Method that Produces Global Precipitation Estimates from Passive Microwave and Infrared Data at High Spatial and Temporal Resolution. *Journal of Hydrometeorology*, 5, 487–503, https://doi.org/10.1175/1525-7541(2004)005<0487:CAMTPG>2.0.CO;2.

Joyce, R.J., and P. Xie, 2011: Kalman filter-based CMORPH. *Journal of Hydrometeorology*, 12, 1547–1563, https://doi.org/10.1175/JHM-D-11-022.1.

Kidd, C., J. Tan, P.-E. Kirstetter and W.A. Petersen, 2018a: Validation of the Version 05 Level 2 precipitation products from the GPM Core Observatory and constellation satellite sensors. *Quarterly Journal of the Royal Meteorological Society*, 144, 313–328, https://doi.org/10.1002/qj.3175.

Kidd, C., R. Roca and E. Stocker, 2018b: Development of the SAPHIR Precipitation Retrieval and Processing Scheme (PRPS). *Geophysical Research Abstracts*, Vol. 20, EGU2018-9356, EGU General Assembly 2018, https://meetingorganizer.copernicus.org/EGU2018/EGU2018-9356.pdf.

Kirstetter, P.-E., Y. Hong, J.J Gourley, S. Chen, Z. Flamig, J. Zhang, M. Schwaller, W. Petersen and E. Amitai, 2012: Toward a Framework for Systematic Error Modeling of Spaceborne Precipitation Radar with NOAA/NSSL Ground Radar–Based National Mosaic QPE. *Journal of Hydrometeorology*, 13, 1285–1300, https://doi.org/10.1175/JHM-D-11-0139.1.

Kirstetter, P.-E., N. Karbalaee, K. Hsu and Y. Hong, 2018a: Probabilistic precipitation rate estimates with space-based infrared sensors. *Quarterly Journal of the Royal Meteorological Society*, 144 (Suppl. 1): 191– 205, https://doi.org/10.1002/qj.3243.

Kirstetter, P.-E., W. Petersen and J.J. Gourley, 2018b: GPM Ground Validation Multi-Radar/Multi-Sensor (MRMS) Precipitation Reanalysis for Satellite Validation Product. Dataset available online from the NASA Global Hydrology Resource Center DAAC, Huntsville, Alabama, U.S.A. DOI: http://dx.doi.org/10.5067/GPMGV/MRMS/DATA101.

Kuligowski, R.J., Y. Li and Y. Zhang, 2013: Impact of TRMM Data on a Low-Latency, High-Resolution Precipitation Algorithm for Flash-Flood Forecasting. *Journal of Applied Meteorology and Climatology*, 52, 1379–1393, https://doi.org/10.1175/JAMC-D-12-0107.1.

Kummerow, C.D., J. Simpson, O. Thiele, W. Barnes, A.T.C. Chang, E. Stocker, R.F. Adler, A. Hou, R. Kakar, F. Wentz, P. Ashcroft, T. Kozu, Y. Hong, K. Okamoto, T. Iguchi, H. Kuroiwa, E. Im, Z. Haddad, G.J. Huffman, B. Ferrier, W.S. Olson, E.J. Zipser, E.A. Smith, T.T. Wilheit, G. North, T. Krishnamurti and K. Nakamura, 2000: The Status of the Tropical Rainfall Measuring Mission (TRMM) after Two Years in Orbit. *Journal of Applied Meteorology*, 39, 1965–1982, https://doi.org/10.1175/1520-0450(2001)040<1965:TSOTTR>2.0.CO;2.

Kummerow, C.D., D.L. Randel, M. Kulie, N.Y. Wang, R. Ferraro, M.S. Joseph and V. Petkovic, 2015: The Evolution of the Goddard profiling algorithm to a fully parametric scheme. *Journal of Atmospheric and Oceanic Technology*, 32, 2265–2280, https://doi.org/10.1175/JTECH-D-15-0039.1.

Le Coz, C., and N. van de Giesen, 2020: Comparison of Rainfall Products over Sub-Saharan Africa. *Journal of Hydrometeorology*, 21, 553–596, https://doi.org/10.1175/JHM-D-18-0256.1.

Maggioni, V., M.R.P. Sapiano, R.F. Adler, Y. Tian and G.J. Huffman, 2014: An Error Model for Uncertainty Quantification in High-Time-Resolution Precipitation Products. *Journal of Hydrometeorology*, 15, 1274–1292, https://doi.org/10.1175/JHM-D-13-0112.1.

Maranan, M., A.H. Fink, P. Knippertz, L.K. Amekudzi, W.A. Atiah and M. Stengel, 2020: A Process-Based Validation of GPM IMERG and Its Sources Using a Mesoscale Rain Gauge Network in the West African Forest Zone. *Journal of Hydrometeorology*, 21, 729–749, https://doi.org/10.1175/JHM-D-19-0257.1.

Meng, H., J. Dong, R. Ferraro, B. Yan, L. Zhao, C. Kongoli, N.-Y. Wang and B. Zavodsky, 2017: A 1DVAR-based snowfall rate retrieval algorithm for passive microwave radiometers. *Journal of Geophysical Research: Atmospheres*, 122, 6520–6540, https://doi.org/10.1002/2016JD026325.

Munchak, S.J., S. Ringerud, L. Brucker, Y. You, I. de Gelis and C. Prigent, 2020: An Active–Passive Microwave Land Surface Database From GPM. *IEEE Transactions on Geoscience and Remote Sensing*, 58, 6224–6242, https://doi.org/10.1109/TGRS.2020.2975477.

Munchak, S.J., R. Meneghini, M. Grecu and W.S. Olson, 2016: A consistent treatment of microwave emissivity and radar backscatter for retrieval of precipitation over water surfaces. *Journal of Atmospheric and Oceanic Technology*, 33, 215–229, https://doi.org/10.1175/JTECH-D-15-0069.1.

Negri, A.J., T.L. Bell and L. Xu, 2002: Sampling of the diurnal cycle of precipitation using TRMM. *Journal of Atmospheric and Oceanic Technology*, 19, 1333–1344, https://doi.org/10.1175/1520-0426(2002)019%3C1333:SOTDCO%3E2.0.CO;2.

Petty, G.W., and K. Li, 2013: Improved passive microwave retrievals of rain rate over land and ocean. Part I: Algorithm description. *Journal of Atmospheric and Oceanic Technology*, 30, 2493–2508, https://doi.org/10.1175/JTECH-D-12-00144.1.

Roca, R., H. Brogniez, P. Chambon, O. Chomette, S. Cloché, M.E. Gosset, J.-F. Mahfouf, P. Raberanto and N. Viltard, 2015: The Megha-Tropiques mission: A review after three years in orbit. *Frontiers in Earth Science* 3, 17, https://doi.org/0.3389/feart.2015.00017.

Seto, S., T. Iguchi and T. Oki, 2013: The Basic Performance of a Precipitation Retrieval Algorithm for the Global Precipitation Measurement Mission's Single/Dual-Frequency Radar Measurements. *IEEE Transactions on Geoscience and Remote Sensing*, 51, 5239–5251, https://doi.org/10.1109/TGRS.2012.2231686.

Sun, Q., C. Miao, Q. Duan, H. Ashouri, S. Sorooshian and K.-L. Hsu, 2018: A review of global precipitation datasets: data sources, estimation, and intercomparisons. *Reviews of Geophysics*, 56, 1–29, https://doi.org/10.1002/2017RG000574.

Takbiri, Z., A. Ebtehaj, E. Foufoula-Georgiou, P.-E. Kirstetter and F.J. Turk, 2019: A Prognostic Nested k-Nearest Approach for Microwave Precipitation Phase Detection over Snow Cover. *Journal of Hydrometeorology*, 20, 251–274, https://doi.org/10.1175/JHM-D-18-0021.1.

Tan, J., W.A. Petersen and A. Tokay, 2016: A Novel Approach to Identify Sources of Errors in IMERG for GPM Ground Validation. *Journal of Hydrometeorology*, 17, 2477–2491, https://doi.org/10.1175/JHM-D-16-0079.1.

Tan, J., G.J. Huffman, D.T. Bolvin and E.J. Nelkin, 2019: IMERG V06: Changes to the Morphing Algorithm. *Journal of Atmospheric and Oceanic Technology*, 36, 2471–2482, https://doi.org/10.1175/JTECH-D-19-0114.1.

Turk, F.J., P. Arkin, M.R.P. Sapiano and E.E. Ebert, 2008: Evaluating high-resolution precipitation products. *Bulletin of the American Meteorological Society*, 89, 1911–1916, https://doi.org/10.1175/2008BAMS2652.1.

Turk, F.J., B.-J. Sohn, H.-J. Oh, E.E. Ebert, V. Levizzani and E.A. Smith, 2009: Validating a rapid-update satellite precipitation analysis across telescoping space and time scales. *Meteorology and Atmospheric Physics*, 105, 99–108, https://doi.org/10.1007/s00703-009-0037-4.

Turk, F.J., Z.S. Haddad, P. Kirstetter, Y. You and S. Ringerud, 2018: An observationally based method for stratifying *a priori* passive microwave observations in a Bayesian-based precipitation retrieval framework. *Quarterly Journal of the Royal Meteorological Society*, 144, Issue S1, 145–164, https://doi.org/10.1002/qj.3203.

Ushio, T., K. Sasashige, T. Kubota, S. Shige, K. Okamoto, K. Aonashi, T. Inoue, N. Takahashi, T. Iguchi and M. Kachi, 2009: A Kalman Filter Approach to the Global Satellite Mapping of Precipitation (GSMaP) from Combined Passive Microwave and Infrared Radiometric Data. *Journal of the Meteorological Society of Japan*, 87A, 137–151, https://doi.org/10.2151/jmsj.87A.137.

Utsumi, N., F.J. Turk, Z. Haddad, G. Huffman and D. Bolvin, 2018: *A Self-Consistent Ensemble Approach to Propagate Estimation, Calibration, and Evolution Uncertainties through Global Precipitation Measurement Surface Precipitation Mapping*. Proceedings from a NASA Precipitation Measurements Mission science team meeting held in Phoenix, Arizona, U.S.A., from 8–11 October 2018, https://gpm.nasa.gov/research/meetings/2018-pmm-science-team-meeting.

Utsumi, N., F.J. Turk, Z.S. Haddad, P.-E. Kirstetter and H. Kim, 2020: Evaluation of precipitation vertical profiles estimated by GPM-era satellite-based passive microwave retrievals. *Journal of Hydrometeorology*, https://doi.org/10.1175/JHM-D-20-0160.1.

You, Y., V. Petkovic, J. Tan, R. Kroodsma, W. Berg, C. Kidd and C. Peters-Lidard, 2020: Evaluation of V05 Precipitation Estimates from GPM Constellation Radiometers Using KuPR as the Reference. *Journal of Hydrometeorology*, 21, 705–728, https://doi.org/10.1175/JHM-D-19-0144.1.

1.2. Validating the intrinsic uncertainty: Implications for hydrologic applications

Pierre-Emmanuel Kirstetter[1]

[1]University of Oklahoma, Norman, OK, USA

Reliable quantitative information on the spatial distribution of precipitation is essential for hydrologic and climatic applications that range from real-time hydrologic hazards forecasting (e.g. floods, droughts, landslides), to water resources and urban drainage management and agriculture, to diagnosing hydroclimate patterns and trends, to evaluating regional and global atmospheric model simulations. Physical processes associated with these applications cover multiple scales, from minutes to decades and from metres to the synoptic scale. The critical importance of accurate water flux estimates for applications explains the large body of verification analyses focusing on precipitation estimates, in terms of occurrence, average and extremes. An abundance of independent validation has been carried out directly on Level-3 products using gauges and sometimes ground radar data from various over-land locations. Very few are implemented at the relevant scales to address the intrinsic uncertainty of precipitation products. Without relevant information on key uncertainty features, applications making use of satellite Level-3 precipitation products are impacted both in terms of outcomes and physical realism.

1.2.1. Benchmarks for satellite precipitation: Sensors

Accurately measuring rainfall has been a challenge for the research community predominantly because of its high variability in space and time. There are primarily three major types of techniques of precipitation measurement: (1) surface-based rain gauge, (2) weather radar and (3) space-based meteorological satellites.

Among precipitation sensors, only the rain gauge directly measures precipitation rates or time accumulations. Rain gauges collect rainfall directly in a small orifice and measure the water depth, weight or volume. Rain gauges provide quite reliable point measurements of precipitation and records frequently span more than 100 years. These are therefore the best source for long-term studies of precipitation extremes and trends. The global distribution of gauges is heterogeneous, with higher densities in more populated regions and lower densities in rural and remote areas. Critically, the number of gauges available also depends on their temporal sampling resolution, with stations sampling at finer scales being rarer. Gauges are routinely used to represent areas of 100 to 3000 m^2 from measurements taken over a few square centimeters. However, their measurements are affected by uncertainties (for example, wind undercatch, evaporation, snow) and lack areal representation, which becomes particularly problematic for intense rainfall with high spatial variability (for example, Zawadzki, 1975). The spatial representativeness of each gauge measurement depends on the autocorrelation distance of precipitation (for example, Delahaye et al., 2015). While the autocorrelation increases with time integration, it varies greatly with precipitation regime and is typically short for extreme events (for example, Lebel et al., 1987). Interpolation of rain gauge observations is mandatory to obtain spatial information. When it comes to comparing gauges with other area-averaged precipitation estimates such as from radars or satellites, the spatial variability of rainfall at small scales and the large resolution difference (as much as nine orders of magnitude in area) may cause large differences in the statistical sampling properties of the extremely variable rainfall process (for example, Habib et al., 2004). The added statistical noise when comparing the two measurements is especially significant for short accumulation periods (1 hour or less; Ciach and Krajewski, 1999).

Precipitation is associated with specific generating processes, such as convection, orographic enhancement in complex terrain or warm rain processes. Measuring variations in the drop size distribution and the vertical structure of events is essential for understanding precipitation processes but cannot be captured by rain gauges. Remote sensing is the only way to explicitly observe the spatial distribution of precipitation. However, complex interactions between the spatiotemporal variability of precipitation processes, sensor resolution, sensitivity, calibration and the indirect nature of precipitation retrievals introduce complications (Section 1.1). In the last decades, weather radar systems have become a valuable tool to fill multiple observational gaps in time, surface 2D and 3D. As active sensors, ground-based radars provide range-resolved information on precipitation that is not available from most satellite sensors. Radar systems reveal precipitation characteristics, including intermittency, types (for example, stratiform, convective, snow and hail) and rates, with better resolution and accuracy than gauges and satellites, respectively. Through real-time and high-resolution volume scanning, weather radars offer more comprehensive information on the horizontal and vertical structure of rainfall. Radar networks upgraded with dual-polarization technology give additional insights into precipitation microphysics specifically on the size, shape, orientation and phase of hydrometeors. Ground-based weather radar data are now widely used by national weather services for quantitative precipitation estimation (QPE) at fine scales (for example, 1 km/5 min). Radar QPE is subject to specific uncertainties (that is, sensor calibration, attenuation depending on the radar frequency, ground clutter and beam blocking, variation of reflectivity with height, conversion from radar moments to precipitation rate, etc.; for example, Delrieu et al., 2009; Villarini and Krajewski, 2010; Berne and Krajewski, 2013). The characterization of these uncertainties has motivated studies for several decades. Radar–rain gauge merging approaches combining the fine spatio-temporal resolution of radar and the local accuracy of gauges have been proposed for QPE (for example, Delrieu et al., 2014) and are applied operationally (for example, Zhang et al., 2016), while novel approaches are being developed to integrate uncertainty as part of the quantitative estimation process (for example, Kirstetter et al., 2015; Neuper and Ehret, 2019).

The last decade has witnessed the growing use of satellite-based observations for seamless observation of precipitation over land and oceans, with quasi-global coverage that is not available with radar or gauge networks (for example, Skofronick-Jackson et al., 2017). As shown in Section 1.1, most instantaneous-level spaceborne precipitation observations are performed with passive MW sensors, providing more indirect observations of surface rainfall amounts than radars. Many multi-sensor precipitation retrievals combine IR and passive MW data to produce near-real time estimates at high spatial and temporal resolution (for example, 30 min, 0.1°). A description and an intercomparison of current global precipitation datasets from stations and satellites can be found in Sun et al. (2017).

Sensor limitations discussed in this section are listed in Section 2.3.1. In order to overcome these limitations, it is crucial to recognize that no single sensor combines accuracy, resolution and representativeness over relevant spatial and temporal scales, which are essential characteristics for applications making use of precipitation inputs. Achieving these characteristics requires the expert combination of observations that maximize each sensor's advantages while minimizing its weaknesses. Ultimately, such a combination does not produce perfects estimates with no uncertainty, but estimates with uncertainties that are deemed sufficiently low.

1.2.2. Benchmarks for satellite precipitation: Requirements for quantifying intrinsic uncertainty

Because precipitation displays variability at all scales, the satellite's intrinsic uncertainty can only be assessed at the primary scale of the precipitation retrievals. Preserving the product's intrinsic characteristics precludes any scale alteration such as interpolation, averaging, smoothing or oversampling, which affects key characteristics such as the retrieved rainfall amount, the rainy area and the distribution of precipitation rates. The true precipitation averaged over the spatial domains and time intervals corresponding to the primary scale of satellite precipitation retrievals is unknown. A reference precipitation used as a proxy for the true precipitation and as a benchmark should spatially and temporally match the satellite retrieval domain and display acceptable levels of accuracy.

Ground sensors constitute a natural choice to create a benchmark because their measurements are more directly sensitive to surface precipitation than satellite sensors. A trustworthy surface reference rainfall dataset should combine the complementary qualities of ground-based sensors, specifically the local accuracy of gauges and the spatial and temporal resolution provided by radars. An example of a satellite precipitation benchmark is the Ground Validation Multi-Radar/Multi-Sensor (GV-MRMS; Kirstetter et al., 2018b) that is derived from the MRMS system (Zhang et al., 2016). MRMS incorporates observations from all polarimetric Weather Surveillance Radar, 1988, Doppler (WSR-88D) radars and from gauge networks in the conterminous U.S. and creates a seamless 3D radar mosaic. Automatic quality controls and corrections procedures mitigate radar uncertainties (section 1.2.1) and generate high-resolution mosaicked radar-based surface precipitation products at a 0.01° horizontal resolution and 2 minute update cycles. Dual-polarization improves the radar data quality and enables the identification of hydrometeors where the ground-radar estimates are the most reliable. The radar-based data are integrated with atmospheric environmental data and rain gauge observations to generate a suite of severe weather and quantitative precipitation estimation (QPE) products. A surface reference precipitation framework is derived from MRMS to support the GPM mission for ground validation and intercompare satellite sensors (Kirstetter et al., 2014; Petersen et al., 2020) and to validate Level-3 precipitation products (Gebregiorgis et al., 2017; Tan et al., 2017). It applies conservative adjustments, quality controls and quantity controls on MRMS products to refine the most trustworthy radar-gauge precipitation estimates towards specific satellite purposes and needs. This processing is designed to maximize accuracy, minimize uncertainties and standardize the GV-MRMS precipitation reference products across the Continental United States (CONUS).

Thanks to their resolution, which is higher than any satellite precipitation product, GV-MRMS data are designed to be pixel-matched in both time and space, and to build statistics for comparing reference precipitation intensities to Level-2 and Level-3 satellite-based estimates. Note that no reference perfectly matches the true precipitation; however, eliminating systematic error sources and non-robust reference values is necessary to improve confidence in the reference precipitation. The reference data covers a broad range of land surface types (mountains, coasts, plains) and precipitation regimes and captures a variety of situations to document representative features of satellite intrinsic uncertainty.

An extended characterization of the reference precipitation should include additional key precipitation properties such as typology. The typology of rainfall can be assessed within the satellite sensor's field of view (FOV) (for Level-2 products) or pixel grid (for Level-3 products) through precipitation properties such as the Convective Percent Index (CPI). CPI quantifies the volume contribution of convective rainfall to the reference precipitation (Kirstetter et al., 2020).

The CPI is expressed in percent between 0% (purely stratiform rainfall within the FOV or pixel) to 100% (purely convective rainfall). CPI values between 0% and 100% indicate mixed precipitation types (Figure 1.2.1).
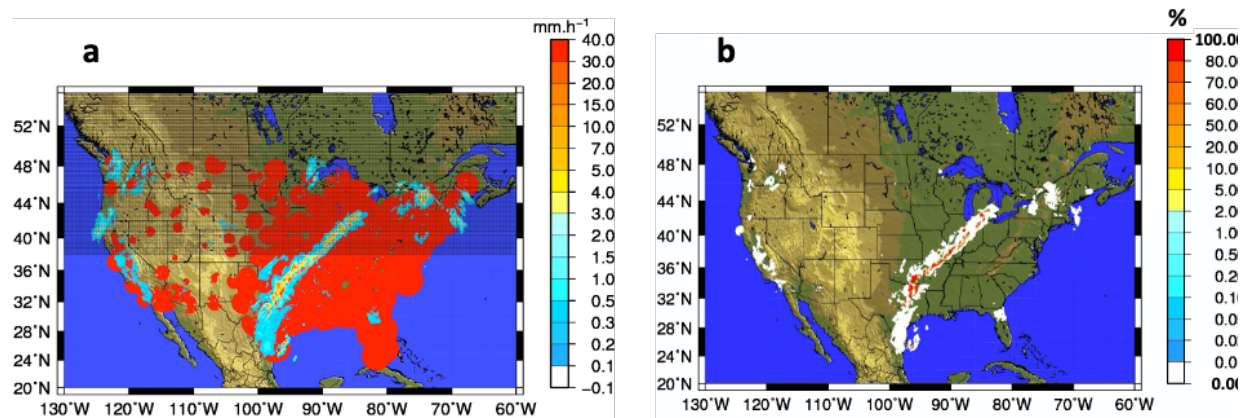
Figure 1.2.1. (a) Map of CONUS area with GV-MRMS instantaneous rain rates at 0725 UTC on 11 April 2011. The red area shows the good quality radar coverage; (b) the convective percent index (CPI).

1.2.3. Non-homogeneity of gridded satellite precipitation products: Implication for their hydrologic assessment

It is essential to recognize that gridded Level-3 satellite precipitation products are not homogeneous because of the dynamical interplay between a variety of error sources described in previous sections. Precipitation characteristics such as convection are a challenge for satellite retrievals, although convective precipitation is a strong driver of extremes. They condition systematic biases at all levels (for example, see Figure 1.2.2). The estimation error varies also depending on which sensor is weighted more in the retrieval. For example, estimates originating from IR display different error patterns from passive MW (for example, see Figure 1.2.2d). Consistency and homogeneity are properties that any Level-3 satellite precipitation product is designed to achieve, but these properties are often overlooked in assessment exercises. It follows that a gap remains with our ability to consistently merge precipitation estimates into gridded products and assess the procedure.

An endemic limitation in the extensive body of literature on satellite precipitation validation and error modeling is that the satellite product is implicitly assumed to be consistent and homogeneous over the spatial and temporal domain of comparison. This is rarely the case because comparison samples gather a variety of precipitation characteristics (for example, intermittency, typology, rates) for which the satellite algorithm (or combination of algorithms for Level-3 merged products) is likely to behave differently. More generally the comparison is always performed with precipitation estimates ambiguously derived from the satellite sensor observation through the retrieval algorithm and associated assumptions. Individual passive MW/IR retrievals are underconstrained by nature and sensitive to unobserved atmospheric parameters (Stephens and Kummerow, 2007). The combined products inherit the varying passive MW/IR performances and create additional uncertainties with temporal/spatial resampling.
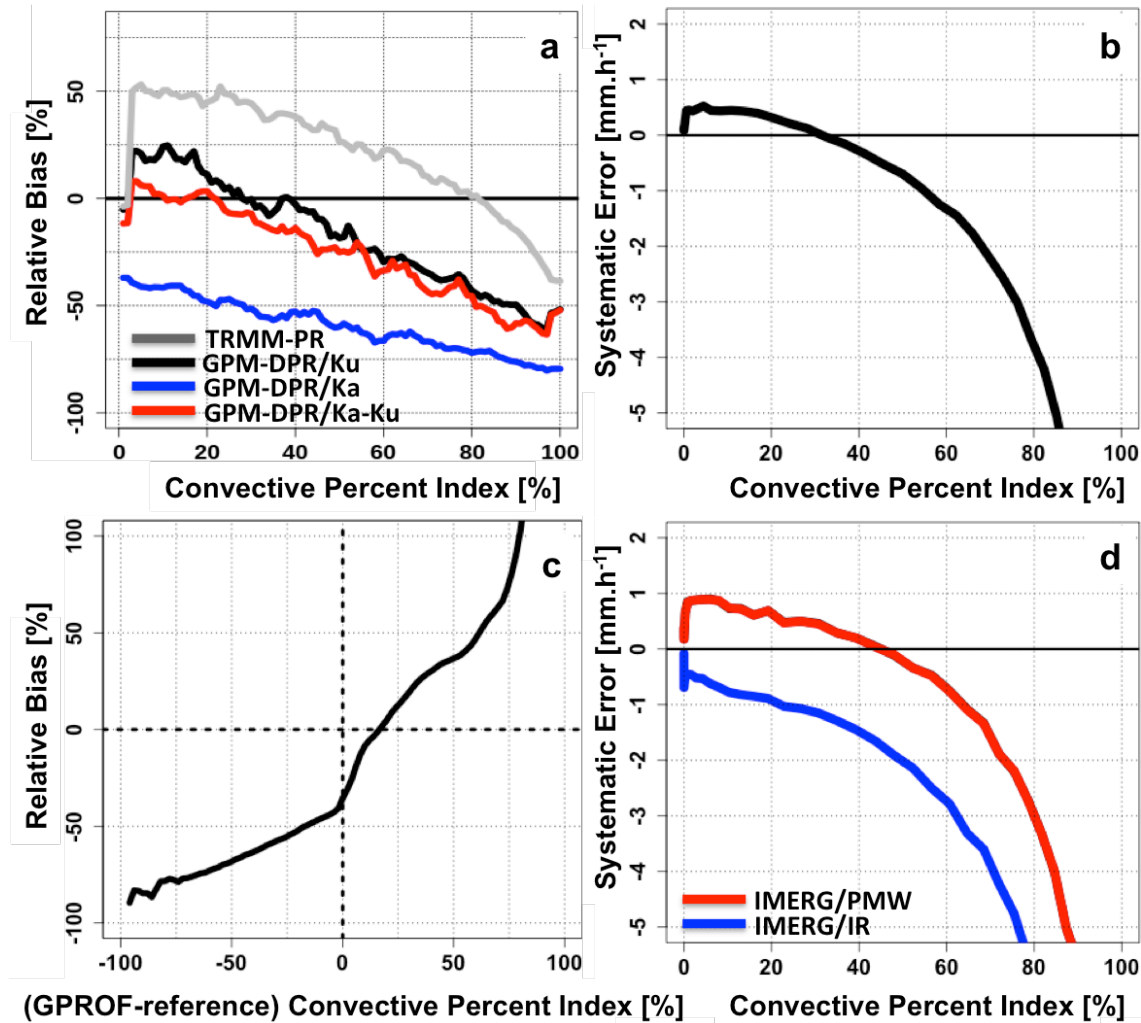
Figure 1.2.2. Performances of space-based QPE as functions of Convective Percent Index with respect to GV-MRMS: (a) space-based radars' relative bias for TRMM-PR (grey), DPR/Ku (black), DPR/Ka (blue) and DPR/Ka-Ku (red); (b) GPROF-GMI systematic error; (c) GPROF-GMI relative bias as a function of CPI difference with GV-MRMS; and (d) IMERG systematic error for the passive MW (red) and IR (blue) components. Convective and stratiform situations correspond to CPI=100% and CPI=0%, respectively. Comparison data include 2M+ matched ground-satellite pairs from June 2014 to September 2016 (from Kirstetter et al., 2020).

Common assessment typically uses bulk comparison metrics (for example, probability of detection, correlation, bias) that depict averaged space/time properties while the errors tend to be non-stationary and sensitive to parameters not accounted for in the assessment formulation. These metrics are sometimes applied without necessarily checking their relevance (for example, the linear correlation is generally insufficient to describe the non-linear and heteroscedastic dependence structure between a satellite precipitation estimate and the precipitation reference). Hence validation practice generally provides limited insight in the complex error characteristics of satellite precipitation estimates.

In addition, the representativeness of any overall satellite QPE assessment or error model is confined to the time and space domain over which it is performed. It tends to be specific to the satellite instrument (for example, resolution), the retrieval algorithm, the space-time-scale and the accuracy of the reference, and has limited applicability for other precipitation regimes, regions, products, etc. The actual benefit of these analyses to satellite precipitation users and

developers is limited. There is a need to formulate the goals of validation and error modeling, and to design appropriate comparison practices.

Integrated assessment of the intrinsic uncertainty across multiple sensors and products is necessary to track the origin of errors and their propagation through various Level-2 active to passive MW to Level-3 merged satellite precipitation estimates. Targeting the most significant factors driving the state of the satellite estimation error (for example, precipitation types) is essential to characterize uncertainties in satellite QPE and lead to a generalization of their assessment (Kirstetter et al., 2020; Shige et al., 2013; Taniguchi et al., 2013; Yamamoto et al., 2017). Figure 1.2.2 illustrates the propagation of uncertainty that arises from precipitation types in the form of systematic biases from spaceborne radars (for example, GPM DPR) through MW precipitation estimates (GPROF-GMI) to the IMERG Level-3 merged product.

1.2.4. Impact of satellite precipitation intrinsic uncertainty on hydrologic applications

Hydrologic applications of satellite data include agriculture, freshwater availability and natural disasters monitoring (for example, floods, droughts, landslides; Serrat-Capdevila et al., 2014). Each application is characterized by specific spatial and temporal requirements that can vary significantly. For example, global hydrological modeling to assess the occurrence of flood events is uniquely enabled with the coverage provided by Level-3 precipitation products (such as the Global Flood Monitoring System, http://flood.umd.edu/; Wu et al., 2014). Anticipating flood events enables the assessment of associated risks and optimized decision making, specifically in developing countries (Kirschbaum et al., 2017). The detection of floods and inundations is critical for hazard response by agencies such as the United Nations World Food Program and the International Federation of Red Cross and Red Crescent Societies (Gray, 2015). On the other side of the precipitation spectrum, precipitation deficits are monitored with satellites as drivers of drought and food and water security (for example, the Famine Early Warning Systems Network, FEWS NET; www.fews.net). Water resources applications are reservoir operations that use precipitation products at monthly time scales (for example, Yang et al., 2017). However, applications of Level-3 products have not been demonstrated yet in contexts involving hydrologic processes over short scales (for example, a few kilometres, hourly), such as flash-flood monitoring, because the Level-3 resolution or latency are limiting factors.

Hydrologic applications often require an understanding of the error structure in the satellite precipitation products. Errors in hydrologic simulations result from a complex interaction between the forcing uncertainty (that is, precipitation), the model structure and approximations, the estimation of model parameters, and observations (for example, gauged streamflow). Hence precipitation errors and uncertainty sources have the potential to affect hydrologic applications (Maggioni and Massari, 2018). For example, simulations using Level-3 products for predicting streamflow and runoff are greatly impacted by their performance in terms of precipitation detection and quantification. Common issues involve systematic bias in the precipitation estimates, since hydrologic simulation highly depends on basin-scale water budget assumptions that directly impact the streamflow simulation (for example, Thiemig et al., 2012). Systematic biases arising at the satellite Level-2 and propagating to the Level-3 products are conditioned on a number of factors, some of which are independent of surface hydrology, such as precipitation physics, climatologies, sensors and algorithms (see Figure 1.2.1).
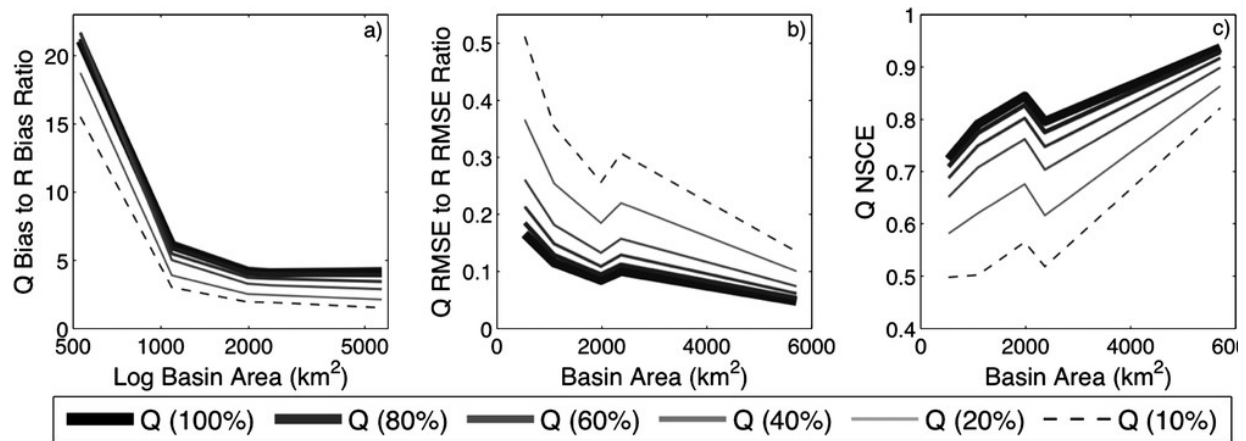
Figure 1.2.3. An example of propagation of resolution-induced rainfall error to streamflow simulations, using a distributed hydrologic model on the Tarboro watershed (North Carolina, U.S.) over the period 2002–2009. Metrics of hydrologic model performance as functions of basin area and streamflow threshold are presented: (a) ratio of streamflow (Q) relative bias to rainfall (R) relative bias, (b) ratio of streamflow (Q) relative RMSE to rainfall (R) relative RMSE and (c) Nash–Sutcliffe coefficient of efficiency (NSCE) of streamflow simulations. The values between parentheses indicate the probability of occurrence of the corresponding threshold. From Vergara et al., 2014

One strategy dealing with the uncertainty is to mitigate it by (1) debiasing for reconciliation with higher-resolution hydrologic models, (2) averaging/filtering/smoothing to obtain coarser-resolution products (typically 1-day 1-degree; see Chapter 2). Applications running at the monthly or seasonal time scales are less affected by biases because Level-3 satellite products increasingly benefit from gauge-based adjustments at coarser scales. However, many applications require spatial resolutions finer than 25 km and temporal resolutions less than 3 hours (Kirschbaum et al., 2017). In many cases, the uncertainty is transferred into the applications. Bias correction techniques can reduce streamflow errors (for example, Serrat-Capdevila et al., 2014); for example, by applying climate-scale bias corrections (for example, Beck et al., 2017). However, the multi-factor and nonstationary nature of satellite-based precipitation biases (that are not well understood yet; see Chapter 1.1) hinders the effectiveness of correction techniques. Another option is to compensate the forcing biases with hydrologic model calibration (for example, Xue et al., 2013; Nikolopoulos et al., 2013). It is made possible because the observed hydrologic response (discharge at the basin outlet) results from unobserved and integrated contributions of surface and subsurface processes. This endemic lack of observational hydrologic constraints leaves a considerable range of options to adjust hydrologic model parameters to reproduce the observed behavior (Beven, 2001), sometimes at the expense of physical realism. Model recalibration has been applied across watersheds with various geomorphologies and climatologies around the world to cope with satellite precipitation biases and improve streamflow prediction. This transfer of uncertainties from the satellite precipitation estimates to modeled hydrologic processes estimates hinders the broad application of hydrologic modeling, especially at sub-basin scales.

Uncertainty also arise due to the resolution of current satellite-based rainfall products and impacts applications of hydrologic modeling and forecasting systems. Resolution modifies the spatial structure of rainfall fields, and its interplay with basin area conditions the propagation of biases in distributed hydrologic models (for example, Vergara et al., 2014; Figure 1.2.3). The effects of precipitation resolution can be accounted for during the calibration of hydrologic models. The systematic analysis of the complex and combined effects arising from satellite uncertainties and resolution, basin geomorphologic characteristics and hydrologic modeling approaches remains a great challenge for the hydrologic application of satellite precipitation estimates. For more reliable flood simulations, additional physical constraints can be brought by observations, such as using soil moisture as a fingerprint of past rain occurrence (for example, Crow et al., 2011; Ciabatta et al., 2015).
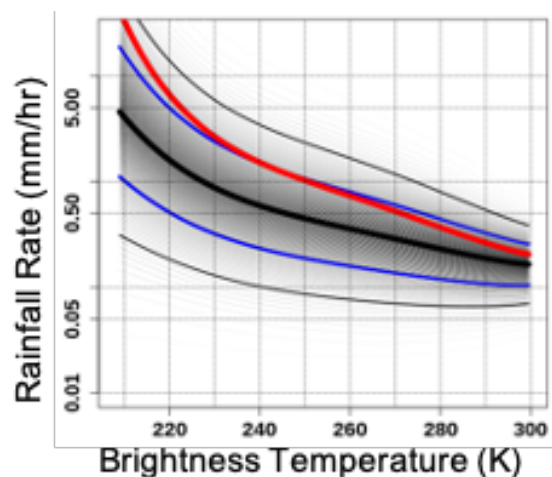
Figure 1.2.4. Precipitation rate distributions conditioned on the IR brightness temperature. The thick black line represents the median (50% quantile), the blue curves represent the 25 and 75% quantiles, the thin black lines represent the 10 and 90% quantiles. The red curve represents the expected value. The intrinsic bias in Figure 1.1.12 is mitigated by the probabilistic approach, while the intrinsic uncertainty is represented by the spread of the conditional precipitation rate distribution (adapted from Kirstetter et al., 2018a).

Another strategy dealing with satellite-based precipitation is to explicitly integrate uncertainty into the precipitation estimation process (see Chapter 3.1). Most precipitation products are deterministic and represent a single "best guess" realization of precipitation but are blind to their intrinsic uncertainty. Recent probabilistic precipitation estimates are developed to explicitly represent uncertainty (Kirstetter et al., 2015, 2018a; Wright et al., 2017), as shown in Figure 1.2.4.

1.2.5. Summary on intrinsic uncertainty and implications for hydrologic applications

Understanding hydrometeorological processes and applications requires more than just one deterministic "best estimate" to adequately cope with the intermittent, highly-skewed distribution that characterizes precipitation. The intrinsic uncertainty structure of satellite-based quantitative precipitation estimates is still largely unknown at the spatiotemporal scales near the sensor measurement scale. Advancing the use of uncertainty as an integral part of QPE in the relationship between sensor measurements and the corresponding "true" precipitation has the potential to provide a framework for diagnosing intrinsic uncertainty when instruments sample raining scenes or processes challenging QPE algorithms' assumptions. It provides the basis for multisensor merging and precipitation assimilation, hydrometeorological hazard mitigation, decision making and hydrological modeling. Hydrologic applications are not generally

configured to directly ingest probabilistic estimates of precipitation, but current research explores this avenue (for example, Hartke et al., 2020).

Numerous validation studies have been performed on satellite precipitation products. Chapter 1.3 summarizes what has been done to date by the IPWG validation subgroup. Limited progress has been made on quantifying the intrinsic uncertainty and its impact on hydrologic applications. This is because few studies are carried out at the primary precipitation retrieval scale. This endeavor requires the expert use of other precipitation sensors such as radar-gauge combinations.

1.2.6. Recommendations

Recommendation 1.2.1: Encourage more satellite precipitation comparisons at the actual satellite retrieval scale to study the intrinsic uncertainty.

The homogeneity of satellite precipitation is often overlooked in the evaluations while it remains an endemic challenge in the generation of such products and their applications. The dynamic interplay between precipitation characteristics, sensors and satellite algorithms is critical to study in order to make progress. There is a need to formulate the goals of validation and error modeling and to design appropriate comparison practices.

Recommendation 1.2.2: The non-homogeneity of satellite estimates at the retrieval scale needs more attention in order to improve products and their applications.

Currently hydrological applications are greatly impacted by the satellite precipitation intrinsic uncertainty. A better understanding of this uncertainty is critical to make progress and mitigate precipitation forcing errors and to avoid error propagation in other modeling components of the water cycle. Explicitly accounting for uncertainty in precipitation products is a promising way to explore coordination with hydrologic applications.

Recommendation 1.2.3: Further means to explicitly represent uncertainty in precipitation products and their hydrologic applications (beyond root mean squared additive error) should be explored.

1.2.7. References

Beck, H.E., A.I.J.M. van Dijk, V. Levizzani, J. Schellekens, D.G. Miralles, B. Martens and A. de Roo, 2017: MSWEP: 3-hourly 0.25° global gridded precipitation (1979–2015) by merging gauge, satellite, and reanalysis data. *Hydrology and Earth System Sciences*, 21, 589–615, https://doi.org/10.5194/hess-21-589-2017.

Berne, A., and W.F. Krajewski, 2013: Radar for hydrology: Unfulfilled promise or unrecognized potential? *Advances in Water Resources*, 51, 357–366, https://doi.org/10.1016/j.advwatres.2012.05.005.

Beven, K., 2001: How far can we go in distributed hydrological modelling? *Hydrology and Earth System Sciences*, 5, 1–12, https://doi.org/10.5194/hess-5-1-2001.

Ciabatta, L., L. Brocca, C. Massari, T. Moramarco, S. Puca, A. Rinollo, S. Gabellani and W. Wagner, 2015: Integration of Satellite Soil Moisture and Rainfall Observations over the Italian Territory. *Journal of Hydrometeorology*, 16, 1341–1355, https://doi.org/10.1175/JHM-D-14-0108.1.

Ciach, G.J., and W.F. Krajewski, 1999: On the estimation of radar rainfall error variance. *Advances in Water Resources*, 22, 585–95, https://doi.org/10.1016/S0309-1708(98)00043-8.

Crow, W.T., M.J. van den Berg, G.J. Huffman and T. Pellarin, 2011: Correcting rainfall using satellite-based surface soil moisture retrievals: The Soil Moisture Analysis Rainfall Tool (SMART). *Water Resources Research*, 47, W08521, doi:10.1029/2011WR010576.

Delahaye, F., P.-E. Kirstetter, V. Dubreuil, L.A.T. Machado, D.A. Vila and R. Clark III, 2015: A consistent gauge database for daily rainfall analysis over the legal Brazilian Amazon. *Journal of Hydrology*, 527, 292–304, https://doi.org/10.1016/j.jhydrol.2015.04.012.

Delrieu, G., B. Boudevillain, J. Nicol, B. Chapon, P.-E. Kirstetter, H. Andrieu and D. Faure, 2009: Bollène-2002 Experiment: Radar Quantitative Precipitation Estimation in the Cévennes–Vivarais Region, France. *Journal of Applied Meteorology and Climatology*, 48, 1422–1447, https://doi.org/10.1175/2008JAMC1987.1.

Delrieu, G., A. Wijbrans, B. Boudevillain, D. Faure, L. Bonnifait and P.-E. Kirstetter, 2014: Geostatistical radar-raingauge merging: A novel method for the quantification of the rain estimation accuracy. *Advances in Water Resources*, 71, 110–24, https://doi.org/10.1016/j.advwatres.2014.06.005.

Gebregiorgis, A., P.-E. Kirstetter, Y.E. Hong, N.J. Carr, J.J. Gourley, W. Petersen and Y. Zheng, 2017: Understanding multi-sensor satellite precipitation error structure in level-3 TRMM products. *Journal of Hydrometeorology*, 18, 285–306, https://doi.org/10.1175/JHM-D-15-0207.1.

Gray, E., 2015: Satellite-based flood monitoring central to relief agencies' disaster response. NASA, July, www.nasa.gov/feature/goddard/satellite-based-flood-monitoring-central-to-relief-agencies-disaster-response.

Habib, E., G.J. Ciach and W.F. Krajewski, 2004: A method for filtering out raingauge representativeness errors from the verification distributions of radar and raingauge rainfall. *Advances in Water Resources*, 27, 967–980, https://doi.org/10.1016/j.advwatres.2004.08.003.

Hartke, S.H., D.B. Wright, D.B. Kirschbaum, T.A. Stanley and Z. Li, 2020: Incorporation of Satellite Precipitation Uncertainty in a Landslide Hazard Nowcasting System. *Journal of Hydrometeorology*, 21, 1741–1759, https://doi.org/10.1175/JHM-D-19-0295.1.

Kirschbaum, D.B., G.J. Huffman, R.F. Adler, S. Braun, K. Garrett, E. Jones, A. McNally, G. Skofronick-Jackson, E. Stocker, H. Wu and B.F. Zaitchik, 2017: NASA's Remotely Sensed Precipitation: A Reservoir for Applications Users. *Bulletin of the American Meteorological Society*, 98, 1169–1184, https://doi.org/10.1175/BAMS-D-15-00296.1.

Kirstetter, P.E., Y. Hong, J.J. Gourley, Q. Cao, M. Schwaller and W. Petersen, 2014: Research framework to bridge from the global precipitation measurement mission core satellite to the constellation sensors using ground-radar-based national Mosaic QPE. In *Remote Sensing of the Terrestrial Water Cycle* (V. Lakshmi, D. Alsdorf, M. Anderson, S. Biancamaria, M. Cosh, J. Entin, G. Huffman, W. Kustas, P. van Oevelen, T. Painter, J. Parajka, M. Rodell and C. Rüdiger, eds.). Hoboken, New Jersey, Wiley, https://doi.org/10.1002/9781118872086.

Kirstetter, P.E., J.J. Gourley, Y. Hong, J. Zhang, S. Moazamigoodarzi, C. Langston and A. Arthur, 2015: Probabilistic precipitation rate estimates with ground-based radar networks. *Water Resources Research*, 51, 1422–1442, https://agupubs.onlinelibrary.wiley.com/doi/full/10.1002/2014WR015672.

Kirstetter, P.-E., N. Karbalaee, K. Hsu and Y. Hong, 2018a: Probabilistic precipitation rate estimates with space-based infrared sensors. *Quarterly Journal of the Royal Meteorological Society*, 144 (Suppl. 1): 191–205, https://doi.org/10.1002/qj.3243.

Kirstetter, P.-E., W. Petersen and J.J. Gourley, 2018b: GPM Ground Validation Multi-Radar/Multi-Sensor (MRMS) Precipitation Reanalysis for Satellite Validation Product. Dataset available online from the NASA Global Hydrology Resource Center DAAC, Huntsville, Alabama, U.S.A., DOI: http://dx.doi.org/10.5067/GPMGV/MRMS/DATA101.

Kirstetter, P.-E., W.A. Petersen, C.D. Kummerow and D.B. Wolff, 2020: Integrated multi-satellite evaluation for the Global Precipitation Measurement mission: Impact of precipitation types on spaceborne precipitation estimation. In: *Satellite Precipitation Measurement*, Chapter 31 (V. Levizzani, C. Kidd, D.B. Kirschbaum, C. Kummerow, K. Nakamura, F.J. Turk, eds.), Advances in Global Change Research, 69, Springer-Nature, Cham, 583–608, https://doi.org/10.1007/978-3-030-35798-6_7.

Lebel, T., G. Bastin, C. Obled and J.D. Creutin, 1987: On the accuracy of areal rainfall estimation: A case study. *Water Resources Research*, 23, 2123–2134, https://doi.org/10.1029/WR023i011p02123.

Maggioni, V., and C. Massari, 2018: On the performance of satellite precipitation products in riverine flood modeling: A review. *Journal of Hydrology*, 558, 214–224, https://doi.org/10.1016/j.jhydrol.2018.01.039.

Neuper, M., and U. Ehret, 2019: Quantitative precipitation estimation with weather radar using a data- and information-based approach. *Hydrology and Earth System Sciences*, 23, 3711–3733, https://doi.org/10.5194/hess-23-3711-2019.

Nikolopoulos, E.I., E.N. Anagnostou and M. Borga, 2013: Using High-Resolution Satellite Rainfall Products to Simulate a Major Flash Flood Event in Northern Italy. *Journal of Hydrometeorology*, 14, 171–185, https://doi.org/10.1175/JHM-D-12-09.1.

Petersen, W.A., P.-E. Kirstetter, J. Wang, D.B. Wolff and A. Tokay, 2020: The GPM Ground Validation Program. In: *Satellite Precipitation Measurement* (V. Levizzani, C. Kidd., D.B. Kirschbaum, C.D. Kummerow, K. Nakamura, F.J. Turk, eds.). Springer Nature, Cham, Advances in Global Change Research, 69, 471–502, https://doi.org/10.1007/978-3-030-35798-6_2.

Serrat-Capdevila, A., J.B. Valdes and E.Z. Stakhiv, 2014: Water Management Applications for Satellite Precipitation Products: Synthesis and Recommendations. *Journal of the American Water Resources Association*, 50(2): 509–525, DOI: 10.1111/jawr.12140.

Shige, S., S. Kida, H. Ashiwake, T. Kubota and K. Aonashi, 2013: Improvement of TMI rain retrievals in mountainous areas. *Journal of Applied Meteorology and Climatology*, 52, 242–254, https://doi.org/10.1175/JAMC-D-12-074.1.

Skofronick-Jackson, G., W.A. Petersen, W. Berg, C. Kidd, E.F. Stocker, D.B. Kirschbaum, R. Kakar, S.A. Braun, G.J. Huffman, T. Iguchi, P.E. Kirstetter, C. Kummerow, R. Meneghini, R. Oki, W.S. Olson, Y.N. Takayabu, K. Furukawa and Thomas Wilheit, 2017: The Global Precipitation Measurement (GPM) mission for science and society. *Bulletin of the American Meteorological Society*, 98, 1679–95, https://doi.org/10.1175/BAMS-D-15-00306.1.

Stephens, G.L., and C.D. Kummerow, 2007: The Remote Sensing of Clouds and Precipitation from Space: A Review. *Journal of the Atmospheric Sciences*, 64(11), 3742–3765, https://doi.org/10.1175/2006JAS2375.1.

Sun, Q., C. Miao, Q. Duan, H. Ashouri, S. Sorooshian and K. Hsu, 2017: A review of global precipitation data sets: data sources, estimation, and intercomparisons. *Reviews of Geophysics*, 56, 79–107, https://doi.org/10.1002/2017RG000574.

Tan, J., W.A. Petersen, P.-E. Kirstetter and Y. Tian, 2017: Performance of IMERG as a Function of Spatiotemporal Scale. *Journal of Hydrometeorology*, 18, 307–319, https://doi.org/10.1175/JHM-D-16-0174.1.

Taniguchi, A., S. Shige, M.K. Yamamoto, T. Mega, S. Kida, T. Kubota, M. Kachi, T. Ushio and K. Aonashi, 2013: Improvement of high-resolution satellite rainfall product for Typhoon Morakot (2009) over Taiwan. *Journal of Hydrometeorology*, 14, 1859–1871, https://doi.org/10.1175/JHM-D-13-047.1.

Thiemig, V., R. Rojas, M. Zambrano-Bigiarini, V. Levizzani and A. De Roo, 2012: Validation of Satellite-Based Precipitation Products over Sparsely Gauged African River Basins. *Journal of Hydrometeorology*, 13, 1760–1783, https://doi.org/10.1175/JHM-D-12-032.1.

Vergara, H., Y. Hong, J.J. Gourley, E.N. Anagnostou, V. Maggioni, D. Stampoulis and P.-E. Kirstetter, 2014: Effects of Resolution of Satellite-Based Rainfall Estimates on Hydrologic Modeling Skill at Different Scales. *Journal of Hydrometeorology*, 15, 593–613, https://doi.org/10.1175/JHM-D-12-0113.1.

Villarini, G., and W.F. Krajewski, 2010: Review of the different sources of uncertainty in single polarization radar-based estimates of rainfall. *Surveys in Geophysics*, 31, 107–19, https://doi.org/10.1007/s10712-009-9079-x.

Wright, D.B., D.B. Kirschbaum and S. Yatheendradas, 2017: Satellite Precipitation Characterization, Error Modeling, and Error Correction Using Censored Shifted Gamma Distributions. *Journal of Hydrometeorology*, 18, 2801–2815, https://doi.org/10.1175/JHM-D-17-0060.1.

Wu, H., R.F. Adler, Y. Tian, G.J. Huffman, H. Li and J. Wang, 2014: Real-time global flood estimation using satellite-based precipitation and a coupled land surface and routing model. *Water Resources Research*, 50, 2693–2717, doi: https://doi.org/10.1002/2013WR014710.

Xue, X., Y. Hong, A.S. Limaye, J.J. Gourley, G.J. Huffman, S.I. Khan, C. Dorji and S. Chen, 2013: Statistical and hydrological evaluation of TRMM-based Multi-satellite Precipitation Analysis over the Wangchu Basin of Bhutan: Are the latest satellite precipitation products 3B42V7 ready for use in ungauged basins? *Journal of Hydrology*, 499, 91–99, https://doi.org/10.1016/j.jhydrol.2013.06.042.

Yamamoto, M.K., S. Shige, C.-K. Yu and L.-W. Cheng, 2017: Further improvement of the heavy orographic rainfall retrievals in the GSMaP algorithm for microwave radiometers. *Journal of Applied Meteorology and Climatology*, 56, 2607–2619, https://doi.org/10.1175/JAMC-D-16-0332.1.

Yang, N., K. Zhang, Y. Hong, Q. Zhao, Q. Huang, Y. Xu, X. Xue and S. Chen, 2017: Evaluation of the TRMM multisatellite precipitation analysis and its applicability in supporting reservoir

operation and water resources management in Hanjiang basin, China. *Journal of Hydrology*, 549, https://doi.org/10.1016/j.jhydrol.2017.04.006.

Zawadzki, I., 1975: On radar-raingauge comparisons. *Journal of Applied Meteorology and Climatology*, 14, 1430–1436, https://doi.org/10.1175/1520-0450(1975)014<1430:ORRC>2.0.CO;2.

Zhang J., K. Howard, C. Langston, B. Kaney, Y. Qi , L. Tang, H. Grams, Y. Wang, S. Cocks, S. Martinaitis, A. Arthur, K. Cooper, J. Brogden and D. Kitzmiller, 2016: Multi-Radar Multi-Sensor (MRMS) quantitative precipitation estimation: initial operating capabilities. *Bulletin of the American Meteorological Society*, 97, 621–38, https://doi.org/10.1175/BAMS-D-14-00174.1.

1.3. Monitoring of satellite precipitation estimates through the IPWG validation studies

Chris Kidd[1] and Viviana Maggioni[2]

[1]Earth System Science Interdisciplinary Center, University of Maryland, College Park, USA and NASA/Goddard Space Flight Center, Greenbelt, USA

[2]Sid and Reva Dewberry Department of Civil, Environmental, and Infrastructure Engineering, George Mason University, Fairfax, VA, USA

1.3.1. Status

The International Precipitation Working Group (IPWG) builds upon the expertise of scientists to provide a focus for the precipitation community to develop and improve precipitation measurements and their utilization, to improve scientific understanding of precipitation, and to further develop international partnerships (Turk and Bauer, 2006; Kidd et al., 2010; Levizzani et al., 2018). A major activity of the IPWG is the verification, validation and intercomparison of precipitation products to enable product developers and users to continually monitor and assess the performance of the available products. This activity has developed an ongoing validation program, comparing surface reference datasets and satellite precipitation products to better inform product developers and the user community.

Several key precipitation intercomparison projects have been organized to assess satellite-based products against surface data. These have included regional and global assessments of the Global Precipitation Climatology Project (GPCP) Algorithm Intercomparison Programme (AIP) series (see Arkin and Xie, 1994; Barrett and Bellerby, 1992; Allam et al., 1993; Ebert, 1996; Ebert et al., 1996), and of the NASA WetNet Precipitation Intercomparison Projects (PIP) series (see Barrett et al., 1994; Smith et al., 1998; Adler et al., 2001). Since 2002, a number of validation sites have been organized by IPWG members, based primarily upon the availability of their regional surface reference datasets (see Kidd et al., 2020). Comparisons of the satellite/model precipitation products against surface data are typically analyzed at the 0.25°x0.25°, daily scale in near real time, although intercomparisons at the full, instantaneous resolution of the products have also be developed (see Kidd et al., 2018.)

The validation work of the IPWG should be seen as complementary to the targeted ground validation (GV) campaigns of mission-specific programs (Skofronick-Jackson et al., 2015; Petersen et al., 2016; Petersen et al., 2020). Key differences relate to the end goal of the validation: the IPWG validation aims to improve satellite precipitation products, focusing upon statistical analysis over regions with existing reference data at moderate temporal/spatial resolutions. Mission-specific validation tends to relate more to the microphysical scale, aimed at improving our fundamental understanding of precipitation-observation capabilities using a multi-tier (satellite, airborne, surface) approach at fine, instantaneous resolutions.

Figure 1.3.1 shows the global distribution of the IPWG validation regions together with the source of their validation data. Note that these are largely operated on a best-effort basis with only a few regions receiving funding, and consequently not all regions operate continuously (also due to cyber-security issues). The development of a validation region over the Indian subcontinent through collaboration with the Indian Meteorological Department is ongoing.
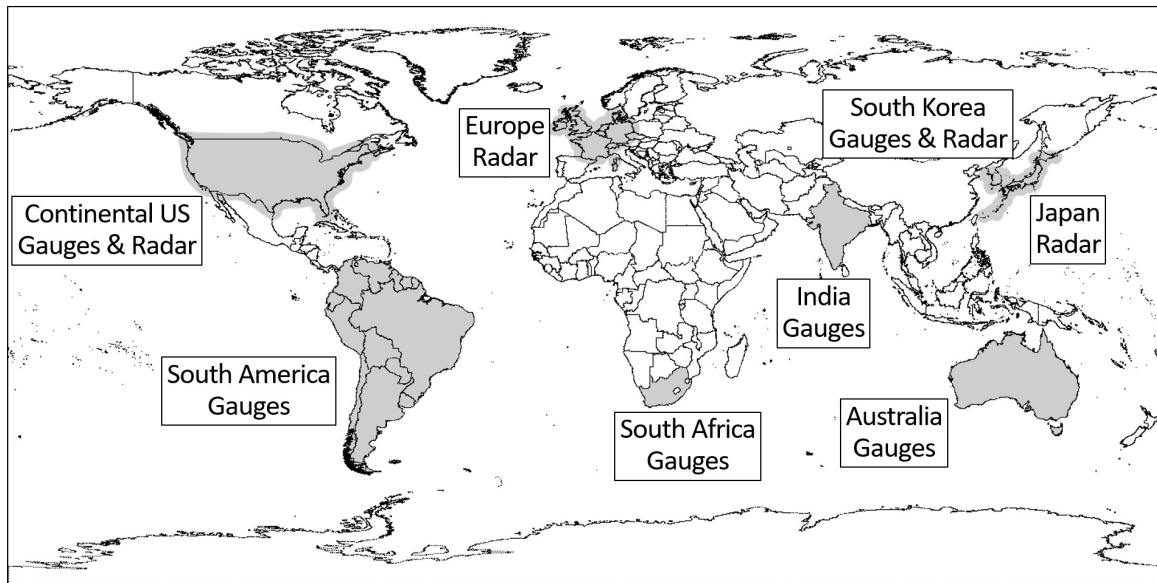
Figure 1.3.1. Distribution of past and current IPWG validation regions and their surface reference datasets.

The surface reference data for the IPWG sites encompasses surface radar and/or gauge datasets. Radar data are in many ways most useful since they provide frequent, regular spatial measures of instantaneous precipitation, which can be easily matched to the satellite data. Aggregating these data into daily totals to match the satellite/model precipitation products is relatively easy. However, care is needed to address artefacts in such data (for example, missing low-level precipitation beam blockage, anomalous propagation errors, etc). Gauge data, at least for these studies, are usually already gridded and reported at (local time) daily scales: as such, the gauge data may not be co-temporal with the satellite products, which usually accumulate midnight–midnight UTC. Some regional variations between the sites is therefore inevitable to ensure that the most is made of the available surface datasets.

Each of the IPWG sites is hosted by local institutions, although all provide similar information on the assessment of the precipitation products and surface data at a common scale (see http://www.isac.cnr.it/~ipwg/calval.html). These assessments follow a strategy of keeping any analysis clear and simple to ensure that they are understandable and pertinent to the user community. An example of a daily validation display for South Korea is shown in Figure 1.3.2. The information contained generally includes images of co-registered satellite/model and surface products for visual analysis and placing the statistics with the context of particular meteorological events. Satellite/model–surface scatterplots, cumulative distribution plots and bar plots provide further visual information on the product performance. Statistical information is provided through categorical statistics of probability of detection (POD), false alarm ratio (FAR) and Heidke Skill Scores (HSS), descriptive statistics for both the estimates and observed precipitation, and statistical scores, that is, bias, ratio (product/validation), RMSE, correlation coefficient and number of samples. Together, this information can be used by both the algorithm/product developer and the user to assess the performance of different algorithms, over different regions, for different meteorological situations.

IMERG (Early) Estimates for 2020.09.15   KMA Radar Analysis for 2020.09.15   Diff. (IMERG vs. KMA Radar) 2020.09.15

No data   < 1   1-2   2-5   5-10   10-20   20-50   50-100   100-200   200 <   (mm/day)   -100 -80 -60 -40 -20 0 20 40 60 80 100

IMERG (Early) vs. KMA Radar

Daily Fraction by Occurrence

Est.

Obs.

0 20 40 60 80 100
Areal Fraction (%)

Daily Fraction of Total Rain

Est.

Obs.

Rainfall Accumulation by Amount

Verification Statistics for 20200915 (N = 6919, Verif. Grid = 0.10°, Units = mm/day)

		IMERG (Early) < 1	IMERG (Early) ≥ 1		KMA Radar	IMERG (Early)
KMA Radar < 1	Correct Rejection	1374	False Alarm 861	Grid Points Raining	4684	4728
				Average Rain	5.84892	6.95664
				Conditional Rain	8.63976	10.18042
				Rain Volume (mm*km²x10⁷)	3.95577	4.70496
KMA Radar ≥ 1	Miss	817	Hits 3867	Maximum Rain	55.70	120.60

Mean Abs. error = 4.90224   RMS error = 9.93258
Correlation Coeff. = 0.56011   Frequency Bias = 1.00939
Probability of Detection = 0.82558   False Alarm Ratio = 0.18211
Hanssen & Kuipers Score = 0.44034   Equitable Threat Score = 0.28421

Figure 1.3.2. Example of IPWG validation over South Korea for the IMERG product versus the Korea Meteorological Administration radar analysis on 15 September 2020.

In addition to the near real time "monitoring" assessments, more detailed studies have been done to evaluate the precipitation products over a longer record and with a greater degree of accuracy. For example, the IPWG validation site over Japan, started in 2003, uses radar data from the Automated Meteorological Data Acquisition System (AMeDAS) network (Makihara et al., 1996; Makihara, 2007). Studies have included the assessment of precipitation products (Kubota et al., 2009) together with the evaluation of their Global Satellite Mapping of Precipitation (GSMaP) product over mountainous regions (Shige et al., 2013, 2014; Taniguchi et al., 2013; Yamamoto and Shige 2015; Yamamoto et al., 2017). They note, however, that validation of heavy, but shallow snowfall (see Murakami et al., 1994) is beyond the scope of this study (and many others). Studies over South America using daily rain gauge data have shown varying biases in satellite estimates on seasonal scales (see Kidd et al., 2020). Other IPWG-related studies have investigated smaller temporal/spatial scale comparisons, such as Kidd et al. (2012) together with the representation of the diurnal cycle at the global scale (Kidd et al., 2013). Maggioni et al. (2016) reviewed satellite precipitation validation efforts during the TRMM era, identifying mountains and semiarid areas as problematic geographic regions, seasonal problems associated with winter, and problems associated with light rainfall, snowfall and mixed-phase precipitation.

1.3.2. Recommendations

Key areas that have been identified for further development within the IPWG validation program are:

i. inclusion errors and uncertainties in the validation process,
ii. validation of snowfall,
iii. validation of precipitation, where possible, over open-ocean regions, and
iv. large scale validation against existing precipitation climatologies [such as from the Global Precipitation Climatology Centre (GPCC)].

Crucial to the validation activities of the IPWG is the need for practical funding since most of this work continues unfunded at present.

1.3.3. References

Adler, R.F., C. Kidd, G. Petty, M. Morissey and H.M. Goodman, 2001: Intercomparison of global precipitation products: The third Precipitation Intercomparison Project (PIP-3). *Bulletin of the American Meteorological Society*, 82, 1377–1396, doi:10.1175/1520-0477(2001)082<1377:IOGPPT>2.3.CO;2.

Allam, R.E., G. Holpin, P. Jackson and G.-L. Liberti, 1993: Second Algorithm Intercomparison Project (AIP-2), U.K. and Northwest Europe, February–April 1991, Pre-Workshop Report. 439pp [available from Satellite Image Applications Group, U.K. Meteorological Office, Bracknell, Berkshire, RG12 2SZ, United Kingdom.]

Arkin, P., and P. Xie, 1994: The Global Precipitation Climatology Project: First Algorithm Intercomparison Project. *Bulletin of the American Meteorological Society*, 75, 401–419.

Barrett, E.C., and T.J. Bellerby, 1992: The application of satellite infrared and passive microwave rainfall estimation techniques to Japan – results from the 1st GPCP Algorithm Intercomparison Project. *Meteorological Magazine,* 121, 34–46.

Barrett, E.C., J. Dodge, M. Goodman, J. Janowiak, C. Kidd and E.A. Smith, 1994: The First WetNet Precipitation Intercomparison Project. *Remote Sensing Reviews*, 11, 49–60.

Ebert, E.E., 1996: *Results of the 3rd Algorithm Intercomparison Project (AIP-3) of the Global Precipitation Climatology Project (GPCP)*. Revision 1. Melbourne, Bureau of Meteorology Research Centre.

Ebert, E.E., M.J. Manton, P.A. Arkin, R.J. Allam, G.E. Holpin and A. Gruber, 1996: Results from the GPCP Algorithm Intercomparison Programme. *Bulletin of the American Meteorological Society*, 77, 2875–2887.

Kidd, C., R.R. Ferraro and V. Levizzani, 2010: The Fourth International Precipitation Working Group. *Bulletin of the American Meteorological Society*, 8, 1095–1099, DOI: 10.1175/2009BAMS2871.1.

Kidd, C., P. Bauer, F.J. Turk, G.J. Huffman, R, Joyce, K.-L. Hsu and D. Braithwaite, 2012: Inter-comparison of high-resolution precipitation products over Northwest Europe. *Journal of Hydrometeorology*, 13, 67–83, DOI:10.1175/JHM-D-11-042.

Kidd, C., E. Dawkins and G. Huffman, 2013: Comparison of Precipitation Derived from the ECMWF Operational Forecast Model and Satellite Precipitation Datasets. *Journal of Hydrometeorology*, 14, 1463–1482.

Kidd, C., J. Tan, P.-E. Kirstetter and W.A. Petersen, 2018: Validation of the Version 05 Level 2 precipitation products from the GPM Core Observatory and constellation satellite sensors. *Quarterly Journal of the Royal Meteorological Society*, DOI:10.1002/qj.3175.

Kidd, C., S. Shige, D. Vila, E. Tarnavsky, M.K. Yamamoto, V. Maggioni and B. Maseko, 2020: The IPWG satellite precipitation validation effort. In: *Satellite Precipitation Measurement* (V. Levizzani, C. Kidd., D.B. Kirschbaum, C.D. Kummerow, K. Nakamura, F.J. Turk, eds.).

Springer Nature, Cham, Advances in Global Change Research, 69, 453–470, https://doi.org/10.1007/978-3-030-35798-6_1.

Kubota, T., T. Ushio, S. Shige, S. Kida, M. Kachi and K. Okamoto, 2009: Verification of high resolution satellite-based rainfall estimates around Japan using gauge-calibrated ground radar dataset. *Journal of the Meteorological Society of Japan*, 87A, 203–222.

Levizzani, V., C. Kidd, K. Aonashi, R. Bennartz, R.R. Ferraro, G.J. Huffman, R. Roca, F.J. Turk and N.-Y. Wang, 2018: The activities of the International Precipitation Working Group. *Quarterly Journal of the Royal Meteorological Society*, doi:10.1002/qj.3214.

Makihara, Y., 2007: Steps towards decreasing heavy rain disasters by short-range precipitation and land-slide forecast using weather radar accompanied by improvement of meteorological operational activities (in Japanese). *Tenki,* 54, 21–33.

Makihara, Y., N. Uekiyo, A. Tabat, and Y. Abe, 1996: Accuracy of Radar-AMeDAS precipitation. *IEICE Transactions on Communications*, 79, 751–762.

Maggioni, V., P.C. Meyers and M.D. Robinson, 2016: A review of merged high-resolution satellite precipitation product accuracy during the Tropical Rainfall Measuring Mission (TRMM) era. *Journal of Hydrometeorology*, 17, 1101–1117.

Murakami, M., T. Matsuo, H. Mizuno and Y. Yamada 1994: Mesoscale and microscale structures of snow clouds over the Sea of Japan Part I: Evolution of microphysical structures in short-lived convective snow clouds. *Journal of the Meteorological Society of Japan*, 72, 671–694.

Petersen, W.A., R.A. Houze, L. McMurdie, J. Zagrodnik, S. Tanelli, J. Lundquist and J. Wurmann, 2016: The Olympic Mountains Experiment (OLMPEX): From ocean to summit. *Meteorological Technology International*, 22–26.

Petersen, W.A., P.-E. Kirstetter, J. Wang, D.B. Wolff and A. Tokay, 2020: The GPM Ground Validation Program. In: *Satellite Precipitation Measurement* (V. Levizzani, C. Kidd, D. Kirschbaum, C. Kummerow, K. Nakamura, F. Turk, eds.). Advances in Global Change Research, vol 69., 471–501, Springer, Cham, https://doi.org/10.1007/978-3-030-35798-6_2.

Shige, S., S. Kida, H. Ashiwake, T. Kubota and K. Aonashi, 2013: Improvement of TMI rain retrievals in mountainous areas. *Journal of Applied Meteorology and Climatology*, 52, 242–254.

Shige, S., M.K. Yamamoto and A. Taniguchi, 2014: Improvement of TMI rain retrieval over the Indian subcontinent. In *Remote Sensing of the Terrestrial Water Cycle* (V. Lakshmi, D. Alsdorf, M. Anderson, S. Biancamaria, M. Cosh, J. Entin, G. Huffman, W. Kustas, P. van Oevelen, T. Painter, J. Parajka, M. Rodell and C. Rüdiger, eds.). Hoboken, New Jersey, Wiley, https://doi.org/10.1002/9781118872086.ch2.

Skofronick-Jackson, G., D. Hudak, W. Petersen, S.W. Nesbitt, V. Chandrasekar, S. Durden, K. J. Gleicher, G.-J. Huang, P. Joe, P. Kollias, K.A. Reed, M.R. Schwaller, R. Stewart, S. Tanelli, A. Tokay, J.R. Wang and M. Wolde, 2015: Global Precipitation Measurement Cold Season Precipitation Experiment (GCPEx): For measurement's sake, let it snow. *Bulletin of the American Meteorological Society*, 96, 1719–1741, DOI:10.1175/BAMS-D-13-00262.1.

Smith, E.A., J.E. Lamm, R. Adler, J. Alishouse, K. Aonashi, E. Barrett, P. Bauer, W. Berg, A. Chang, R. Ferraro, J. Ferriday, S. Goodman, N. Grody, C. Kidd, D. Kniveton, C. Kummerow, G. Liu, F. Marzano, A. Mugnai, W. Olson, G. Petty, A. Shibata, R. Spencer, F. Wentz, T. Wilheit

and E. Zipser, 1998: Results of WetNet PIP-2 project. *Journal of the Atmospheric Sciences*, 55, 1483–1536, DOI: 10.1175/1520-0469(1998)055<1483:ROWPP>2.0.CO;2.

Taniguchi, A., S. Shige, M.K. Yamamoto, T. Mega, S. Kida, T. Kubota, M. Kachi, T. Ushio and K. Aonashi, 2013: Improvement of high-resolution satellite rainfall product for Typhoon Morakot (2009) over Taiwan. *Journal of Hydrometeorology*, 14, 1859–1871, https://doi.org/10.1175/JHM-D-13-047.1.

Turk, J., and P. Bauer, 2006: The International Precipitation Working Group and Its Role in the Improvement of Quantitative Precipitation Measurements. *Bulletin of the American Meteorological Society*, 87, 643–647, DOI: 10.1175/BAMS-87-5-643.

Yamamoto, M.K. and S. Shige, 2015: Implementation of an orographic/nonorographic rainfall classification scheme in the GSMaP algorithm for microwave radiometers. *Atmospheric Research*, 163, 36–47.

Yamamoto, M.K., S. Shige, C.-K. Yu and L.-W. Cheng, 2017: Further improvement of the heavy orographic rainfall retrievals in the GSMaP algorithm for microwave radiometers. *Journal of Applied Meteorology and Climatology*, 56, 2607–2619.

2. Climate Applications

2.1 Energy and water closure

Rémy Roca[1], Seiji Kato[2] and Tristan L'Ecuyer[3]

[1]Laboratoire d'Études en Géophysique et Océanographie Spatiales (Université de Toulouse III, CNRS, CNES, IRD), Toulouse, France

[2]NASA Langley Research Center, Hampton, Virginia

[3]University of Wisconsin–Madison, Madison, Wisconsin

2.1.1 Introduction

The water cycle of the Earth distributes water mass through the various water storage reservoirs of the planet. The water cycle is tightly related to the energy cycle of the Earth through diabatic heating in the atmosphere when water changes its phase (Stephens et al., 2012). The energy cycle of the Earth is represented by the flux of solar and terrestrial radiation, turbulent fluxes and moist static energy divergence within the Earth climate system. One notorious example of the coupling between the water and energy cycle in the climate system is manifested in the water vapor feedback process (Ramanathan, 1981). When radiative forcing is imposed by increasing the concentration of CO_2 in the atmosphere, the direct radiative effect is to warm the surface and the lower troposphere and cool the stratosphere. As surface temperature increases, evaporation also increases, allowing further increase in water vapor concentration in the warmer atmosphere. The increase of water vapor concentration is roughly 7% for each 1 K increase in temperature, following the Clausius-Clapeyron equation (Held and Soden, 2006). Water vapor itself is a strong greenhouse gas. It reinforces the initial warming, which induces a positive feedback on the climate system. Increased evaporation from the surface and a larger water vapor concentration in the atmosphere also imply an enhanced precipitation rate that also contributes to the warming of the atmosphere. More precisely, the increase in global precipitation rate in response to global warming is driven by the atmospheric radiative cooling rate, and is currently estimated to be around 2–3% for each 1 K increase in temperature (Stephens and Ellis, 2008). The slower increase in the precipitation rate than the increase in water vapor concentration is clear evidence of a tight relationship between the energy and water cycles. This coupling is an important aspect that has profound ramifications up to the climate sensitivity estimate because it is strongly related to hydrological sensitivity (Mauritsen and Stevens, 2015; Watanabe et al., 2018).

This prompted earlier investigators to explore the consistency among water and energy cycle elements and assess the closure of the water-energy budget observational capabilities. Budget assessments from observations of the water cycle only (Sheffield et al., 2009) or of both water and energy cycles (Stephens et al., 2012) further identified some significant deficits of closure in the observational portfolio. These studies lead to the conclusion that there is a need to adjust some fluxes to tend towards closure (Meyssignac et al., 2019). Significant progress in Earth observations of the water cycle prompt further assessment of the state of the art in our observational capabilities (Stephens et al., 2020).

Recently, optimal techniques that perform the adjustments objectively have been brought forward (L'Ecuyer et al., 2015; Rodell et al., 2015). These optimization techniques rely on enforcing global conservation laws playing with the uncertainty information that comes along with the data products. Modifications to the original datasets when closure is enforced are performed assuming changes lay within the stated uncertainty of each data product. This

approach allows the assessment of whether the various fluxes are consistent (or not) among each other. In this approach, the closure of the water and energy cycles is enforced objectively and the consistency of the different fluxes is assessed. The paradigm of assessing the closure is shifted to the new paradigm: "enforcing the closure to assess consistency".

We assess here both aspects; that is, how global and regional precipitation observations are closing budgets, and when closure is enforced, how consistent the precipitation estimates are. It is interesting to note that water and energy closure studies are a good complement to more classic evaluations of the gridded products using ground reference observations, particularly in data-scarce regions.

2.1.2. Water-only budget

At continental scales, the terrestrial water balance equation links precipitation (P) with river runoff (R), evapotranspiration (E) and water storage (S) as

P-E-R=dS/dt

Closure estimates rely to some extent on precipitation, but also on the other terms and their consistency, providing an integrated way to assess the performance of the precipitation. Note that bias in P and E can compensate easily in the water closure. The usually less-accurate evapotranspiration and runoff products may also not provide a strong constraint on precipitation.

2.1.2.1. Global land and globally-distributed basins studies

Munier and Aires (2018) explore the water budget closure framework over global land areas and perform optimization for 1°x1°grid boxes at a monthly scale. They use four satellite precipitation products (3B42v7, GPCP v2.2, CMORPH v1 uncorrected and PERSIANN-CDR v1).

The optimization using the closure only improves the original product's scores for 60% of the stations (Figure 2.1.1). There, the improvements in RMS remains moderate, around 19%. This suggests that the original multi-product average is already close to reference ground-based observations and that other elements of the budget can only slightly improve the situation overall in this framework. Most of the evaluation is performed over the U.S. and Europe, which prevents drawing conclusions over the tropical regions.
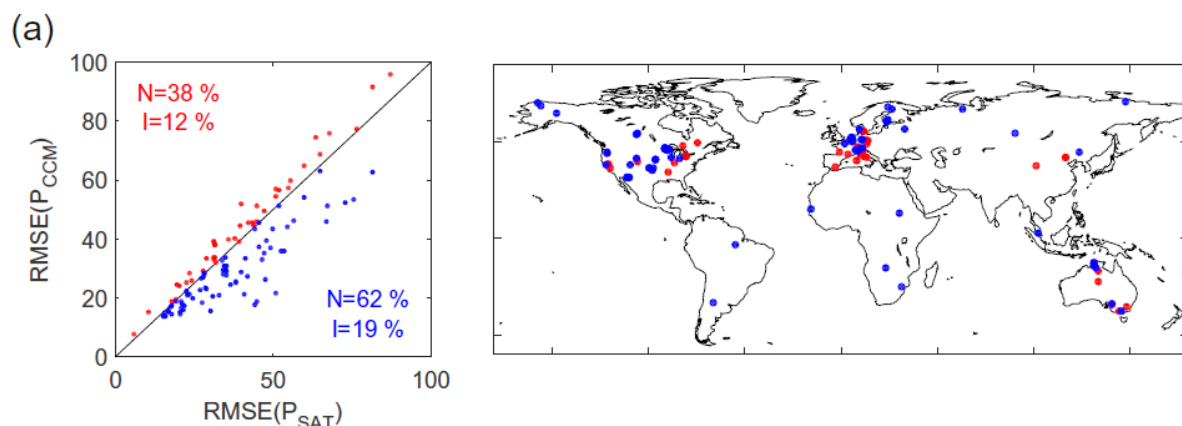

Figure 2.1.1. Comparison of corrected precipitation using CCM+CIC with FLUXNET observations. Left: scatter plot of RMSE of original satellite datasets and CCM corrected dataset (N is the percentage of stations where CCM improves P, I is the average relative improvement). Right: location of stations where the CCM improves (blue) or degrades (red) P. Adapted from Munier and Aires, 2018

Focusing on 96 globally-distributed catchments of various size and under various climates, Lorenz et al. (2014) explore the water closure of different datasets, including for ground-based precipitation products [GPCC data, National Weather Service Climate Prediction Center retrospective analysis (CPC), The University of East Anglia's Climatic Research Unit's global climate dataset (CRU) and data from Willmott, Matsuura and collaborators at the University of Delaware (UDEL)] and one satellite product (GPCP). Water budget closure is reasonably achieved only in a few cases with a given combination of datasets. In most catchments, the major characteristic is a significant imbalance. Precipitation strongly influences the budget in the tropics; the GPCC and GPCP products show best scores. In the Arctic, GPCP provides the best results, probably owing to the undercatch correction. The study emphasizes that performance over an individual catchment does not hold for the other regions.

2.1.2.2. Regional land studies

While a systematic exploration of all the ongoing regional studies about precipitation and closure is out of the scope of the present chapter, we have selected a few references that convey the main messages.

2.1.2.2.1.   *High Mountain Asia*

Yoon et al. (2019) explore the regional water closure using a water balance model and ten gridded precipitation datasets over 17 years. It includes in situ, reanalysis and satellite-based products. The products that incorporate rain gauges are shown to reach higher accuracy in the surface balance estimates. Satellite products exhibit systematic underestimation and low correlations over the Tibetan Plateau and high elevation areas. The spread in the precipitation estimates at the regional scale is significantly large than those from global studies. Generally, the in situ-based products outperform the other datasets.

2.1.2.2.2.   *Mediterranean Area*

Pellet et al. (2019) estimate the closure of the water budget over Mediterranean catchments using a few observational precipitation products (the same as Munier and Aires, 2018) and various other fluxes estimates. The optimization method brings only a marginal improvement on the original multi product simple average with a 10–15% improvement on the RMS and no change on the correlation with the ENSEMBLES Observation EOBS reference dataset. This is indicative of the relative proper accuracy of the gauge corrected satellite products over this area at this scale.

2.1.2.2.3.   *Mississippi Basin*

Munier et al. (2014) focus on this well-gauged basin to assess their methodology at the regional scale. The study is limited to a few sets of precipitation products [3B43 V7 CMORPH, V1.0, the NRL blended technique, and the Global Precipitation Climatology Project (GPCP, V2.2)]. It reveals a strong discrepancy between NRL and CMORPH and the gauge adjusted products. Yet enforcing the water budget closure at the catchment scale permits optimization of the products reaching very high R2 scores (>0.85) for each of the 4 products at the monthly scales. The corrected product seems to be fit for future hydrological analysis.

2.1.3. Regional atmospheric budget over ocean

The vertically-integrated atmospheric water budget links precipitation (P), evaporation (E) and the convergence of water vapor in the atmosphere (∇Q) after neglecting the storage term

$E-P=\nabla Q$

∇Q is nominally obtained from atmospheric reanalysis and as with the previous hydrologic budget equation, it allows the assessment of the consistency of the precipitation products with the other data sources, but compensating errors will not be revealed.

Brown and Kummerow (2014) perform such budget calculations over various tropical oceanic basins using the precipitation from GPCP. Figure 2.1.2 indicates a remarkably good ability to close the budget at these scales over this 10-year period.
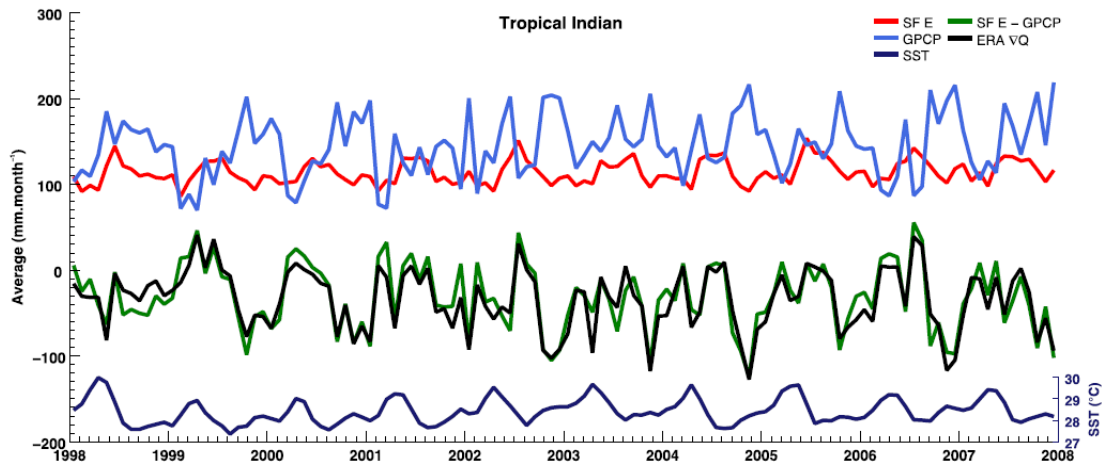
Figure 2.1.2. Monthly average time series of SeaFlux evaporation (SF E) and GPCP precipitation over the Tropical Indian Ocean region. Observation-based freshwater flux (E-P), European Centre for Medium-Range Weather Forecasts Re-Analysis dataset (ERA-Interim) atmospheric moisture divergence (∇Q) and sea surface temperature (SST) are also shown.

The accuracy of the GPCP estimate hence revealed is of similar magnitude over the other basin with some slight changes in the Pacific Ocean along the time yet to be fully understood. Since a number of satellite products eventually adjust onto GPCP monthly over the ocean (CMORPH, PERSIANN-CDR), this good behavior is likely to hold for these products as well. The E-P ocean freshwater budget is linked to the salinity of the ocean. Recent measurements of surface salinity could contribute to further constrain E-P estimates over the world's oceans. The relationship between E-P and salinity is governed by upper ocean dynamics, ice sheets melting, and other phenomenon, making it somewhat difficult to infer from salinity observations. Salinity could nevertheless bring additional consistency constraints that could eventually help to assess E-P over the ocean (Yu et al., 2020).

2.1.4. Water and energy budget

The water and energy cycles follow water mass and energy conservation laws respectively. The conservation of water mass and energy at the surface are coupled through evaporation (see also Kato et al., 2016). The water mass balance for a regional land surface is

$dS/dt_i = P-E-R$

where S is the land water storage, P and E are precipitation and evaporation rate, and R is runoff. At an annual global scale, the evaporation rate at the surface balances with the precipitation rate. The energy balance at the surface is

$NET = DLW+DSW–ULW–USW–SH–L_eE$

45

NET is the surface net energy, DLW (DSW) the downward longwave (shortwave) radiation, ULW (USW) is the upward longwave (shortwave) surface radiation, SH is the sensible heat flux, and L_eE is evaporation rate multiplied by the enthalpy of vaporization. Note that bias in P and E can compensate easily in the water closure and less so in the water and energy closure owing to the radiation constraint. The usually more-accurate radiation estimates can also provide a stronger constraint on the precipitation.

2.1.4.1. Global

Previous studies have demonstrated that, in the current climate, variability in atmospheric energy balance, ∆NETATM, is primarily governed by changes in longwave radiation (ULW - DLW) and precipitation (P) (Allen and Ingram, 2002; Held and Soden, 2006). As a result, atmospheric longwave cooling exerts a robust control on global precipitation in the equilibrium climate as demonstrated by Stephens and Ellis (2008). The implications of this link between the energy and water cycle are readily evident in recent reconstructions of Earth's energy budget. When energy and water cycle fluxes from state-of-the-art satellite observations or reanalysis are combined to reconstruct the global atmospheric and oceanic energy budgets, large residuals emerge that exceed in situ estimates of atmospheric and ocean heat uptake by an order of magnitude. One or more fluxes must be adjusted to resolve these imbalances. Two approaches emerged for reconciling the implied energy imbalances with in situ observations. Trenberth et al. (2009) chose to reduce the downwelling radiation (primarily DLW) into the surface while Stephens et al. (2012) argued that global precipitation estimates should be increased, sparking intense debate as to which flux datasets were more accurate. While subjective arguments could be made for adjusting either precipitation or DLW, the discrepancies in the resulting global, annual-mean precipitation estimates exceeded 10%.

The debate fueled by these competing energy budget reconstructions led a large group of investigators in NASA's Energy and Water cycle Study (NEWS) to develop an objective approach to imposing energy and water cycle closure constraints. By adjusting fluxes using a 1D-VAR framework that explicitly accounted for uncertainties in component fluxes, L'Ecuyer et al. (2015) and Rodell et al. (2015) generated closed energy and water budgets on global and continental scales. This work suggests that current satellite-based estimates of global precipitation need to be increased by 4%, an adjustment that falls within existing error bars, to properly balance global evaporation and close the atmospheric and surface energy budgets (Rodell et al., 2015).

2.1.4.1.1. *Towards assessing multiple precipitation products water and energy closure*

As a preliminary step towards assessing the various precipitation products' consistency within the optimized framework, a first comparison of the global diabatic heating variability is needed. Indeed, on the global and annual scale, net atmospheric irradiance divergence must be balanced by surface sensible heating and diabatic heating rate by precipitation (Stephens and Ellis, 2008). The net atmospheric radiation divergence is derived from Clouds and the Earth's Radiant Energy System (CERES) Energy Balanced and Filled (EBAF) edition 4 and the global latent heat value is derived from a subset of global precipitation products from Frequent Rainfall Observations on GridS (FROGS: Roca et al., 2019). The quasi-global satellite products have been completed poleward using the GPCP "truly" global product data, forming a larger ensemble of products to assess. In complement to satellite-based estimates, a handful of reanalysis products is also included in the study.

The variability of monthly anomalies is +-1 Wm-2 (Figure 2.1.3). The results indicate a strong lack of consistency of the precipitation products with the exception the GPCP estimates and

that of European Centre for Medium-Range Weather Forecasts Reanalysis version 5 (ERA5), especially after 2007. The PERSIANN and the CMORPH products also seem to track the net atmospheric irradiance well, which is not surprising since the products are scaled on GPCP at monthly scale (only over ocean for CMORPH). Most of the precipitation products overestimate the diabatic heating variability and some show substantial trends with no equivalent in the radiation-derived budget.
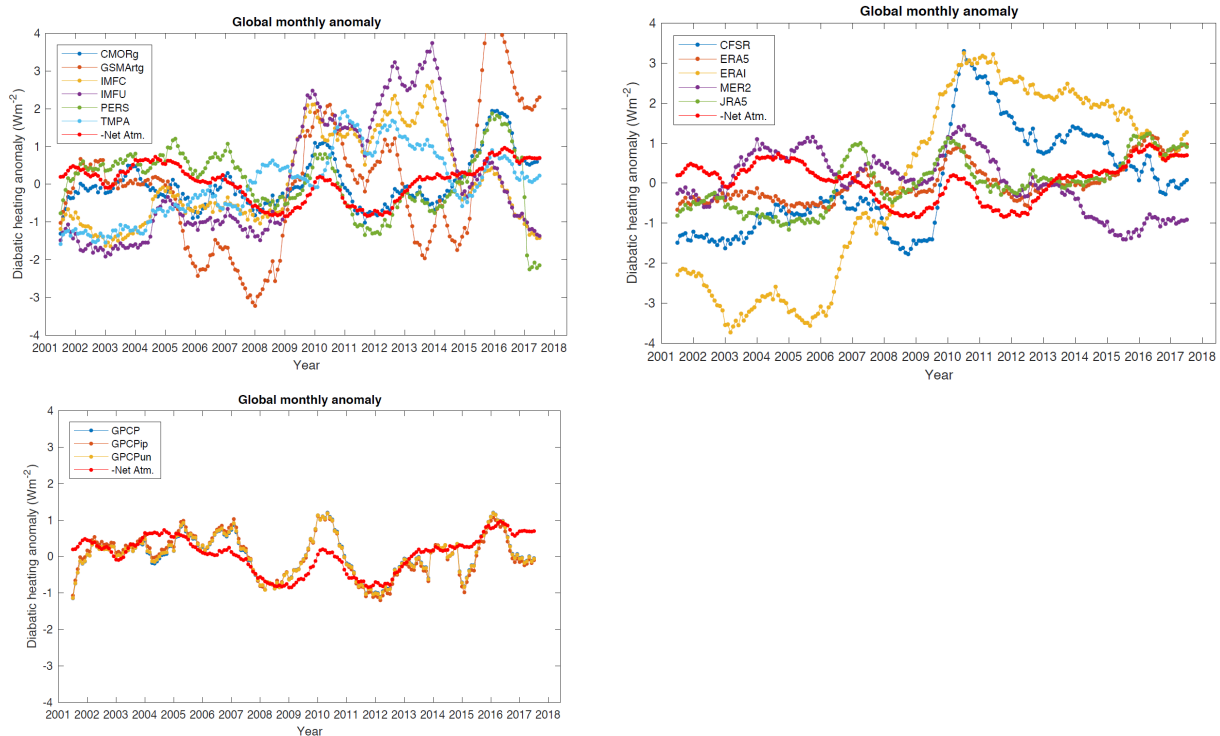
Figure 2.1.3. Time series of the deseasonalized monthly anomaly of global diabatic heating for various filled satellite (top left) and reanalysis (top right) and truly global satellite (bottom left) products. In both panels, anomalies of net atmospheric irradiance are shown by the red line.

2.1.4.1.2. *Multiple precipitation products using water budget only closure*

Hobeichi et al. (2020a) investigate five global products, two from satellite (IMERG, GPCP), two ground-based [GPCC, Rainfall Estimates on a Gridded Network (REGEN)] and one reanalysis, the second Modern-Era Retrospective analysis for Research and Applications (MERRA-2). The assimilation-based method of Hobeichi et al. (2020b) is used. It is implemented globally at the resolution of half a degree and at monthly time scales and performs a simultaneous enforcement of the closure of the surface water and energy budgets. Using various metrics, the analysis shows that GPCC best closes the budget of the high latitudes while GPCP leads in the tropics. The REGEN data test seems to best perform over semi-arid regions of northern Africa and the Middle East and in the moist Southeast Asia. IMERG outperforms the other products only over Australia.

Figure 2.1.4 indicates that despite having a significantly lesser performance, the MERRA-2 uncertainty characterization is relevant as the adjustments due to the closure remain bounded by the uncertainty. Unlike MERRA-2, the satellite and ground-based products' uncertainty appears not to be adequate in most of the regions, suggesting a deeper elaboration on uncertainty for these products.

47
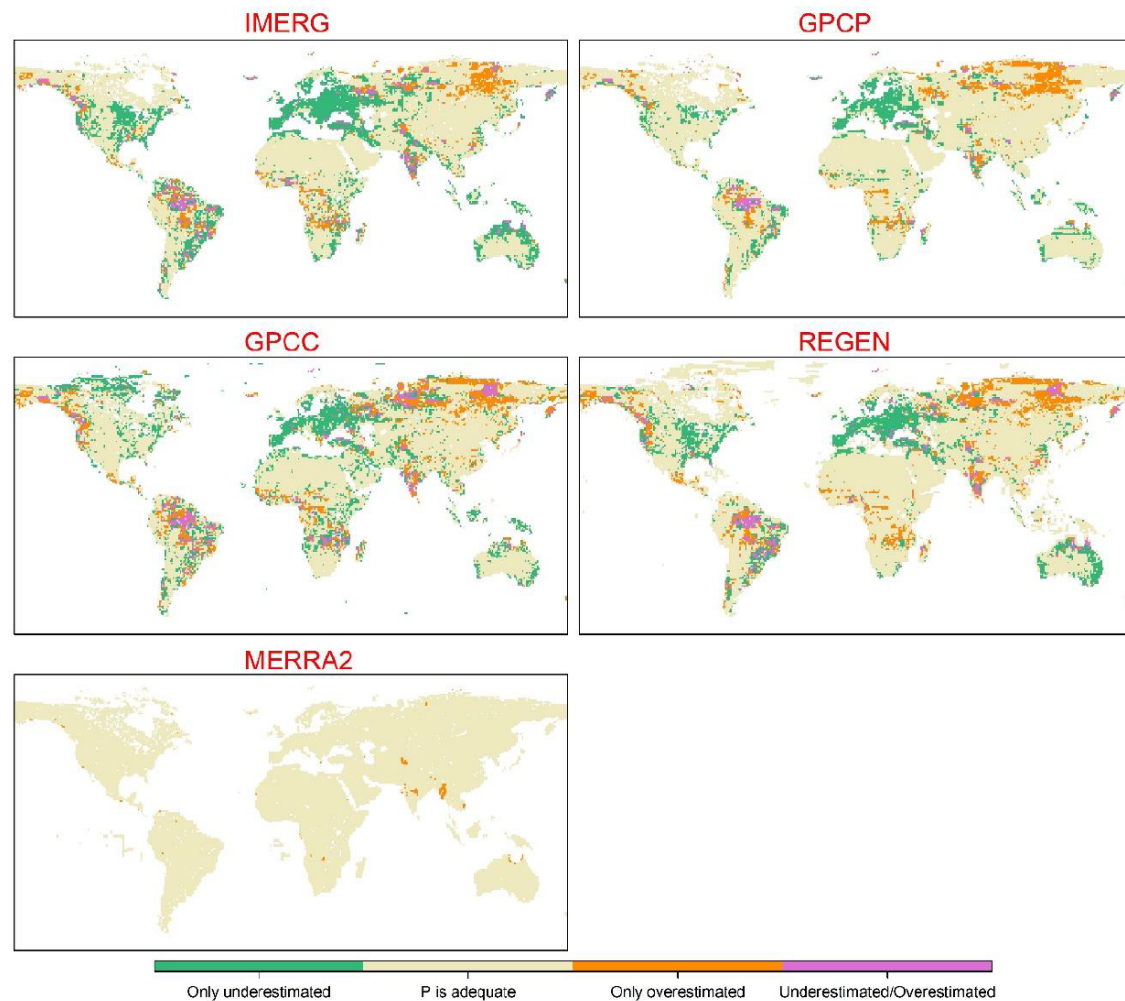
Figure 2.1.4. Regions where a P dataset had to undergo adjustments beyond its uncertainty bounds, indicating that it was originally underestimated or overestimated. Green grid cells are locations where P was found to be underestimated in at least one calendar month, but never overestimated. Orange grid cells refer to locations where P was found overestimated in at least one calendar month but never underestimated. Magenta grid cells show regions where P exhibited different behaviors (underestimated/overestimated) in difference calendar months. Beige grid cells are regions where changes applied to P do not exceed its uncertainty. From Hobeichi et al., 2020a

2.1.5. Summary

Optimization techniques have provided a useful way to assess the capability of the existing observations to close the water budget or the water and energy budget as well as the consistency of the estimated fluxes, once the closure is enforced. This leap forward enables the assessment of the new generation of products at the global scale as well as regionally, including the oceans, for which precipitation products' performances is usually poorly known. The emergence of new observational constraints on the surface freshwater budget via surface salinity measurements can further help with the consistency analysis over the ocean.

Water balance studies at a regional scale emphasize the better accuracy of the rain gauge-based products compared to the reanalysis and satellite datasets. Water budget only

optimization yields only moderate changes and improvements of a few precipitation products, suggesting a relatively good consistency with evaporation and runoff. This status is of no use for global investigations and embodies the difficulty of benefiting from numerous regional land investigations from a global climate perspective.

Water and energy budget simultaneous closure optimization at global, multi-year scales shows that current global precipitation estimations need an adjustment that falls within existing error bars. Preliminary time series comparisons between energy and precipitation at the global scale, on the other hand, show large spread from the various precipitation products and significant unrealistic variability.

Systematic evaluation of the breadth of products available remains challenging, as most of the studies explore one or two products, making it difficult so far to reach a community-centric overview. Preliminary efforts using a dozen *global* datasets nevertheless reveal the large inconsistency between the precipitation and radiation budget, except for GPCP and ERA5.

2.1.6. Recommendations

Based on this first and partial attempt to assess the capability of precipitation products to contribute to water and energy cycle closure as well as their consistency with other fluxes, we are in a position to formulate some recommendations for the agencies and the community.

General recommendations:

- Validation/intercomparison/assessment studies should embrace the large breadth of existing products and not be restricted to one or two products
- Consolidate present findings; elaborate and refine the current set of diagnostics
- Improve the products, as the assessment has identified some non-robust features that deserve further attention. Provide feedback to the dataset providers on the details, perhaps with specific workshops.
- Fill the gaps in the assessment.
- Communicate the robust features of the datasets to support further research using the datasets.

2.1.6.1.1. *Specific recommendations*

- Better convey the optimization results at regional scales with ongoing field programs (for example, the GEWEX Hydroclimatology Panel)
- The documentation of the precipitation products' uncertainty should be advanced to fully benefit the optimization framework. This includes auto-correlation and structural error characterization at the monthly scale.
- Support the systematic use of the various precipitation products instead of the single product approach to help better identify the strengths and weaknesses of the products.

2.1.7. Acknowledgments

2.1.8. References

Allen, M.R., and W.J. Ingram, 2002: Constraints on future changes in climate and the hydrologic cycle. *Nature*, 419, 224–232, https://doi.org/10.1038/nature01092.

Brown, P.J., and C.D. Kummerow, 2014: An assessment of atmospheric water budget components over tropical oceans. *Journal of Climate*, 27(5), 2054–2071, doi:10.1175/JCLI-D-13-00385.1.

Held, I.M., and B.J. Soden, 2006. Robust Responses of the Hydrological Cycle to Global Warming. *Journal of Climate*, 19, 21, 5686–5699, https://doi.org/10.1175/JCLI3990.1.

Hobeichi, S., G. Abramowitz, S. Contractor and J. Evans, 2020a: Evaluating precipitation datasets using surface water and energy budget closure. *Journal of Hydrometeorology*, 1–49, doi:10.1175/jhm-d-19-0255.1.

Hobeichi, S., G. Abramowitz and J. Evans, 2020b: Conserving Land–Atmosphere Synthesis Suite (CLASS). *Journal of Climate*, 33, 1821–1844, https://doi.org/10.1175/JCLI-D-19-0036.1.

Kato, S., K.M. Xu, T. Wong, N.G. Loeb, F.G. Rose, K.E. Trenberth and T.J. Thorsen, 2016: Investigation of the residual in column-integrated atmospheric energy balance using cloud objects. *Journal of Climate*, 29(20), 7435–7452, doi:10.1175/JCLI-D-15-0782.1.

L'Ecuyer, T., H.K. Beaudoing, M. Rodell, W. Olson, B. Lin, S. Kato, C.A. Clayson, E. Wood, J. Sheffield, R. Adler, G. Huffman, M. Bosilovich, G. Gu, F. Robertson, P.R. Houser, D. Chambers, J.S. Famiglietti, E. Fetzer, W.T. Liu, X. Gao, C.A. Schlosser, E. Clark, D.P. Lettenmaier and K. Hilburn, 2015: The Observed State of the Energy Budget in the Early Twenty-First Century. *Journal of Climate*, 28, 21, 8319–8346, https://doi.org/10.1175/JCLI-D-14-00556.1.

Lorenz, C., H. Kunstmann, B. Devaraju, M.J. Tourian, N. Sneeuw and J. Riegger, 2014: Large-scale runoff from landmasses: A global assessment of the closure of the hydrological and atmospheric water balances. *Journal of Hydrometeorology*, 15(6), 2111–2139, doi:10.1175/JHM-D-13-0157.1.

Mauritsen, T., and B. Stevens, 2015: Missing iris effect as a possible cause of muted hydrological change and high climate sensitivity in models. *Nature Geoscience*, 8, 346–351, http://dx.doi.org/10.1038/ngeo2414.

Meyssignac, B., T. Boyer, Z. Zhao, M.Z. Hakuba, F.W. Landerer, D. Stammer, A. Köhl, S. Kato, T. L'Ecuyer, M. Ablain, J.P. Abraham, A. Blazquez, A. Cazenave, J.A. Church, R. Cowley, L. Cheng, C.M. Domingues, D. Giglio, V. Gouretski, M. Ishii, G.C. Johnson, R.E. Killick, D. Legler, W. Llovel, J. Lyman, M.D. Palmer, S. Piotrowicz, S.G. Purkey, D. Roemmich, R. Roca, A. Savita, K. von Schuckmann, S. Speich, G. Stephens, G. Wang, S.E. Wijffels and N. Zilberman, 2019: Measuring Global Ocean Heat Content to Estimate the Earth Energy Imbalance. *Frontiers in Marine Science*, 6, 1–31, doi:10.3389/fmars.2019.00432.

Munier, S., F. Aires, S. Schlaffer, C. Prigent, F. Papa, P. Maisongrande and M. Pan, 2014: Combining data sets of satellite-retrieved products for basin-scale water balance study: 2. Evaluation on the Mississippi basin and closure correction model. *Journal of Geophysical Research*, 119(21), 12,100–12,116, doi:10.1002/2014JD021953.

Munier, S., and F. Aires, 2018: A new global method of satellite dataset merging and quality characterization constrained by the terrestrial water budget. *Remote Sensing of Environment*, 205, 119–130, https://doi.org/10.1016/j.rse.2017.11.008.

Pellet, V., F. Aires, S. Munier, D. Fernández Prieto, G. Jordá, W.A. Dorigo, J. Polcher and L. Brocca, 2019: Integrating multiple satellite observations into a coherent dataset to monitor the full water cycle – application to the Mediterranean region. *Hydrology and Earth System Sciences*, 23, 465–491, https://doi.org/10.5194/hess-23-465-2019.

Ramanathan, V., 1981: The role of ocean-atmosphere interactions in the CO_2 climate problem. *Journal of the Atmospheric Sciences*, 38, 918–930.

Roca, R., L.V. Alexander, G. Potter, M. Bador, R. Jucá, S. Contractor, M.G. Bosilovich and S. Cloché, 2019: FROGS: a daily 1° × 1° gridded precipitation database of rain gauge, satellite and reanalysis products. *Earth System Science Data*, 11, 1017–1035, https://doi.org/10.5194/essd-11-1017-2019.

Rodell, M., H.K. Beaudoing, T.S. L'Ecuyer, W.S. Olson, J.S. Famiglietti, P.R. Houser, R. Adler, M.G. Bosilovich, C.A. Clayson, D. Chambers, E. Clark, E.J. Fetzer, X. Gao, G. Gu, K. Hilburn, G.J. Huffman, D.P. Lettenmaier, W.T. Liu, F.R. Robertson, C.A. Schlosser, J. Sheffield and E.F. Wood, 2015: The Observed State of the Water Cycle in the Early Twenty-First Century. *Journal of Climate*, 28.21, 8289–8318, https://doi.org/10.1175/JCLI-D-14-00555.1.

Sheffield, J., C.R. Ferguson, T.J. Troy, E.F. Wood and M.F. McCabe, 2009: Closing the terrestrial water budget from satellite remote sensing. *Geophysical Research Letters*, 36(7), doi:10.1029/2009GL037338.

Stephens, G.L., and T.D. Ellis, 2008: Controls of global-mean precipitation increases in global warming GCM experiments. *Journal of Climate*, 21, 6141–6155, doi:10.1175/2008JCLI2144.1.

Stephens, G.L., J. Li, M. Wild, C.A. Clayson, N. Loeb, S. Kato, T. L'Ecuyer, P.W. Stackhouse Jr., M. Lebsock and T. Andrews, 2012: An update on Earth's energy balance in light of the latest global observations. *Nature Geoscience*, 5, 691–696, http://dx.doi.org/10.1038/ngeo1580.

Stephens, G.L., J.M. Slingo, E. Rignot, J.T. Reager, M.Z. Hakuba, P.J. Durack, J. Worden and R. Rocca, 2020: Earth's water reservoirs in a changing climate. *The Royal Academy Proceedings: Mathematical, Physical and Engineering Sciences*, 476(2236), doi:10.1098/rspa.2019.0458, 2020.

Trenberth, K.E., J.T. Fasullo and J. Kiehl, 2009: Earth's global energy budget. *Bulletin of the American Meteorological Society*, 90, 311–323, https://doi.org/10.1175/2008BAMS2634.1.

Watanabe, M., Y. Kamae, H. Shiogama, A.M. DeAngelis and K. Suzuki, 2018: Low clouds link equilibrium climate sensitivity to hydrological sensitivity. *Nature Climate Change*, 8, 901–906, http://dx.doi.org/10.1038/s41558-018-0272-0.

Yoon, Y., S.V. Kumar, B.A. Forman, B.F. Zaitchik, Y. Kwon, Y. Qian, S. Rupper, V. Maggioni, P. Houser, D. Kirschbaum, A. Richey, A. Arendt, D. Mocko, J. Jacob, S. Bhanja and A. Mukherjee, 2019: Evaluating the Uncertainty of Terrestrial Water Budget Components Over High Mountain Asia. *Frontiers in Earth Science*, 7:120, doi: 10.3389/feart.2019.00120.

Yu, L., S.A. Josey, F.M. Bingham and T. Lee, 2020: Intensification of the global water cycle and evidence from ocean salinity: a synthesis review. *Annals of the New York Academy of Sciences*, 1–19, doi:10.1111/nyas.14354.

2.2. Climate variability and trends

Francisco J. Tapiador

University of Castilla-La Mancha (UCLM), Spain

"Climate variability" is defined as the temporal variations of the atmosphere-ocean system around a mean state. The term "natural climate variability" is further used to identify climate variations that are not attributable to or influenced by any activity related to humans (American Meteorological Society, 2021). Regarding "climatic trends", those are defined as a climate change characterized by a reasonably smooth, monotonic increase or decrease of the average value of one or more climatic elements during the period of record (American Meteorological Society, 2021).

The variability of precipitation has two dimensions in climate. The first one is how precipitation departs from the average over a number of years, say the 1990–2020 mean over the 1960–1990 mean, at each location on the globe. The second one is how to gauge climate variability as a whole looking at precipitation. The latest is the province of studies analyzing the dominant modes of variability and includes research on the Pacific Decadal Oscillation (PDO), the Atlantic Multidecadal Oscillation (AMO), the Indian Ocean Dipole (IOD) and the El Niño Southern Oscillation (ENSO). Good climate models correctly simulate the Madden-Julian Oscillation (MJO), ENSO and the mean Intertropical Convergence Zone (ITCZ). Those processes are also precisely identified as a fingerprint in the precipitation field. Thus, satellite precipitation estimates are fundamental to achieve a proper representation of such climate variability and to validate models (cf. Chapter 2.3 below).

Precision and accuracy of the precipitation estimates are both important, as is the global scope. It is known that the changes in global mean precipitation are determined by changes in radiative cooling of the atmosphere (Stephens and Ellis, 2008), so it is extremely important to be as precise as possible in determining such changes to understand changes in the radiative forcing, either by natural or anthropogenic causes. Regional estimates are also a must. In the tropics, mean precipitation and the extreme of the distribution is largely dominated by organized mesoscale convective systems (Roca et al., 2014; Rossow et al., 2013), and the trends in precipitation are related to the fate of organized convection (Tan et al., 2015). Latent heating algorithms that have been developed for satellite rain data diagnose the convective/stratiform partitioning from characteristics of the rain and reflectivity fields to produce realistic heating profiles and thus to improve the modeling of the climate variability. Indeed, model parameterization errors become obvious only when higher-order variability metrics such as PDO, AMO, IOD, MJO and ENSO are used. The continental diurnal cycle, which depends on the timing of the transition from bottom-heavy to top-heavy latent heating profiles, is also relevant for climate variability and trends analyses. In fact, precipitation was instrumental in documenting the existence and propagation of MJO anomalies (Madden and Julian, 1994; Del Genio et al., 2015; Wang et al., 2015). Here, the advantage of precipitation over the more commonly-used outgoing longwave radiation (OLR) is that OLR anomalies over the Maritime Continent can be affected by the fairly ubiquitous high cloud cover. Instead, the rain anomalies have proved to be very helpful in isolating the onset phase of the MJO, when shallow and congestus rain dominate as the biggest sources of error in GCM cumulus parameterizations and in preventing the development of a robust MJO. This particular case illustrates that it is precisely because of its complexity that precipitation can be superior to other variables: OLR-based indices of convection greatly overestimate surface rain over Africa, because they sense only the high cold clouds and cannot tell that rain is evaporating more strongly into the relatively dry lower troposphere there and not reaching the ground to the

extent that it does in humid regions such as the Amazon (Liu and Zipser, 2005; Ling and Zhang, 2011).

Regarding the ENSO, a precipitation-based definition of an extreme El Niño event (those events for which the Niño-3 rainfall index is above 5 mm day^{-1}) has been proposed. It is based on the precipitation anomalies averaged over the Niño-3 (5°S–5°N, 150°–90°W) region (Cai et al., 2014, 2017). Based on this precipitation-based index, Cai et al. (2014) analyzed Coupled Model Intercomparison Project (CMIP) phase 3 (CMIP3) and CMIP5 models and found a doubling in the occurrence of extreme El Niño events in the future in response to greenhouse warming, while no significant change in statistics in extreme El Niño events is found based on the "classical" Niño-3.4 SST index. Power et al. (2013) also shows that ENSO-driven precipitation exhibits a clearer longer-term change than SST anomalies. Thus, precipitation may be seen as a better field to reveal, diagnose and quantify the nonlinear relationship between the variability in the climate system and changes in mean state. There is more evidence on the central role of precipitation: the precipitation response to SST during strong El Niño events encapsulates the process associated with the nonlinear amplification of the Bjerknes feedback (Takahashi and Dewitte, 2016) and therein can be considered a better metric of El Niño–Southern Oscillation (ENSO) extremes than SST anomalies alone. Thus, the relationship between precipitation in the eastern equatorial Pacific (Niño-3 region) and the SST gradient near the equatorial region during El Niño exhibits a marked nonlinear pattern that enhances or eases the detection of extreme events.

There are many available precipitation datasets suitable for climate validation (Tapiador et al., 2017). The existence of different approaches and merging methods is a plus in climate variability and trends studies. When satellite estimates differ, important information is revealed. Identifying trends and breakpoints in precipitation series is not trivial, but has proved useful in the context of validating climate models (Figure 2.2.1, Tapiador et al., 2018; Tan et al., 2015). For example, the considerable discrepancy between passive microwave and radar estimates of rain rate in the eastern Pacific ITCZ (Liu and Zipser, 2013) revealed that assumptions about the depth or microphysical properties of rain-producing clouds are valid. While the issue has been known for a long time, the specific details, and crucially the mechanistic description, are better

Figure 2.2.1. Time series of tropical (30S–30N) precipitation (mm/day) over land for 1980–2000. From Tapiador et al., 2018

expressed in terms of precipitation. Therein, it is important to keep and maintain a host of precipitation datasets from different sources and methodologies. Single, one-instrument and multisource datasets are both valuable for analyzing different aspects of the climate variability and the trends. Section 2.4 below delves more deeply into the nature of 11 comprehensive datasets and acknowledges that none of them can be considered as the "true" representation of global precipitation. A first-order metric such as the global (60N-60S) mean precipitation over land can vary from 1.81 mm/day (GSMap) to 2.33 mm/day [PERSIANN-Climate Data Record (PERSIANN-CDR)]. Differences in the polar areas are larger. Such discrepancies raise several challenges on the appropriate approach to follow in the validation of climate models for present climate simulations (cf. Chapter 2.3 below). Careful consideration of the algorithmic choices and the sampling errors (cf. Chapter 1.1 above) is also required when these datasets are used for analyzing climate variability and trends. Large uncertainties in extremes in both reanalysis and observations (Chapter 2.5 below) also raise issues on their fitness-for-purpose on this realm. Error modeling (Chapter 3.2 below) is fundamental for the use of satellite precipitation datasets for these applications.

There are more examples of the need for satellite precipitation data in climate variability research. Processes of SST-wind-precipitation interaction are also likely involved in long-term trends and variability in the surface circulation in the tropics (Tapiador et al., 2019). For instance, while in the subtropical eastern boundary upwelling regions, an increase of the equatorward winds is expected (and observed in some regions) owing to the poleward displacement and intensification of the anticyclone/Hadley cells. In the tropical Pacific region, the trends in upwelling-favorable winds are more ambiguous and are sensitive to concurrent changes in SST and rainfall, as observed off Peru from coupled model experiments (Belmadani et al., 2014). Therefore, processes associated with moist convection and subsidence in the far eastern Pacific are likely important to understand trends in upwelling systems, and their investigation will benefit from precipitation observations and will require model evaluations based on those.

Regarding climate variability in precipitation, the fingerprints have been observed following different methods and approaches (Hidalgo et al., 2017; Kenyon and Hegerl, 2010). The impact of anthropic activity in climate variability is a major driver (Vera et al., 2019). Multidimensional analyses involving other environmental sciences also require detailed precipitation data (Trauernicht, 2019; Suarez and Kitzberger, 2010). The use of precipitation data for analyzing extremes in the climate variability realm is also valuable (van Pelt et al., 2015; Shawul and Chakma, 2020; Liu and Allan, 2012; Ummenhofer and England, 2007; Teegavarapu, 2016). Precipitation estimates over the poles are also of interest: Antarctica is significantly colder and more prone to climate variability than the Arctic, although both regions are strongly responsive to large-scale variability including the northern and southern annular modes (Screen et al., 2018).

To conclude this section, it is worth noting that climate variability and trends are relevant for a number of applications. Climate services are mostly targeted at informing adaptation to them, widely recognized as an important challenge for sustainable development. The role of satellite precipitation datasets is central in this realm. Better identification of the modes of climate variability, the definition of new precipitation-based metrics and novel methods to gauge trends and changes, all depend on the continuous availability of long, continuous and global measurements of liquid and solid precipitation (cf. Chapter 3.1 below). The need to continually improve the precipitation estimates from satellite and new developments in the observation network should follow the path imposed by progresses in modeling.

2.2.1. References

American Meteorological Society, 2021: Natural Climate Variability. Glossary of Meteorology, https://glossary.ametsoc.org/wiki/Climate_variability.

American Meteorological Society, 2021: Climatic Trend. Glossary of Meteorology, https://glossary.ametsoc.org/wiki/Climatic_trend.

Belmadani, A., V. Echevin, F. Codron, K. Takahashi and C. Junquas, 2014: What dynamics drive future wind scenarios for coastal upwelling off Peru and Chile? *Climate Dynamics*, 43, 1893-1914, doi:10.1007/s00382-013-2015-2.

Cai, W., S. Borlace, M. Lengaigne, P. van Rensch, M. Collins, G. Vecchi, A. Timmermann, A. Santoso, M. McPhaden, L. Wu, M.H. England, G. Wang, E. Guilyardi and F.-F. Jin, 2014: Increasing Frequency of Extreme El Niño Events due to Greenhouse Warming. *Nature Climate Change*, 4, 111–116, DOI: 10.1038/nclimate2100.

Cai, W., G. Wang, A. Santoso, X. Lin and L. Wu, 2017: Definition of Extreme El Niño and Its Impact on Projected Increase in Extreme El Niño Frequency. *Geophysical Research Letters,* https://doi.org/10.1002/2017GL075635.

Del Genio, A.D., J. Wu, A.B. Wolf, Y. Chen, M. Yao and D. Kim, 2015: Constraints on Cumulus Parameterization from Simulations of Observed MJO Events. *Journal of Climate*, 28, 6419–6442, https://doi.org/10.1175/JCLI-D-14-00832.1.

Hidalgo, H.G., E.J. Alfaro and B. Quesada-Montano, 2017: Observed (1970–1999) climate variability in Central America using a high-resolution meteorological dataset with implication to climate change studies. *Climatic Change* 141, 13–28, https://doi:10.1007/s10584-016-1786-y.

Kenyon, J., and G.C. Hegerl, 2010: Influence of modes of climate variability on global precipitation extremes. *Journal of Climate*, **23**(23), 6248–6262, https://doi.org/10.1175/2010JCLI3617.1.

Ling, J., and C. Zhang, 2011: Structural evolution in heating profiles of the MJO in global reanalyses and TRMM retrievals. *Journal of Climate*, 24, 825–842, doi:10.1175/2010JCLI3826.1.

Liu, C., and R.P. Allan, 2012: Multisatellite observed responses of precipitation and its extremes to interannual climate variability. *Journal of Geophysical Research Atmospheres*, vol. 117, D3, https://doi.org/10.1029/2011JD016568.

Liu, C., and E.J. Zipser, 2005: Global distribution of convection penetrating the tropical tropopause, *Journal of Geophysical Research,* 110, D23104, doi:10.1029/2005JD006063.

Liu C., and E. Zipser, 2013: Regional variation of morphology of the organized convection in the tropics and subtropics, Part I: regional variation, *Journal of Geophysical Research,* 118, 453–466, doi:10.1029/2012JD018409.

Madden, R.E., and P.R. Julian, 1994: Observations of the 40-50 day tropical oscillation-A review. *Monthly Weather Review*, 122: 814–837.

Power, S., F. Delage, C. Chung, G. Kociuba and K. Keay, 2013: Robust twenty-first-century projections of El Niño and related precipitation variability. *Nature*, 502, 541–545.

Roca, R., J. Aublanc, P. Chambon, T. Fiolleau and N. Viltard, 2014: Robust observational quantification of the contribution of mesoscale convective systems to rainfall in the tropics. *Journal of Climate*, 27, 4952–4958, doi:10.1175/JCLI-D-13-00628.1.

Rossow, W.B., A. Mekonnen, C. Pearl and W. Goncalves, 2013: Tropical precipitation extremes. *Journal of Climate*, 26, 1457–1466, doi:10.1175/JCLI-D-11-00725.1.

Screen, J.A., C. Deser, D.M. Smith, X. Zhang, R. Blackport, P.J. Kushner, T. Oudar, K.E. McCusker and L. Sun, 2018: Consistency and discrepancy in the atmospheric response to Arctic sea-ice loss across climate models. *Nature Geoscience*, 11, 3, 155–163, DOI:10.1038/s41561-018-0059-y.

Shawul, A.A., and S. Chakma, 2020: Trend of extreme precipitation indices and analysis of long-term climate variability in the Upper Awash basin, Ethiopia. *Theoretical and Applied Climatology*, 140, 635–652, https://doi.org/10.1007/s00704-020-03112-8.

Suarez, M.L., and T. Kitzberger, 2010: Differential effects of climate variability on forest dynamics along a precipitation gradient in northern Patagonia. *Journal of Ecology*, https://doi.org/10.1111/j.1365-2745.2010.01698.x.

Takahashi, K., and B. Dewitte, 2016: Strong and Moderate nonlinear El Niño regimes. *Climate Dynamics*, doi: 10.1007/s00382-015-2665-3.

Tan, J., C. Jakob, W. B. Rossow and G. Tselioudis, 2015: Increases in tropical rainfall driven by changes in frequency of organized deep convection. *Nature*, 519, 451–454, doi:10.1038/nature14339, http://dx.doi.org/10.1038/nature14339.

Tapiador, F.J., A. Navarro, A. Jiménez, R. Moreno and E. García-Ortega, E. 2018: Discrepancies with satellite observations in the spatial structure of global precipitation as derived from global climate models. *Quarterly Journal of the Royal Meteorological Society*, 144, 419-435, https://doi.org/10.1002/qj.3289.

Tapiador, F.J., A. Navarro, V. Levizzani, E. García-Ortega, G.J. Huffman, C. Kidd, P.A. Kucera, C.D. Kummerow, H. Masunaga, W.A. Petersen, R. Roca, J.-L. Sánchez, W.-K. Tao and F.J. Turk, 2017: Global precipitation measurements for validating climate models. *Atmospheric Research*, 197, 1–20, https://doi.org/10.1016/j.atmosres.2017.06.021.

Tapiador, F.J., R. Roca, A. Del Genio, B. Dewitt, W. Petersen and F. Zhang, 2019: Is precipitation a good metric for model performance? *Bulletin of the American Meteorological Society*, 100(2), 223–233, https://doi.org/10.1175/BAMS-D-17-0218.1.

Teegavarapu, R.S.V., 2016: Climate variability and changes in precipitation extremes and characteristics. In: *Sustainable Water Resources Planning and Management Under Climate Change* (E. Kolokytha, S. Oishi, R. Teegavarapu, eds.). Springer, Singapore, https://doi.org/10.1007/978-981-10-2051-3_1.

Trauernicht, C., 2019: Vegetation—Rainfall interactions reveal how climate variability and climate change alter spatial patterns of wildland fire probability on Big Island, Hawaii. *Science of the Total Environment*, 650, 459–469, https://doi:10.1016/j.scitotenv.2018.08.347.

Ummenhofer, C.C., and M.H. England, 2007: Interannual extremes in New Zealand precipitation linked to modes of Southern Hemisphere climate variability. *Journal of Climate*, 20(21), 5418–5440, https://doi.org/10.1175/2007JCLI1430.1.

van Pelt, S.C., J.J. Beersma, T.A. Buishand, B.J.J. van den Hurk and J. Schellekens, 2015: Uncertainty in the future change of extreme precipitation over the Rhine basin: the role of internal climate variability. *Climate Dynamics*, 44, 1789–1800, https://doi.org/10.1007/s00382-014-2312-4.

Vera, C.S., L.B. Díaz and R.I. Saurral, 2019: Influence of anthropogenically-forced global warming and natural. Climate variability in the rainfall changes observed over the South American Altiplano. *Frontiers in Environmental Science*, https://doi:10.3389/fenvs.2019.00087.

Wang, S., A.H. Sobel, F. Zhang, Y. Qiang Sun, Y. Yue and L. Zhou, 2015: Regional Simulation of the October and November MJO Events Observed during the CINDY/DYNAMO Field Campaign at Gray Zone Resolution. *Journal of Climate*, 28, 2097–2119.

2.3. Climate model validation

Francisco J. Tapiador[1] and Vincenzo Levizzani[2]

[1]University of Castilla-La Mancha (UCLM), Spain

[2]National Research Council of Italy-Institute of Atmospheric Sciences and Climate (CNR-ISAC)

As of 2020, climate models include traditional Global Circulation/Climate Models (GCMs), Regional Climate Models (RCMs) and, more recently, Earth System Models (ESMs). All these models are different from Numerical Weather Prediction (NWP) models in that they are intended to provide estimates of the climate rather than meteorological forecasts: they produce "climates", that is, mean values and other statistical moments of the distribution, but not realistic sequences of the actual weather. The World Meteorological Organization (WMO)'s standard length for constructing climatologies is 30 years, with the standard period being the 1960–1990 interval (the "historical climate"). More recently, the 1980–2010 period is used, which is more into the "satellite-era" of meteorological observations.

Climate model outputs are generically named "simulations". They are deemed "projections" when they aim to gauge the climates of the future based on a set of assumptions of anthropogenic forcings and therefore ultimately of social behavior (scenarios). Working in hindsight or to derive estimates of past geological eras, climate models produce "present-climate climatologies" and "paleoclimates" respectively. By going back in time, they can benefit from ancillary data and historical information to fine-tune the simulations, but in the case of experiments on future climate change, such advantage is naturally absent, so different challenges appear.

Validation of climate models is mostly circumscribed to simulations of the present-day climatologies (say 1960–1990) and comparison with meteorological observations. While paleoclimates can also be validated, the absence of an instrumental record obliges us to rely on proxies, which are indirect. Assuming the "rosy" and ceteris paribus assumptions (Smith, 2002), simulations of future climates are useful to understand our changing climate. Nonetheless, the first step to trust such simulations is ensuring models provide a faithful picture of current climate.

Model developers routinely compare their partial results in the developing phase with observations and adjust their models accordingly (Voosen, 2016). While this is unavoidable, it can hardly be considered as scientific validation. First, validation requires independence both in data not used to develop the model, and in the group of people who do the validation. However important self-validation by the developers is for model consistency, it is not a substitute for proper scientific scrutiny by independent, unrelated teams. Secondly, there is a set of protocols and standards that make validation a field in itself. Quality Control (QC) standards have been proposed for this field to address the increasingly pressing requirement as climate becomes more and more interwoven with activities of mitigation and adaptation to global warming. The public and the decision makers demand that the science behind policies is traceable, transparent and auditable, and that includes the validation of climate model outputs.

A major issue in the field of validating present climates is that in the development stage, climate models are tuned to current conditions. The empirical values and assumptions implied in the procedure may vary in the future due to ongoing human emissions and land use changes, and therefore must be fully documented.

Quality Control is now an integral part of climate model validation, as it has long been in the remote sensing field where International Organization for Standardization (ISO) requirements are strictly followed. Failure to do so may result in catastrophic mission failures. International standardization techniques are slowly permeating the procedures of climate validation. It needs to be noted that providing confidence that quality requirements will be fulfilled (e.g., ISO 9000) implies not only that the product is suited for the specific purpose it was conceived in the first place (a dataset or a climate model in our case), but also that the product has been created following a well-defined set of rules and methods that builds confidence in the whole production process. Quality Assurance (QA) procedures are designed to minimize errors and mistakes, setting double-blind evaluations and sanity checks and providing a traceable flow of several stages of the process of generating the product.

To achieve a QA-standard, each step of the production process has to be clearly defined and subject to auditing. This is not a problem for most merged precipitation datasets, since these are carefully-designed products whose science can be traced back to an Algorithm Theoretical Basis Document (ATBD). The ATBDs are the cornerstone of the confidence in merged precipitation datasets, in the same way that metadata and technical notes perform for pure observational datasets. They provide the rationale of the many decisions taken over the process of developing the product, and allow users to trace back each step, also permitting duplication of the product by another party. Reputable climate models also have the equivalent to the ATBD in the form of model documentation describing the physics of the dynamical core, the numerical methods employed, the parameterizations and the empirical choices used to fine-tune the model.

Validating climate model outputs of prognostic variables such as temperature is a difficult exercise per se and becomes even more problematic when dealing with diagnostic variables such as precipitation. Precipitation has been considered "the ultimate test" for validating models for a number of reasons (Tapiador et al., 2019). However, it is difficult to find homogeneous precipitation datasets over reasonably long time periods that cover the whole globe. These are hard to find among ground-based observing systems, which are obviously limited to land areas. Indeed, until 2010 validations of climate models were done by the same teams that develop the software and for grid-point, rain gauge measurements only. Moving to independent, satellite and gauge-satellite combined data, Tapiador (2010) (see Figure 2.3.1) relied on increased availability of robust and public datasets such as those described in Tapiador et al. (2017). The latest published Intergovernmental Panel on Climate Change (IPCC) report, the Fifth Assessment Report (AR5) (IPCC, 2015), acknowledged that the detection and attribution of regional precipitation changes had generally focused on continental areas using in situ data because observational coverage over oceans was limited to a few island stations, although model-data comparisons over continents also illustrated large observational uncertainties. The report also noted that available satellite datasets that could supplement oceanic studies are short and their long-term homogeneity is still unclear, and that accordingly they have not yet been used for detection and attribution of changes. The IPCC concluded in 2014 that "continuing uncertainties in climate model simulations of precipitation make quantitative model/data comparisons difficult (e.g., Stephens et al., 2010), which also limits confidence in detection and attribution."
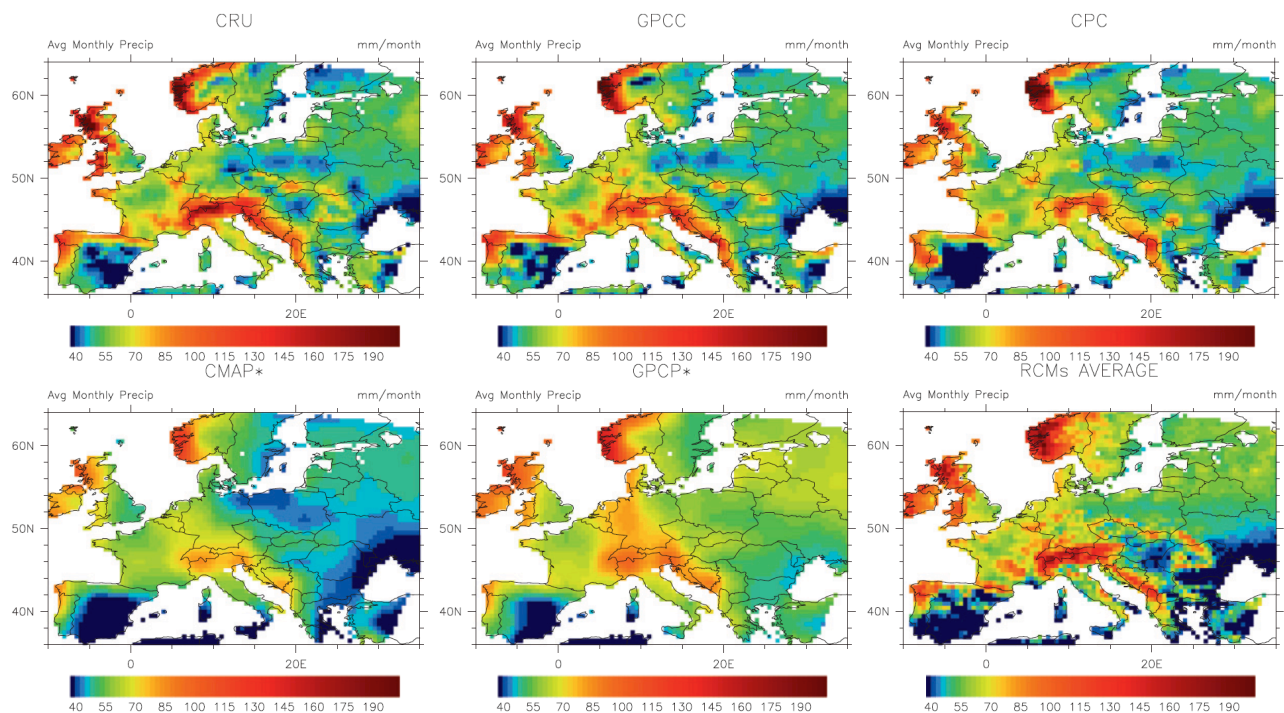
Figure 2.3.1. An example of the first validation of regional climate outputs using several precipitation datasets instead of gauge-only data. From Tapiador, 2010

Tapiador et al. (2017) first conducted a thorough analysis of the existing satellite-based precipitation datasets in view of their application for climate model validation. The authors provide guidance on the use of precipitation datasets for climate research, including model validation and verification for improving physical parameterizations. Strengths and limitations of the datasets for climate modeling applications are presented, underlining that not all datasets are suitable for this purpose. The checklist of items that must be considered in the field of validation of precipitation outputs from climate models includes several crucial points that we will now try to separate between facts and recommendations.

2.3.1. Facts

1. Rain gauges provide pointwise measurements that may not be fully representative of the area, especially for large areas with few observations (for example, the Amazon basin).

2. Rain gauges have known technical limitations and biases and the spatial distribution/length record of the instruments is highly variable.

3. Ground radars are characterized by many sources of uncertainty that have diverse natures (beam blockage, attenuation, anomalous propagation, etc.).

4. Precipitation (solid, liquid and mixed phase) has a large spatial and temporal variability.

5. Satellite estimates are indirect and have limited temporal sampling.

6. Satellite estimates over land, coast and ocean are derived using different methods and assumptions.

7. Merged precipitation databases are not intended for trend analyses as sensor drifts are present over limited time spans.

8. Many of the techniques used in Level-2 products are built upon Bayesian estimates (that is, they require an a priori estimate).

9. The quality of Level-3 precipitation products is driven by microwave observations and therefore is dependent on their availability and quality.

10. There are significant latitudinal differences in the satellite and ground-based estimates in terms of known biases and uncertainties.

11. The error characteristics resulting from the merging of disparate datasets are not well known.

12. There are known uncertainties in the estimation of diabatic heating fields that affect how models represent some precipitation processes.

13. Model outputs that have been bias-corrected or that are the results of model output statistic techniques cannot be validated.

14. Series derived from global circulation model (GCM)-driven regional climate models (RCMs) cannot be directly compared with time series of observations.

15. High-resolution global cloud-resolving models (G-CRM) are becoming better suited than RCMs to inform policies and advance our knowledge of the physics of precipitation.

16. End-to-end characteristics of the satellite-based retrieval process are not yet fully understood.

17. There is less agreement among satellite products in trends and variability at global scale than in regional variability.

2.3.2. Recommendations

i. Uncertainty figures from ground radars should be considered when assimilating data.

ii. Challenges posed to the validation of precipitation by its spatiotemporal variability need to be considered, paying attention when using precipitation datasets in model validation.

iii. The indirect character of satellite estimates and their limited temporal sampling should be considered in the comparisons.

iv. The tuning of the models with specific datasets must be considered for ensuring a truly independent validation.

v. Parameterizations must be validated with data not used in their development and tuning.

vi. Global measurements of microphysics are important to avoid overfitting models to empirical parameters.

vii. Ground validation campaigns are essential for improving the representation of precipitation in models.

viii. "Scope principle": a model cannot claim performances at better resolutions that those at which it has been validated.

ix. Blending methods in deriving global precipitation products involves subtleties than must be considered in any validation process.

x. Parameters and techniques used in the estimation process using satellites and rain gauges may not be universally applicable, both in space and time.

xi. The precise measurement of shallow and very light precipitation still represents a scientific challenge and more research is needed in this direction.

xii. While precipitation is a key variable to validate models, there is no agreement on the reference to be compared with. More research and targeted observations are required to fill this gap.

xiii. Public auditing of model code and precipitation database algorithms is required if models are used for policy-making and societal applications other than pure research.

xiv. Every aspect of model and database development should be subject to QC methods and be fully traceable, transparent and auditable.

xv. Models must be independently validated by scientists not involved in their development or belonging to the same research network.

xvi. Users should be made fully aware of the confidence level that can be attributed to model outputs and observational databases.

When considering the need for validation campaigns that produce new insights for a correct representation of precipitation processes in the models, under-represented areas and processes come first. This is particularly true for tropical forests. In this latter case, the problem is still to make sure that the correct microphysics is understood for its inclusion into the precipitation estimation algorithms prior to conducting any meaningful validation exercise. Recently the project Cloud Processes of the Main Precipitation Systems in Brazil: A Contribution to Cloud-Resolving Modeling and to the Global Precipitation Measurement (CHUVA), held in Brazil, has substantially contributed to improving our level of understanding in this direction (Machado et al., 2014). Another key example is the need for characterizing the relation of mid-latitude frontal precipitation mechanisms and their modification by terrain to rainfall estimation uncertainties. The Olympic Mountain Experiment (OLYMPEX) (Houze et al., 2017) assessed satellite measurements made by the GPM along the northeastern Pacific coastline. At the same time, warm rain processes are still not completely understood, and the Integrated Precipitation and Hydrology EXperiment (IPHEX) sought to characterize warm season orographic precipitation regimes and the relationship between precipitation regimes and hydrologic processes in regions of complex terrain (Erlingis et al., 2018).

There are a number of considerations that need to be made before approaching satellite precipitation datasets for model validation. Validation can be performed on the precipitation model means, which are those most used for applications, or on other first-order statistics. These include the modeling of the ENSO phenomenon (Neale et al., 2008), the representation of the diurnal cycle of rainfall (Betts and Jakob, 2002) and the frequency of occurrence of high- and low-intensity rainfall events (Sun et al., 2006). Validation can also be performed on more

physical quantities such as latent heat (LH) and in the intricacies of the microphysics of precipitation in models.

1. **Latent heat release**. It is a consequence of phase changes between the vapor, liquid and frozen states of water, which cannot be measured or detected using present observational instruments. The vertical distribution of LH has, however, a strong influence on the atmosphere, controlling large-scale tropical circulations, exciting and modulating tropical waves, maintaining the intensities of tropical cyclones, and even providing the energetics of midlatitude cyclones and other midlatitude weather systems (Li et al., 2017). The launch of the Tropical Rainfall Measuring Mission (TRMM) satellite in November 1997 provided a much-needed and accurate measurement of rainfall as well as the ability to estimate the four-dimensional (4D) structure of LH over the global tropics (Simpson et al., 1988, 1996). The success of TRMM made it possible to have another major precipitation measuring mission from the National Aeronautics and Space Administration (NASA), the Global Precipitation Measurement (GPM) mission. GPM is considered by NASA to be the centerpiece mission of its Global Water & Energy Cycle research program. On the modeling side, Cloud resolving models (CRMs) have been identified as being a valuable tool for algorithm developers and are considered a key component for one of the major GPM ground validation (GV) sites. In addition, CRMs are one of the most important tools used to establish quantitative relationships between diabatic heating and rainfall. Thus, simulated data from the Goddard Cumulus Ensemble (GCE) model have been used extensively in TRMM for the development of both rainfall and heating retrieval algorithms (Simpson et al., 1996; Tao et al., 2006). Five different TRMM LH algorithms designed for application with satellite-estimated surface rain rate and precipitation profile inputs have been developed, compared, validated and applied for over two decades (Tao et al., 2001, 2006, 2016b). They are the: (1) Goddard Convective-Stratiform Heating (CSH) algorithm, (2) Spectral Latent Heating (SLH) algorithm, (3) Goddard Trained Radiometer (TRAIN) algorithm, (4) Hydrometeor Heating (HH) algorithm, and (5) Precipitation Radar Heating (PRH) algorithm. The strengths and weaknesses of each algorithm are discussed in Tao et al. (2006). Ling and Zhang (2011) compared the heating profiles between TRMM retrieved (CSH, SLH and TRAIN) and global reanalyses [(ERA-I, Japanese 25-year ReAnalysis (JRA-25) and Climate Forecast System Reanalysis (CFSR)]. All heating data exhibit three longitudinal maxima but with different amplitudes; for example, heating over South America and Africa is much stronger in three models (CSH, SLH, and CFSR) than in the others. Heating is weaker over the Maritime Continent than over the eastern Indian Ocean and western Pacific in some data [for example, apparent heat source Q_1 (Q_1), TRAIN LH, ERA-I Q_1, and JRA25 Q_1], but not so in others. Among all, TRAIN has the largest low-level heating over the east Pacific, which might be an overestimate owing to shallow convection (Grecu et al., 2009). Low-level heating over the eastern Pacific is also present with smaller amplitudes in Q1 from ERA-I and LH from CFSR. The distribution of boundary heating of the LH from CFSR is almost the same, and it may also be related to precipitating marine stratus clouds over the ocean (vanZanten and Stevens, 2005). It is reasonable to say that the upper peak is related to precipitation by cold (ice or mixed phase) clouds and the lower one to precipitation by warm (liquid phase) clouds. LH in TRAIN and CFSR and Q_1 in JRA25 do not have any obvious double-peak structure. Ling and Zhang (2011) also pointed out that the discrepancies among the heating datasets are not merely between the TRMM and reanalysis datasets or between LH and Q_1. Differences within the TRMM

and reanalysis products, respectively, and within various products of LH or Q_1 are no less than those between the TRMM and reanalysis data and between LH and Q_1. These differences reflect our current level of estimating diabatic heating fields: we may get some basic properties of the heating field (for example, longitudinal locations of maxima) correct, but there are many details with large uncertainties. These uncertainties should by no means stop us from cautiously using the currently available heating products to provide as much information as they may credibly provide.

2. **Microphysics of precipitation**. This is the framework through which to understand the links between interactive water vapor, aerosol, cloud and precipitation processes. Global measurements of microphysics are important to avoid overfitting the models to specific places when tuning the empirical parameters, which is the standard procedure to adjust models to observations (Voosen, 2016). CRMs with advanced microphysical schemes have been used to study the interactions between aerosol, cloud and precipitation processes at high resolution. These processes play a critical role in the global water and energy cycle. Validation of CRMs with observational databases is important both to ascertain the fidelity of the outputs and to improve the models. The interest in this topic lies in the many uncertainties associated with various microphysics schemes. In part, this reflects the fact that microphysical processes cannot always be measured (or observed) directly. Herein cloud properties, which can be estimated, have been used to validate model results. The spectral bin microphysical (SBM) schemes represent the most sophisticated representations of microphysical processes. They generally perform better in simulating realistic cloud properties and surface precipitation compared with bulk microphysical schemes (Li et al., 2010). SBM schemes have helped to improve the bulk scheme [Lang et al., 2014; Tao et al., 2016a also used the microphysics bin scheme from the Regional Atmospheric Modeling System (RAMS) to parameterize their cloud activation]. However useful, SBM schemes are not perfect, though they are more direct (and realistic) than the bulk MP parameterizations used in GCMs. Uncertainties in these can be expected to be larger.

There are also additional considerations to be made to validate climate models with precipitation datasets drawing on recent results. Apart from time span, spatial resolution and calibration quality of the data, there are very important subjects that need attention:

1. First, we need to consider the way the retrieval of precipitation was conducted. As stated by Stephens and Kummerow (2007), precipitation retrievals from space are highly sensitive to the specific radiative and microphysical model used in the retrieval process. Identifying a cloud as precipitating is not a trivial exercise and can result in large errors that make the dataset almost useless. This is the reason why most recent datasets including observations from passive and active sensors are necessary for improving cloud and precipitation retrievals (Levizzani et al., 2020a, 2020b).

2. The second crucial aspect concerns the precipitation phase. When validating climate models, precipitation type should be known, but this is a kind of knowledge that is far from being totally achieved. For the time being, only data from the MODerate resolution Imaging Spectroradiometer (MODIS) were used to verify climate model outputs such as in the case of Matiu et al. (2020) within the European Coordinated Regional Downscaling Experiment (EURO-CORDEX).

3. However, failure to accurately predict the location, magnitude and frequency of precipitation, including snowfall, heavily impacts climate modeling (for example, Field and Heymsfield, 2015). This is why a number of studies have recently started using observations and climate models to identify deficiencies in the actual modeling and validation approaches. Fowler et al. (2020), for example, show results that underscore the importance of evaluating clouds, their optical properties, and the top-of-the-atmosphere radiation budget in addition to precipitation when performing mesh refinement global simulations. Heymsfield et al. (2020) have been the first to produce a global view of the precipitation process partitioning, using a combination of satellite and global climate modeling data (Figure 2.3.2). They showed that significant differences between satellite- and model-based results are found and the reasons require investigations far more complex than the simple traditional surface precipitation differences. Note also that increasing temperatures may also imply increasing melting level height, which obviously impacts surface precipitation phase and intensity and thus model verification (Prein and Heymsfield, 2020). At the same time, care must be taken in improving frozen hydrometeors representation in the climate models (especially at the regional scale) since large discrepancies (up to 5 times) are found between modeled and observed brightness temperatures in the microwave that may undermine the value of intercomparison results (for example, Rysman et al., 2018).

4. Precipitation intensity at the ground is thus not sufficient to characterize the changing climate. The mean and the other statistical moments are just a first step in validation. Trenberth et al. (2003) argued that advancing understanding and the ability to model and predict the character of precipitation is vital and requires new approaches to examining data and models. The timing, duration and intensity of precipitation can be explored via the diurnal cycle (Betts and Jakob, 2002), whose correct simulation in models remains an unsolved challenge of vital importance in global climate change. This can only be done with truly global datasets such as those derived from satellite observations. Here, reanalyses are expected to play a dominant role in the near future.

5. Observational uncertainty quantification is essential for climate studies, climate model evaluation and statistical post-processing. Recently, Tang et al. (2020) have shown variable performance of the IMERG product with respect to other precipitation datasets and reanalyses. Prein and Gobiet (2017) have in turn demonstrated that differences between global precipitation datasets have the same magnitude as precipitation errors found in regional climate models.

6. Finally, precipitation is the most important process for a deeper understanding of climatic changes, but it is linked to several other processes within the water cycle and thus a combined use of precipitation datasets with other datasets (for example, soil moisture, sea surface temperature, evapotranspiration, wind fields, etc.) is unavoidable when assessing climate model outputs (Levizzani and Cattani, 2019).

After considering all possible caveats in using satellite precipitation datasets for climate model validation, nonetheless we register their increasing use in this field.
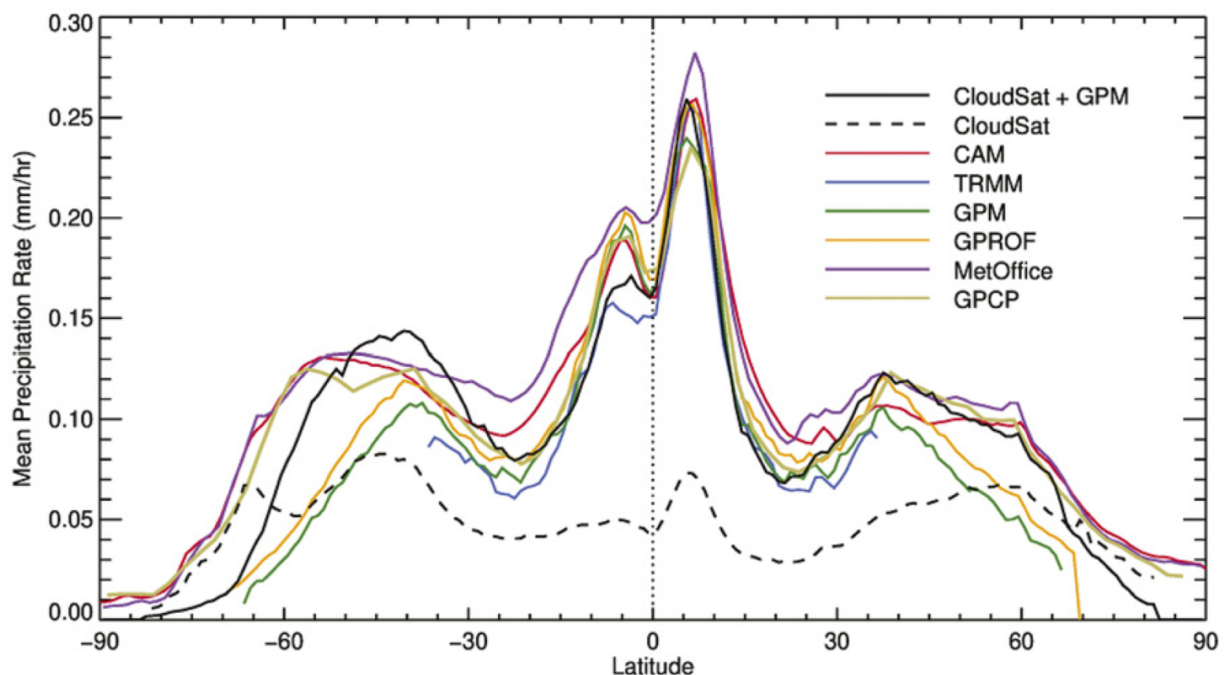
Figure 2.3.2. Mean surface precipitation rate retrieved from CloudSat, Global Precipitation Measurement (GPM) mission, Goddard Profiling (GPROF) algorithm, and Tropical Rainfall Measurement Mission (TRMM), derived from output from the Community Atmosphere Model (CAM) and the Met Office models, and from the Global Precipitation Climatology Project (GPCP) product. These are for land and ocean areas. [from Heymsfield et al. 2020; courtesy American Meteorological Society]. Note that model results are not independent from the satellite observations.

In the RCMs realm, satellite precipitation datasets were widely used during the Coordinated Regional Climate Downscaling Experiment (CORDEX) and the Coupled Model Intercomparison Project (CMIP) both sponsored by the World Climate Research Programme (WCRP) of the WMO. Target areas have been mostly Africa and Asia with special attention to the Tropics using a range of RCMs. Before that, data from the Ensemble-based Predictions of Climate Changes and their Impacts (ENSEMBLES) and Prediction of Regional scenarios and Uncertainties for Defining EuropeaN Climate change risks and Effects (PRUDENCE) projects were used to compare satellite datasets with RCM outputs. Biases of the single model depending on the African region and season were identified during CORDEX while simulating the West African summer monsoon (Akinsanola et al., 2015). In a previous study during CORDEX-Africa, Nikulin et al. (2012) showed that a multimodel average generally outperforms any individual simulation, showing biases of similar magnitude to differences across a number of observational datasets. At the same time, the authors confirmed that a common problem in the majority of the RCMs is that precipitation is triggered too early during the diurnal cycle with differences among the models as first suggested by Dai (2006). More recently, Wu et al. (2020) results show that improvements in the ability of RCMs to simulate precipitation in Africa compared to their driving reanalysis in many cases are simply related to model formulation and not necessarily to higher resolution. Such model formulation-related improvements are strongly model dependent.

The precipitation datasets have proved instrumental also in identifying deficiencies in the simulation of the CMIP5 models. Figure 2.3.3 shows the climatologies of 40 CMIP5 models and several precipitation reference data. Over the Tropics, model output and satellite precipitation dataset intercomparisons represent a substantial added value in identifying strengths and
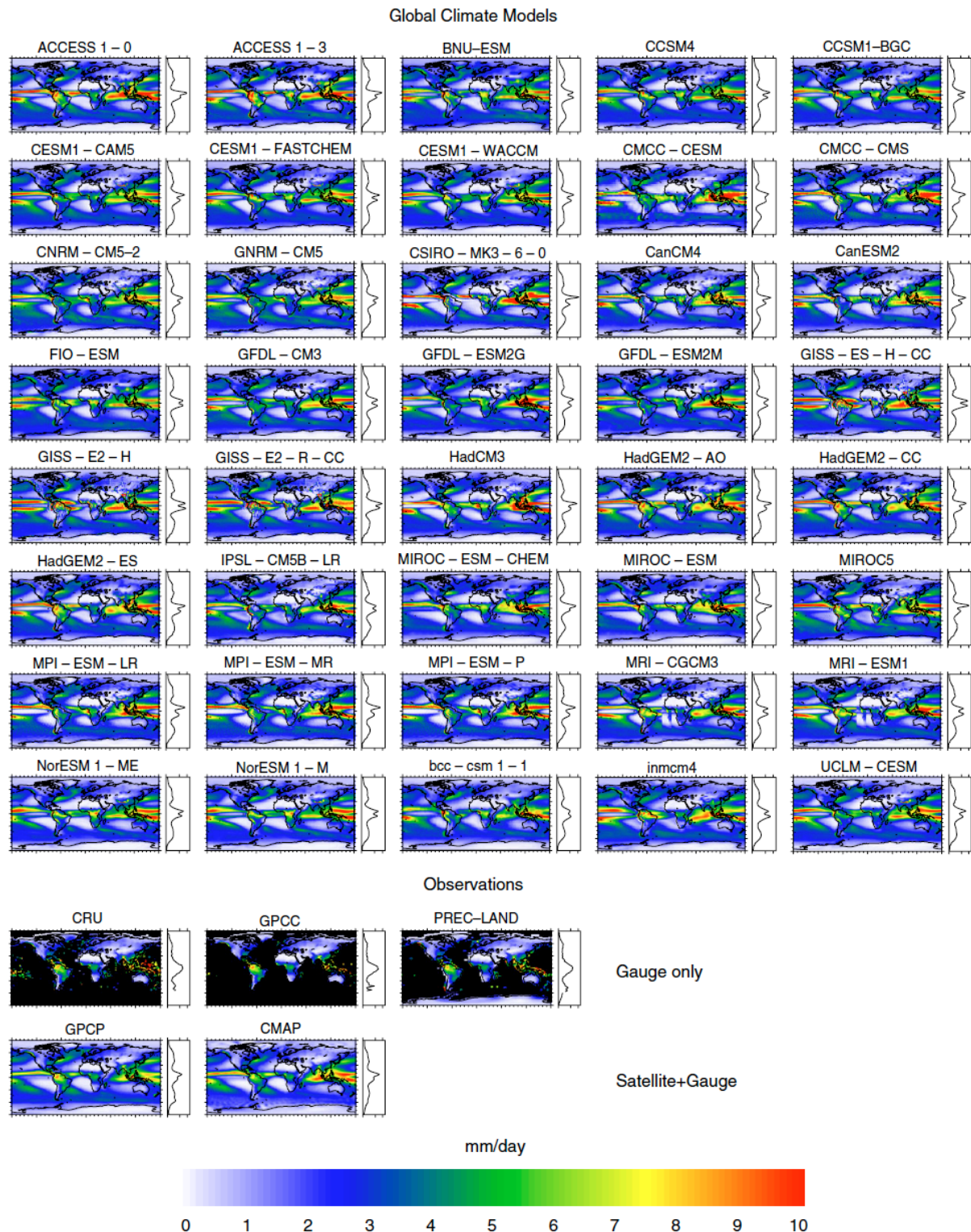
Figure 2.3.3. An example of the use of satellite-derived precipitation datasets in order to validate 40 Global Climate Models (GCMs) and Earth System Models (ESMs). The data represents the 1980–2000 climatology of the mean precipitation. From Tapiador et al. (2018)

weaknesses of the approaches of the various models to predict water cycle changes. For example, when considering one of the key convective areas of the planet, the Congo basin in Central Africa, there appears to be little agreement as to the distribution and quantity of rainfall across the basin with datasets differing by an order of magnitude in some seasons

67

(Washington et al., 2013). Higher-resolution satellite data can surely help in disentangling persisting uncertainties in the area. Over the ocean, the satellite precipitation datasets have contributed to find that precipitation in CMIP5 models is overestimated in most areas (Yang et al., 2018). This is consistent with the previous results of Hirota and Takayabu (2013), who concluded that a proper representation of the sensitivity of deep convection to humidity and higher resolution of the ocean models with better equatorial trades are important for reducing the double ITCZ and the cold tongue biases.

Another key aspect of climate model studies is the need for verifying improvements among different versions of the models and of their ensembles. An example of the application of satellite precipitation datasets is provided by Kumar et al. (2014), whose results show little change in the central tendency, variability, uncertainty of historical skills or consensus across CMIP3 and CMIP5. At the same time, there are regions and seasons where significant changes, performance improvements and even degradation in skills are suggested. This fact clearly demonstrates the potential of using satellite-derived datasets at the global as well as the regional scales. In fact, Pathak et al. (2019) have found that over the south Asian region, some of the convective and large-scale precipitation biases are common across CMIP5 model groups, emphasizing that although on a global scale the bias patterns may be sufficiently different to cluster the models into different groups, regionally, it may not be true.

Substantial work is still needed in examining the ability of both satellite observations and models in capturing extremes, droughts and floods. While observations need to be done at very high resolution and for long time periods, posing problems for using the available global datasets, models need to better represent convection. Kendon et al. (2019) argue that with a more accurate representation of convection in the models, projected changes in both wet and dry extremes over Africa may be more severe than they are actually predicted. Such conclusions need, however, to be linked to the way we conduct intercomparisons and numerical experiments. Recently, Yosef et al. (2020) have concluded that the use of percentile-based indices, such as those of the Expert Team on Climate Change Detection and Indices (ETCCDI), gives very different results when choosing a base period that included records from the last two decades (e.g., 1981–2010, 1988–2017) over Israel. At the same time, Alexander et al. (2019) argue that to advance the use of satellite precipitation data in the applications on extremes differences between data products, limitations in satellite-based estimation processes, and the inherent challenges of scale need to be better understood. Several efforts are on their way in recent times to come to the production of global datasets able to account for extremes (for example, Beck et al., 2020). We will most surely witness an intense activity in this field because it is crucial for climate change studies and to make sure that global precipitation datasets contain the necessary information for all types of events, especially the most severe ones that should be linked to changed climatic conditions.

Alongside research for clarifying the number and intensity of extremes per se, one more subject has come up in recent times. The understanding of short-duration rainfall extremes is also crucial, but data are often subject to errors and inhomogeneities and these events are poorly quantified in projections of future climate change. Consequently, knowledge of the processes contributing to intense, short-duration rainfall is less complete compared with those on daily timescales as argued by Blenkinsop et al. (2018) who launched the project INTENSE to overcome this lack of knowledge via sub-daily gauge dataset collection. Satellite datasets should help in this direction as they acquire higher temporal resolution.

2.3.3. References

Akinsanola, A.A., K.O. Ogunjobi, I.E. Gbode and V.O. Ajayi, 2015: Assessing the capabilities of three regional climate models over CORDEX Africa in simulating West African summer monsoon precipitation. *Advances in Meteorology*, 935431, https://doi.org/10.1155/2015/935431.

Alexander, L.V., H.J. Fowler, M. Bador, A. Behrangi, M.G. Donat, R. Dunn, C. Funk, J. Goldie, E. Lewis, M. Rogé, S.I. Seneviratne and V. Venugopal, 2019: On the use of indices to study extreme precipitation on sub-daily and daily timescales. *Environmental Research Letters*, **14**, 125008, https://doi.org/10.1088/1748-9326/ab51b6.

Beck, H.E., S. Westra, J. Tan, F. Pappenberger, G.J. Huffman, T.R. McVicar, G.J. Gründemann, N. Vergopolan, H.J. Fowler, E. Lewis, K. Verbist and E.F. Wood, 2020: PPDIST, global 0.1° daily and 3-hourly precipitation probability distribution climatologies for 1979–2018. *Scientific Data*, **7**, 302, https://doi.org/10.1038/s41597-020-00631-x.

Betts, A.K., and C. Jakob, 2002: Study of diurnal cycle of convective precipitation over Amazonia using a single column model. *Journal of Geophysical Research: Atmospheres*, **107**, D23, ACL 25-1-ACL 25-13, https://doi.org/10.1029/2002JD002264.

Blenkinsop, S., H.J. Fowler, R. Barbero, S.C. Chan, S.B. Guerreiro, E. Kendon, G. Lenderink, E. Lewis, X.-F. Li, S. Westra, L. Alexander, R.P. Allan, P. Berg, R.J.H. Dunn, M. Ekström, J.P. Evans, G. Holland, R. Jones, E. Kjellström, A. Klein-Tank, D. Lettenmaier, V. Mishra, A.F. Prein, J. Sheffield and M.R. Tye, 2018: The INTENSE project: using observations and models to understand the past, present and future of sub-daily rainfall extremes. *Advances in Science and Research*, **15**, 117–126, https://doi.org/10.5194/asr-15-117-2018.

Dai, A., 2006: Precipitation characteristics in eighteen coupled climate models. *Journal of Climate,* **19***(*18*),* 4605–4630, https://doi.org/10.1175/JCLI3884.1.

Erlingis, J.M., J.J. Gourley, P.-E. Kirstetter, E.N. Anagnostou, J. Kalogiros, M.N. Anagnostou and W. Petersen, 2018: Evaluation of operational and experimental precipitation algorithms and microphysical insights during IPHEx. *Journal of Hydrometeorology*, **19**, 113–125, https://doi.org/10.1175/JHM-D-17-0080.1.

Field, P.R., and A.J. Heymsfield, 2015: Importance of snow to global precipitation. *Geophysical Research Letters*, **42**, 9512–9520, https://doi.org/10.1002/2015GL065497.

Fowler, L.D., M.C. Barth and K. Alapaty, 2020: Impact of scale-aware deep convection on the cloud liquid and ice water paths and precipitation using the Model for Prediction Across Scales (MPAS-v5.2). *Geoscientific Model Development*, **13**, 2851–2877, https://doi.org/10.5194/gmd-13-2851-2020.

Grecu, M., W.S. Olson, C.-L. Shie, T.S. L'Ecuyer and W.-K. Tao, 2009: Combining satellite microwave radiometer and radar observations to estimate atmospheric heating profiles. *Journal of Climate*, **22**, 6356–6376, https://doi.org/10.1175/2009JCLI3020.1.

Heymsfield, A.J., C. Schmitt, C-C. J. Chen, A. Bansemer, A. Gettelman, P.R. Field and C. Liu, 2020: Contributions of the liquid and ice phases to global surface precipitation: Observations and global climate modeling. *Journal of the Atmospheric Sciences*, **77**, 2629–2648, https://doi.org/10.1175/JAS-D-19-0352.1.

Hirota, N., and Y.N. Takayabu, 2013: Reproducibility of precipitation distribution over the tropical oceans in CMIP5 multi-climate models compared to CMIP3. *Climate Dynamics*, **41**, 2909–2920, https://doi.org/10.1007/s00382-013-1839-0.

Houze, R.A. Jr., L.A. McMurdie, W.A. Petersen, M.R. Schwaller, W. Baccus, J.D. Lundquist, C.F. Mass, B. Nijssen, S.A. Rutledge, D.R. Hudak, S. Tanelli, G.G. Mace, M.R. Poellot, D.P. Lettenmaier, J.P. Zagrodnik, A.K. Rowe, J.C. DeHart, L.E. Madaus, H.C. Barnes and V. Chandrasekar, 2017: The Olympic Mountains Experiment (OLYMPEX). *Bulletin of the American Meteorological Society*, **98**, 2167–2188, https://doi.org/10.1175/BAMS-D-16-0182.1.

Intergovernmental Panel on Climate Change, 2015: *Climate Change 2014: Synthesis Report*. Contribution of Working Groups I, II and III to the Fifth Assessment Report of the Intergovernmental Panel on Climate Change [Core Writing Team, R.K. Pachauri and L.A. Meyer (eds.)]. IPCC, Geneva, Switzerland, ISBN:978-92-9169-143-2, 151 pp.

Kendon, E.J., R.A. Stratton, S. Tucker, J.H. Marsham, S. Berthou, D.P. Rowell and C.A. Senior, 2019: Enhanced future changes in wet and dry extremes over Africa at convection-permitting scale. *Nature Communications*, **10**, 1794, https://doi.org/10.1038/s41467-019-09776-9.

Kumar, D., E. Kodra and A.R. Ganguly, 2014: Regional and seasonal intercomparison of CMIP3 and CMIP5 climate model ensembles for temperature and precipitation. *Climate Dynamics*, **43**, 1–28, https://doi.org/10.1007/s00382-014-2070-3.

Lang, S., W.-K. Tao, J.-D. Chern, D. Wu and X. Li, 2014: Benefits of a 4th ice class in the simulated radar reflectivities of convective systems using a bulk microphysics scheme. *Journal of the Atmospheric Science*, **71**, 3583–3612, https://doi.org/10.1175/JAS-D-13-0330.1.

Levizzani, V., and E. Cattani, 2019: Satellite remote sensing of precipitation and the terrestrial water cycle in a changing climate. *Remote Sensing*, **11**, 2301, https://doi.org/10.3390/rs11192301.

Levizzani, V., C. Kidd, D.B. Kirschbaum, C.D. Kummerow, K. Nakamura and F.J. Turk (eds.), 2020a: *Satellite Precipitation Measurement*. Vol. 1, Springer Nature, Cham, *Advances Global Change Research*, **67**, 450 pp, https://doi.org/10.1007/978-3-030-24568-9.

Levizzani, V., C. Kidd, D.B. Kirschbaum, C.D. Kummerow, K. Nakamura and F.J. Turk (eds.), 2020b: *Satellite Precipitation Measurement*. Vol. 2, Springer Nature, Cham, *Advances in Global Change Research*, **69**, 712 pp, https://doi.org/10.1007/978-3-030-35798-6.

Li, R.C.Y., W. Zhou, C.M. Shun and T.C. Lee, 2017: Change in destructiveness of landfalling tropical cyclones over China in recent decades. *Journal of Climate*, **30**, 3367–3379, https://doi.org/10.1175/JCLI-D-16-0258.1.

Li, X., W.-K. Tao, T. Matsui, C. Liu and H. Masunaga, 2010: Improving a spectral bin microphysics scheme using TRMM satellite observations. *Quarterly Journal of the Royal Meteorological Society*, **136**, 382–399, https://doi.org/10.1002/qj.569.

Ling, J., and C. Zhang, 2011: Diabatic heating profiles in recent global reanalyses. *Journal of Climate*, **26**, 3307-3325, https://doi.org/10.1175/JCLI-D-12-00384.1.

Machado, L.A.T., M.A.F. Silva Dias, C. Morales, G. Fisch, D. Vila, R. Albrecht, S.J. Goodman, A.J.P. Calheiros, T. Biscaro, C. Kummerow, J. Cohen, D. Fitzjarrald, E.L. Nascimento, M.S.

Sakamoto, C. Cunningham, J.-P. Chaboureau, W.A. Petersen, D.K. Adams, L. Baldini, C.F. Angelis, L.F. Sapucci , P. Salio, H.M.J. Barbosa, E. Landulfo, R.A.F. Souza, R.J. Blakeslee, J. Bailey, S. Freitas, W.F.A. Lima and A. Tokay, 2014: The Chuva Project: How does convection vary across Brazil? *Bulletin of the American Meteorological Society*, 95, 1365–1380, https://doi.org/10.1175/BAMS-D-13-00084.1.

Matiu, M., M. Petitta, C. Notarnicola and M. Zebisch, 2020: Evaluating snow in EURO-CORDEX regional climate models with observations for the European Alps: Biases and their relationship to orography, temperature, and precipitation mismatches. *Atmosphere*, **11**, 46, https://doi.org/10.3390/atmos11010046.

Neale, R.B., J.H. Richter and M. Jochum, 2008: The impact of convection on ENSO: From a delayed oscillator to a series of events. *Journal of Climate*, **21**, 5904-5924, https://doi.org/10.1175/2008JCLI2244.1.

Nikulin, G., C. Jones, F. Giorgi, G. Asrar, M. Büchner, R. Cerezo-Mota, O. Bøssing Christensen, M. Déqué, J. Fernandez, A. Hänsler, E. van Meijgaard, P. Samuelsson, M. Bamba Sylla and L. Sushama, 2012: Precipitation climatology in an ensemble of CORDEX-Africa regional climate simulations. *Journal of Climate*, **25**, 6057–6078, https://doi.org/10.1175/JCLI-D-11-00375.1.

Pathak, R., S. Sahany, S.K. Mishra and S.K. Dash, 2019: Precipitation biases in CMIP5 models over the South Asian region. *Scientific Reports*, **9**, 9589, https://doi.org/10.1038/s41598-019-45907-4.

Prein, A.F., and A. Gobiet, 2017: Impacts of uncertainties in European gridded precipitation observations on regional climate analysis. *International Journal of Climatology*, **37**, 305–327, https://doi.org/10.1002/joc.4706.

Prein, A.F., and A.J. Heymsfield, 2020: Increased melting level height impacts surface precipitation phase and intensity. *Nature Climate Change*, https://doi.org10.1038/s41558-020-0825-x.

Rysman, J.-F., S. Berthou, C. Claud, P. Drobinski, J.-P. Chaboureau and J. Delanoë, 2018: Potential of microwave observations for the evaluation of rainfall and convection in a regional climate model in the frame of HyMeX and MED-CORDEX. *Climate Dynamics*, **51**, 837–855, https://doi.org/10.1007/s00382-016-3203-7.

Simpson, J., R.F. Adler and R.F. North, 1988: A proposed Tropical Rainfall Measuring Mission (TRMM) satellite. *Bulletin of the American Meteorological Society*, **69**, 278–295, https://doi.org/10.1175/1520-0477(1988)069<0278:APTRMM>2.0.CO;2.

Simpson, J., C. Kummerow, W.-K. Tao and R.F. Adler, 1996: On the Tropical Rainfall Measuring Mission (TRMM). *Meteorology and Atmospheric Physics*, **60**, 19–36, https://doi.org/10.1007/BF01029783.

Smith, L.A., 2002: What might we learn from climate forecasts? *Proceedings of the National Academy of Sciences of the United States of America*, **99**, 2478–2492, https://doi.org/10.1073/pnas.012580599.

Stephens, G.L., and C.D. Kummerow, 2007: The remote sensing of clouds and precipitation from space: A review. *Journal of the Atmospheric Sciences*, **64**, 3742–3765, https://doi.org/10.1175/2006JAS2375.1.

Stephens, G.L., T. L'Ecuyer, R. Forbes, A. Gettlemen, J.-C. Golaz, A. Bodas-Salcedo, K. Suzuki, P. Gabriel and J. Haynes, 2010: Dreary state of precipitation in global models. *Journal of Geophysical Research: Atmospheres*, **115**, D24211, https://doi.org/10.1029/2010JD014532.

Sun, Y., S. Solomon, A. Dai and R.W. Portmann, 2006: How often does it rain? *Journal of Climate*, **19**, 916–934, https://doi.org/10.1175/JCLI3672.1.

Tang, G., M.P. Clark, S.M. Papalexiou, Z. Ma and Y. Hong, 2020: Have satellite precipitation products improved over last two decades? A comprehensive comparison of GPM IMERG with nine satellite and reanalysis datasets. *Remote Sensing of Environment*, **240**, 111696, https://doi.org/10.1016/j.rse.2020.111697.

Tao, W.-K., S. Lang, W. Olson, R. Meneghini, Y. Yang, J. Simpson, C. Kummerow, E. Smith and J. Halverson, 2001: Retrieved vertical profiles of latent heat release using TRMM rainfall products for February 1998. *The Journal of Applied Meteorology and Climatology*, **40**, 957–982, https://doi.org/10.1175/1520-0450(2001)040%3C0957:RVPOLH%3E2.0.CO;2.

Tao, W.-K., E. Smith, R. Adler, Z. Haddad, A. Hou, T. Iguchi, R. Kakar, T.N. Krishnamurti, C. Kummerow, S. Lang, R. Meneghini, N. Nakamura, T. Nakazawa, K. Okamoto, W. Olson, S. Satoh, S. Shige, J. Simpson, Y. Takayabu, G. Tripoli and S. Yang, 2006: Retrieval of latent heating from TRMM measurements. *Bulletin of the American Meteorological Society*, **87**, 1555–1572, https://doi.org/10.1175/BAMS-87-11-1555.

Tao, W.-K., D. Wu, S. Lang, J. Chern, A. Fridlind, C. Peters-Lidard and T. Matsui, 2016a: High-resolution model simulations of MC3E, deep convective-precipitation systems: Comparisons between Goddard microphysics schemes and observations. *Journal of Geophysical Research: Atmospheres*, **121**, 1278–1306, https://doi.org/10.1002/2015JD023986.

Tao, W.-K., Y.N. Takayabu, S. Lang, S. Shige, W. Olson, A. Hou, G. Skofronick-Jackson, X. Jiang, C. Zhang, W. Lau, T. Krishnamurti, D. Waliser, M. Grecu, P.E. Ciesielski, R.H. Johnson, R. Houze, R. Kakar, K. Nakamura, S. Braun, S. Hagos, R. Oki and A. Bhardwaj, 2016b: TRMM latent heating retrieval: Applications and comparisons with field campaigns and large-scale analyses. *Meteorological Monographs*, **56**, 2.1–2.34, https://doi.org/10.1175/AMSMONOGRAPHS-D-15-0013.1.

Tapiador, F.J., 2010: A joint estimate of the precipitation climate signal in Europe using eight regional models and five observational datasets. *Journal of Climate*, **23(7)**, 1719–1738, https://doi.org/10.1175/2009JCLI2956.1.

Tapiador, F.J., A. Navarro, A. Jiménez, R. Moreno and E. García-Ortega, 2018: Discrepancies with satellite observations in the spatial structure of global precipitation as derived from global climate models. *Quarterly Journal of the Royal Meteorological Society*, **144**, 419–435, https://doi.org/10.1002/qj.3289.

Tapiador, F.J., A. Navarro, V. Levizzani, E. García-Ortega, G.J. Huffman, C. Kidd, P.A. Kucera, C.D. Kummerow, H. Masunaga, W.A. Petersen, R. Roca, J.-L. Sánchez, W.-K. Tao and F.J. Turk, 2017: Global precipitation measurements for validating climate models. *Atmospheric Research*, **197**, 1–20, https://doi.org/10.1016/j.atmosres.2017.06.021.

Tapiador, F.J., R. Roca, A. Del Genio, B. Dewitt, W. Petersen and F. Zhang, 2019: Is precipitation a good metric for model performance? *Bulletin of the American Meteorological Society*, **100**(2), 223–233, https://doi.org/10.1175/BAMS-D-17-0218.1.

Trenberth, K.E., A. Dai, R.M. Rasmussen and D.B. Parsons, 2003: The changing character of precipitation. *Bulletin of the American Meteorological Society*, **84**, 1205–1218, https://doi.org/10.1175/BAMS-84-9-1205.

vanZanten, M.C., and B. Stevens, 2005: Observations of the structure of heavily precipitating marine stratocumulus. *Journal of the Atmospheric Sciences*, **62**, 4327– 4342, https://doi.org/10.1175/JAS3611.1.

Voosen, P., 2016: Climate scientists open up their black boxes to scrutiny. *Science*, **354**, 401–402, https://doi.org/10.1126/science.354.6311.401.

Washington, R., R. James, H. Pearce, W.M. Poka, and W. Moufouma-Okia, 2013: Congo Basin rainfall climatology: Can we believe the climate models? *Philosophical Transactions of the Royal Society B: Biological Sciences*, **368**, 20120296, https://doi.org/10.1098/rstb.2012.0296.

Wu, M., G. Nikulin, E. Kjellström, D. Belušić, C. Jones and D. Lindstedt, 2020: The impact of regional climate model formulation and resolution on simulated precipitation in Africa. *Earth System Dynamics*, **11**, 377–394, https://doi.org/10.5194/esd-11-377-2020.

Yang, M., G.J. Zhang and D.-Z. Sun, 2018: Precipitation and moisture in four leading CMIP5 models: Biases across large-scale circulation regimes and their attribution to dynamic and thermodynamic factors. *Journal of Climate*, **31**, 5089–5106, https://doi.org/10.1175/JCLI-D-17-0718.1.

Yosef, Y., E. Aguilar and P. Alpert, 2020: Is it possible to fit extreme climate change indices together seamlessly in the era of accelerated warming? *International Journal of Climatology*, https://doi.org/10.1002/joc.6740.

2.4. Intercomparison of products for climate applications

Hirohiko Masunaga[1], Fumie F. Akimoto[1], Takuji Kubota[2], Chris Kummerow[3] and Marc Schröder[4]

[1] Institute for Space-Earth Environmental Research, Nagoya University, Nagoya, Japan

[2] Earth Observation Research Center, Japan Aerospace Exploration Agency, Tsukuba, Japan

[3] Department of Atmospheric Science, Colorado State University, Fort Collins, CO, USA

[4] Satellite-Based Climate Monitoring, Deutscher Wetterdienst, Offenbach, Germany

2.4.1. Introduction

Observational datasets of global precipitation are widely used for a range of climate applications, including atmospheric water and energy budget analyses (section 2.1) and climate model assessment (section 2.3), as well as meteorological studies on regional scales (for example, extreme events, see section 2.5) and synoptic scales (for example, tropical disturbances such as MJO). The precipitation products, however, are not strictly a "true" representation of nature but have their own uncertainties related to issues such as sampling errors and algorithmic assumptions. Extensive efforts have been made to document the biases in existing precipitation products. Such studies include the systematic assessment of numerous products on a global scale (for example, Gruber and Levizzani, 2008; Gehne et al., 2016; Beck et al., 2017; Sun et al., 2018) as well as a large body of literature on regional (typically continental-scale) intercomparisons (see review by Maggioni et al., 2016).

This assessment report is a concise update to existing efforts on the assessment of global precipitation products. Particular attention is paid to the potential bias characteristics in geographical pattern, ocean-land contrasts and mean versus extreme precipitation.

2.4.2. Data

In this sub-chapter, we analyze 11 global products consisting of the Climate Hazards Group InfraRed Precipitation with Station version 2 (CHIRPS v2.0, Funk et al., 2015), CMORPH v1.0 (Joyce et al., 2004; Xie et al., 2017), CPC v1.0 (Xie et al., 2007), GPCC Full Data Daily v2018 (Becker et al., 2013; Ziese et al., 2018), GPCP v1.3 daily (Huffman et al., 2001), GSMaP v6 (Kubota et al., 2007, 2020), Hamburg Ocean Atmosphere Parameters and Fluxes from Satellite Data (HOAPS) v4.0 (Andersson et al., 2010), IMERG v5 (Huffman et al., 2015, 2020), PERSIANN-CDR v1r1 (Ashouri et al., 2015), the Tropical Amount of Rainfall with Estimation of ERors (TAPEER) v1.5 (Roca et al., 2018), and TRMM Precipitation L3 1 day 0.25 degree x 0.25 degree V7 (TRMM 3B42 V7; Huffman et al., 2007). Note that HOAPS is an over-ocean product and the CHIRPS, CPC and GPCC data are available only over land. All estimates are adjusted to a daily 1°×1° grid in accordance with the FROGS data format (Roca et al., 2019). The analysis shown here is largely based on the results recently published by Masunaga et al. (2019).

Among these products, CMORPH, GPCP, GSMaP, IMERG, TAPEER and TRMM 3B42 all rely on the Low Earth Orbit (LEO) microwave radiometry and/or sounding data for baseline estimates of precipitation, with the GEO infrared measurements incorporated to fill in spatial and temporal gaps (see Section 1.1 for extended discussion on the methodology and error characterizations). In GPCP, GSMaP, IMERG and 3B42, a further adjustment is made with in situ measurements from gauge networks over land. See the individual documents cited above for product-specific details in the algorithmic strategy.

2.4.3. Results

Figure 2.4.1 shows the global (60°S-60°N) mean precipitation for different products with the daily data aggregated over 20 years from 1998 to 2017. The oceanic mean precipitation ranges from 2.39 mm/d to 3.4 mm/d, and the land mean precipitation varies between 1.81 mm/d and 2.28 mm/d. Note that the two gauge-only products (CPC and GPCC) largely disagree against each other, suggesting that uncertainties specific to gauge measurements such as sampling errors and the wind-induced undercatch may be as much responsible for the inter-product discrepancies as retrieval uncertainties in satellite algorithms (see section 1.2 for additional discussion on the utility and limitations of gauge measurements). This discrepancy partially accounts for the spread over land in the merged products as well, since IMERG is adjusted to GPCC over land and the daily GPCP is calibrated with GPCC through the monthly GPCP, while GSMaP and CMORPH adopt CPC for the gauge correction.
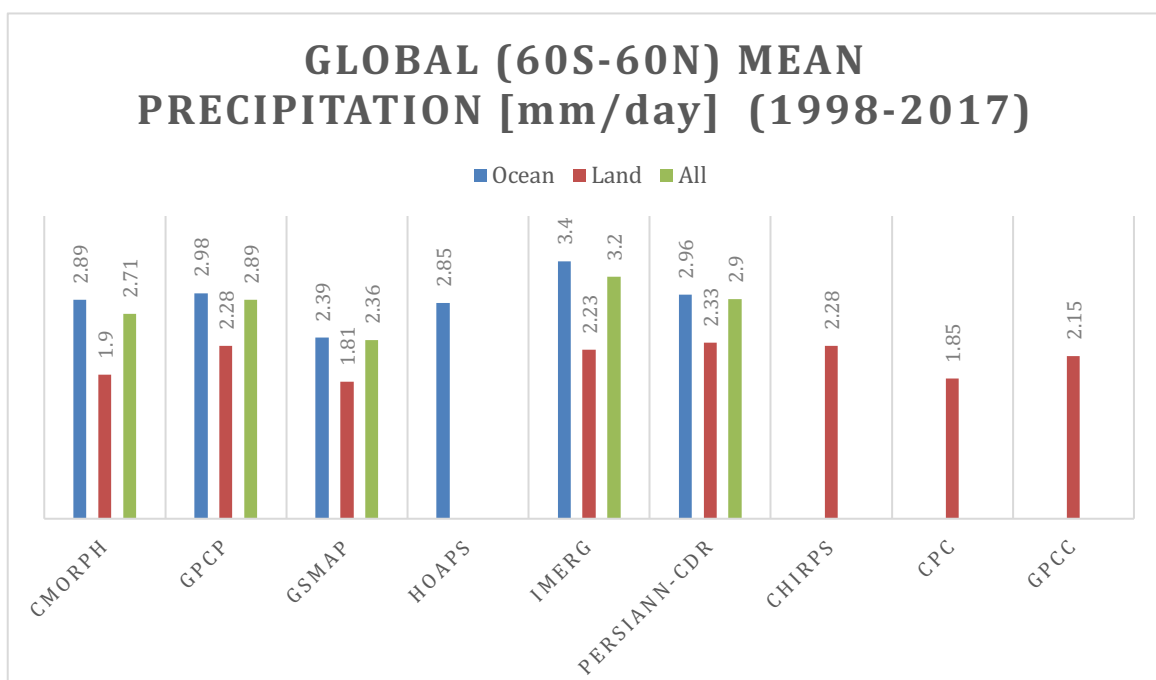

Figure 2.4.1. Global mean precipitation (mm/d) for each product (60°S-60°N, 1998–2017) over ocean (blue), land (orange) and all surfaces (gray). TAPEER and TRMM 3B42 are not included because these datasets do not cover the whole 60°S-60°N band.

Figure 2.4.2 presents the zonal-mean precipitation of different products for the year of 2015. All products qualitatively agree in the meridional structure of precipitation. A systematic bias, however, is evident in a quantitative sense, with the peak rainfall over ocean, representing the ITCZ, varying from 7 mm/d to 9 mm/d. The zonal-mean precipitation agrees better in the sub-tropics, but the spread expands over ocean for latitudes higher than 40°, where lighter precipitation that is difficult for radiometers to separate from cloud water, as well as some solid precipitation, makes the retrieval technically challenging (see also section 3.1). GSMaP marks the lowest while IMERG hits the highest at high latitudes as found in the global mean precipitation (Figure 2.4.1), while this order is reversed in the tropics. The uncertainty at high latitudes is a primary driver of the inter-product spread in the global-mean precipitation. Precipitation over land in the northern high latitudes reasonably agrees among different products, presumably owning to the dense gauge networks there to which satellite estimates are adjusted.
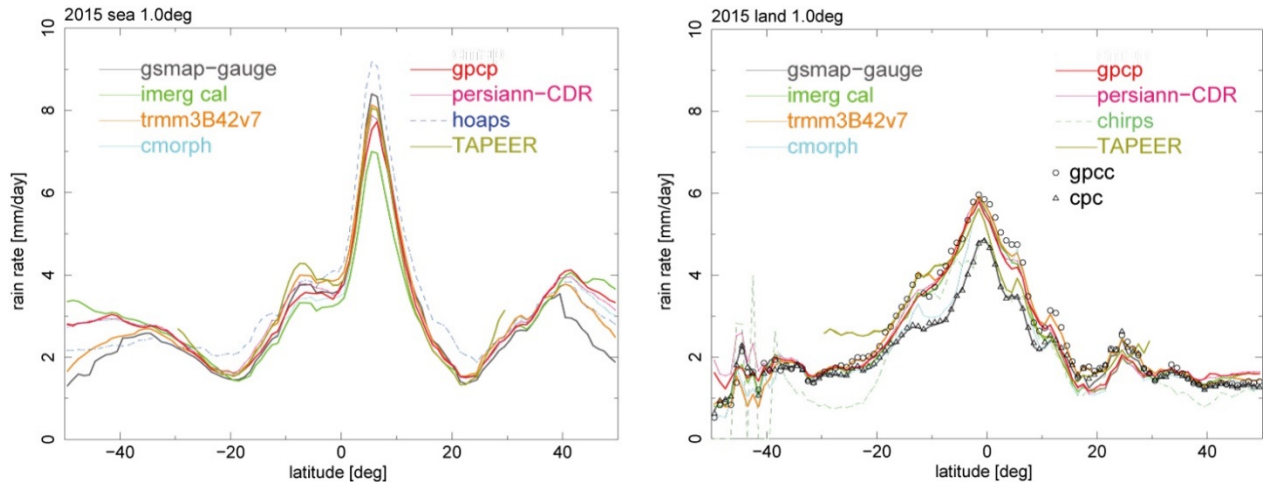
Figure 2.4.2. Zonal mean precipitation (mm/d) over ocean (left) and over land (right) for the year of 2015. Adopted from Masunaga et al. (2019)

The global distribution of all the products averaged together and the anomalous geographical pattern for selected products from the ensemble mean is depicted in Figure 2.4.3. The GSMaP annual-mean precipitation is higher in the Pacific ITCZ and lower elsewhere than the ensemble mean, while the IMERG precipitation is just opposite in geographical pattern to GSMaP. This striking contrast is somewhat surprising, given that GSMaP and IMERG share aspects of the fundamental product design such as the native grid resolution (0.5°), temporal sampling (hourly for GSMaP and half-hourly for IMERG), and the overall algorithmic flow (LEO microwave → GEO infrared morphing → gauge adjustment). When compared in extreme (ninety-ninth percentile) precipitation, GSMaP and IMERG, however, have fundamentally different anomaly patterns relative to their annual means. Both the two products stay lower than the ensemble mean across global oceans, while the anomaly is opposite in sign over land. This particular case offers an illustrative example that the bias characteristics in the climatological precipitation are generally a poor predictor of the extreme rain biases. See Masunaga et al. (2019) for the global maps of the other products included in the assessment.
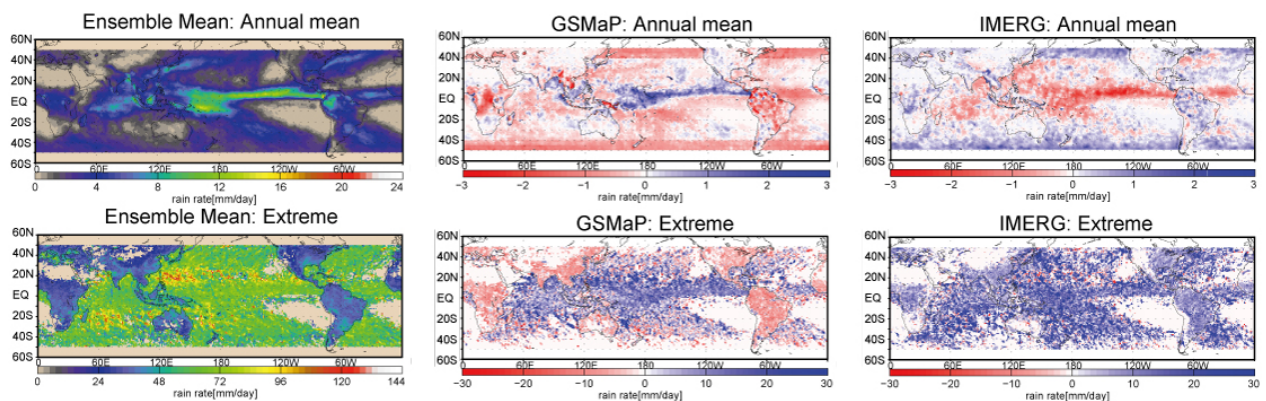

Figure 2.4.3. Global map of annual-mean precipitation (top) and ninety-ninth percentile extreme precipitation or R99p (bottom) for the year of 2015. The ensemble mean of all products (left) and the anomaly from the ensemble mean for selected products: GSMaP (middle) and IMERG (right). Adopted from Masunaga et al. (2019)

Finally, the deseasonalized time series of different products are shown in Figure 2.4.4. Different curves are found to be clustered into a few groups rather than spread widely. The monthly-mean precipitation agrees relatively well over oceans with the exception of GSMaP, staying somewhat lower. Some products exhibit more pronounced interannual variability than others: HOAPS has a striking peak associated with the 1997 El Niño, and PERSIANN shows a sharp minimum of unknown origin in 2017. Over land, the monthly-mean precipitation appears to be divided into two groups anchored to the two-gauge products (GPCC and CPC). This may be partly due to the gauge adjustment procedure carried out in each product. The ninety-ninth percentile extremes are spread more widely than the monthly mean. Oceanic extremes in GPCP and PERSIANN, the latter of which is adjusted to the former in monthly mean, are modest in intensity relative to other datasets. As such, the bias characteristics specific to each product are essentially different between the mean and extreme precipitation as noted above.
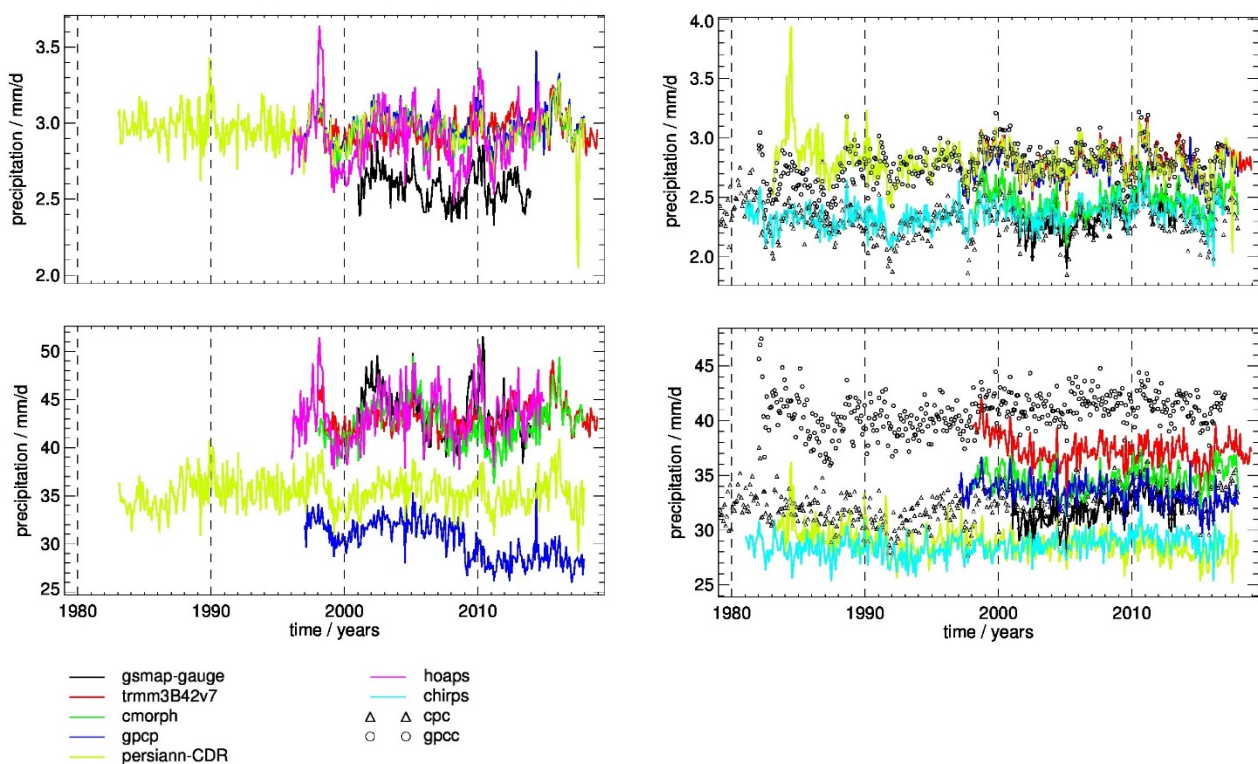
Figure 2.4.4. Time series of monthly mean precipitation with the annual cycle being removed: global ocean (left column) and global land within 50°N/S (right column), mean over all defined values (top row), and ninety-ninth percentile (bottom row). Adopted from Masunaga et al. (2019)

2.4.4. Fitness of gridded daily observations for different applications

Spatial and temporal resolutions and the period of data record depend largely on the products. Those with fine grid intervals include CHIRPS (0.05°) and GSMaP and IMERG (0.1°). The temporal sampling is as dense as half-hourly for IMERG and hourly for GSMaP. The data record dates back to the late nineteenth century for a monthly version of GPCC, but is otherwise limited to more recent decades. Most satellite-based products are available only after late 1990s with a few exceptions, including the monthly GPCP, which is available for 1979 onwards. The products with fine resolutions may be of great utility for regional hazard monitoring, while those with decades of data record would be optimal for climate studies focused on long-term changes in the water cycle. It is noted that a grid size as small as 0.1°

does not necessarily guarantee that the information content is as fine as 10 km, since low-frequency microwave FOVs are significantly larger than 10 km.

Among the critical requirements for operational applications is data latency. Many of the products (CMORPH, GSMaP, IMERG, and PERSIANN, for instance) offer a near-real-time option in which the data are distributed to the users as quickly as possible at the expense of accuracy (for example, Kubota et al., 2020). The same products often provide a better calibrated version at a later time for general users who prioritize reliability over latency.

This assessment is not intended to show which product is "better" than another because the absolute reference does not exist. One of the primary goals of the assessment is to document the characteristics of structural bias in hopes to help the dataset providers further refine the algorithm. The intercomparison results shown above would change as the participating products are upgraded to future versions. The assessment will need to be regularly updated as well to accommodate the continuous evolution of the products.

2.4.5. Summary

We presented in this sub-chapter an intercomparison of 11 global precipitation datasets. Major conclusions are:

i. While the overall geographical pattern of precipitation is coherent among products, the magnitude varies from one dataset to the other. The agreement is poor particularly at high latitudes, since light and/or solid precipitation typical of high latitudes is difficult to estimate accurately from satellite microwave radiometry.

ii. A systematic bias is present between gridded gauge products (GPCC and CPC), which is presumably partially responsible for the spread in merged multi-satellite datasets adjusted to the gauge products.

iii. The bias characteristics in the annual/monthly mean precipitation are a poor predictor of those in extreme precipitation.

2.4.6. Recommendations

Specific recommendations to this chapter are:

i. An accurate estimation of the tropical precipitation is important as an observational constraint on the tropical dynamics (Hadley cells, MJO, etc.) and the Earth energy budget. The current uncertainty in the ITCZ rainfall (7 mm/d–9 mm/d) could be problematic and further effort is urged to reconcile this discrepancy.

ii. The inter-product spread is large at latitudes higher than 40°S/N. This high-latitude uncertainty is among the major factors responsible for the disagreement in the global-mean precipitation. To mitigate this issue, further improvement is critically important on the estimation of cold-season precipitation. The difficulty in separating cloud water from light rainfall is likely another source of uncertainty in the microwave retrieval of precipitation and requires better modeling in the algorithm.

iii. Many products apply a gauge adjustment to satellite-based precipitation estimates over land. The present intercomparison reveals that the uncertainties intrinsic of gridded gauge datasets (GPCC and CPC) can be a bottleneck for all the products internally using these data as a reference. Better consistency between different gauge products is critically desired.

iv.   Uncertainties in accumulations have not been reduced significantly from many regional validation studies. More emphasis on physically derived uncertainties for weather and climate applications will be critical to gain confidence in these products going forward.

2.4.7. References

Andersson, A., K. Fennig, C. Klepp, S. Bakan, H. Grassl and J. Schulz, 2010: The Hamburg Ocean Atmosphere Parameters and Fluxes from Satellite Data - HOAPS-3. *Earth System Science Data*, **2**, 215–234.

Ashouri, H., K.-L. Hsu, S. Sorooshian, D.K. Braithwaite, K.R. Knapp, L.D. Cecil, B.R. Nelson and O.P. Prat, 2015: PERSIANN-CDR: Daily precipitation climate data record frommulti-satellite observations for hydrological and climate studies. *Bulletin of the American Meteorological Society*, 96, 69–83.

Beck, H.E., N. Vergopolan, M. Pan, V. Levizzani, A.I.J.M. Van Dijk, G.P. Weedon, L. Brocca, F. Pappenberger, G.J. Huffman and E.F. Wood, 2017: Global-scale evaluation of 22 precipitation datasets using gauge observations and hydrological modeling. *Hydrology and Earth System Sciences*, 21(12), 6201–6217, doi:10.5194/hess-21-6201-2017.

Becker, A., P. Finger, A. Meyer-Christoffer, B. Rudolf, K. Schamm, U. Schneider and M. Ziese, 2013: A description of the global land-surface precipitation data products of the Global Precipitation Climatology Centre with sample applications including centennial (trend) analysis from 1901–present. *Earth System Science Data*, **5**, 71–99.

Funk, C., P. Peterson, M. Landsfeld, D. Pedreros, J. Verdin, S. Shukla, G. Husak, J. Rowland, L. Harrison, A. Hoell and J. Michaelsen, 2015: The climate hazards infrared precipitation with stations–A new environmental record for monitoring extremes. *Scientific Data,* **2,** 1–21.

Gehne, M., T.M. Hamill, G.N. Kiladis and K.E. Trenberth, 2016: Comparison of global precipitation estimates across a range of temporal and spatial scales. *Journal of Climate*, 29, 7773–7795.

Gruber, A., and V. Levizzani (eds.), 2008: *Assessment of global precipitation products*. WCRP Series Report No. 128 and WMO TD−no. 1430, Geneva.

Huffman, G.J., R.F. Adler, M.M. Morrissey, D.T. Bolvin, S. Curtis, R. Joyce, B. McGavock and J. Susskind, 2001: Global Precipitation at One-Degree Daily Resolution from Multisatellite Observations, *Journal of Hydrometeorology*, **2,** 36–50.

Huffman, G.J., R.F. Adler, D.T. Bolvin, G. Gu, E.J. Nelkin, K.P. Bowman, Y. Hong, E.F. Stocker and D.B. Wolff, 2007: The TRMM Multi-satellite Precipitation Analysis: Quasi-global, multi-year, combined-sensor precipitation estimates at fine scale. *Journal of Hydrometeorology,* **8**, 38–55.

Huffman, G.J., D.T. Bolvin and E.J. Nelkin, 2015: *Day 1 IMERG Final Run Release Notes.* https://gpm.nasa.gov/sites/default/files/document_files/IMERG_FinalRun_Day1_release_notes.pdf.

Huffman, G.J., D.T. Bolvin, D. Braithwaite, K.-L. Hsu, R.J. Joyce, C. Kidd, E. J. Nelkin, S. Sorooshian, E.F. Stocker, J. Tan, D.B. Wolff and P. Xie, 2020: Integrated Multi-satellite Retrievals for the Global Precipitation Measurement (GPM) Mission (IMERG). In: *Satellite Precipitation Measurement* (V. Levizzani, C. Kidd., D.B. Kirschbaum, C.D. Kummerow, K.

Nakamura, F.J. Turk, eds.). Springer Nature, Cham, Advances in Global Change Research, 67, 343–353, https://doi.org/10.1007/978-3-030-24568-9_19.

Joyce, R.J., J.E. Janowiak, P.A. Arkin and P. Xie, 2004: CMORPH: A Method that Produces Global Precipitation Estimates from Passive Microwave and Infrared Data at High Spatial and Temporal Resolution. *Journal of Hydrometeorology*, **5,** 487–503.

Kubota, T., S. Shige, H. Hashizume, A. Aonashi, N. Takahashi, S. Seto, M. Hirose, Y.N. Takayabu, T. Ushio, K. Nakagawa, K. Iwanami, M. Kachi and K. Okamoto, 2007: Global Precipitation Map Using Satellite-Borne Microwave Radiometers by the GSMaP Project: Production and Validation. *IEEE Transactions on Geoscience and Remote Sensing*, **45**, 2259–2275.

Kubota, T., K. Aonashi, T. Ushio, S. Shige, Y.N. Takayabu, M. Kachi, Y. Arai, T. Tashima, T. Masaki, N. Kawamoto, T. Mega, M.K. Yamamoto, A. Hamada, M. Yamaji, G. Liu and R. Oki, 2020: Global Satellite Mapping of Precipitation (GSMaP) products in the GPM era. In: *Satellite Precipitation Measurement* (V. Levizzani, C. Kidd., D. B. Kirschbaum, C. D. Kummerow, K. Nakamura, F.J. Turk, eds.), Springer Nature, Cham, Advances in Global Change Research, 67, 355–373, https://doi.org/10.1007/978-3-030-24568-9_20.

Maggioni, V., P. Meyers and M. Robinson, 2016: A review of merged high resolution satellite precipitation product accuracy during the Tropical Rainfall Measuring Mission (TRMM)-Era. *Journal of Hydrometeorology,* **17,** 1101–1117.

Masunaga, H., M. Schröder, F.A. Furuzawa, C. Kummerow, E. Rustemeier and U. Schneider, 2019: Inter-product biases in global precipitation extremes. *Environmental Research Letters*, **14**, 125016, doi:10.1088/1748-9326/ab5da9.

Roca, R., N. Taburet, E. Lorant, P. Chambon, M. Alcoba, H. Brogniez, S. Cloché, C. Dufour, M. Gosset and C. Guilloteau, 2018: Quantifying the contribution of the Megha-Tropiques mission to the estimation of daily accumulated rainfall in the Tropics. *Quarterly Journal of the Royal Meteorological Society*, **144** (Suppl. 1), 49–63.

Roca, R., L.V. Alexander, G. Potter, M. Bador, R. Jucá, S. Contractor, M.G. Bosilovich and S. Cloché, 2019: FROGS: a daily 1° × 1° gridded precipitation database of rain gauge, satellite and reanalysis products. *Earth System Science Data*, 11, 1017–1035, https://doi.org/10.5194/essd-11-1017-2019.

Sun, Q., C. Miao, Q. Duan, H. Ashouri, S. Sorooshian and K.L. Hsu, 2018: A Review of Global Precipitation Data Sets: Data Sources, Estimation, and Intercomparisons. *Reviews of Geophysics*, 56(1), 79–107, doi:10.1002/2017RG000574.

Xie, P., A. Yatagai, M. Chen, T. Hayasaka, Y. Fukushima, C. Liu and S. Yang, 2007: A gauge-based analysis of daily precipitation over East Asia. *Journal of Hydrometeorology*, **8**, 607–626.

Xie, P., R. Joyce, S. Wu, S. Yoo, Y. Yarosh, F. Sun and R. Lin, 2017: Reprocessed, Bias-Corrected CMORPH Global High-Resolution Precipitation Estimates from 1998. *Journal of Hydrometeorology*, **18**, 1617–1641.

Ziese, M., A. Rauthe-Schöch, A. Becker, P. Finger, A. Meyer-Christoffer and U. Schneider, 2018: GPCC Full Data Daily Version 2018 at 1.0°: Daily Land-Surface Precipitation from Rain-Gauges built on GTS-based and Historic Data. DOI: 10.5676/DWD_GPCC/FD_D_V2018_100.

2.5. Extreme and intense precipitation

Rémy Roca[1], Hirohiko Masunaga[2] and Lisa Alexander[3,4]

[1] Laboratoire d'Études en Géophysique et Océanographie Spatiales (Université de Toulouse III, CNRS, CNES, IRD), Toulouse, France

[2] Institute for Space-Earth Environmental Research, Nagoya University, Nagoya, Japan

[3] Climate Change Research Centre, University of New South Wales, Sydney, Australia

[4] ARC Centre of Excellence for Climate Extremes, University of New South Wales, Sydney, Australia

2.5.1. Introduction

Extreme and intense precipitation is at the core of many scientific and societal concerns, both from a meteorological and a climate change perspective. In recognition of this central role and the need to enhance research efforts, WCRP established a Grand Challenge on Weather and Climate Extremes, a core research focus of which was on heavy precipitation (Alexander et al., 2016). The maturity of new precipitation observational datasets has triggered interest in their ability to help document extreme precipitation. In this chapter, we summarize our current assessment and we focus on intense precipitation, the wet end of extreme precipitation, leaving the dry end of the spectrum (droughts) for a later time.

The recent emergence of multiple satellite-based datasets, reanalyses from multiple centers and a new set of ground-based gridded datasets indeed prompts the need to assess how extreme intense situations are described by these renewed observational-based capabilities (Roca et al., 2019). This is even more urgent, as none of these efforts have been purposely constructed for very intense rainfall conditions. We note that the following condensed review is not a guidance document and we do not address the technicalities here (order of operation, selection of an extreme index; the requirement for length of the record, etc). Rather, we focus on what our current ability is to document extreme precipitation.

Intense precipitation can arise from either a short burst of very precipitating deep convection and/or a long spell of moderately raining systems, or both. The definition of "extreme" precipitation therefore remains scale-dependent, and here we put the emphasis on daily precipitation at ~100 km scale.

The chapter is organized by first exploring global land and ocean. Then a limited regional investigation is proposed along with a process-oriented assessment of the products' capability. A third section is dedicated to showcasing a few subjectively-selected studies where the data are actually used for a scientific application. Finally, a list of recommendations is offered.

2.5.2. Global land

Owing to the conventional networks of rain gauges, the documentation of precipitation over global land benefits from a large number of datasets including in situ gridded, satellite-based on atmospheric reanalysis. Alexander et al. (2020) used many extreme indices based on those recommended by ETCCDI (Zhang et al., 2011). Figure 2.5.1 shows the large discrepancies across observationally-based products characterized by a factor of 2 in magnitude. The figure also shows how the various sub-ensemble of products (in situ, satellite uncorrected, satellite gauge corrected and reanalyses) contribute to the overall spread. This intercomparison generally emphasizes that global space-based precipitation products show the potential for
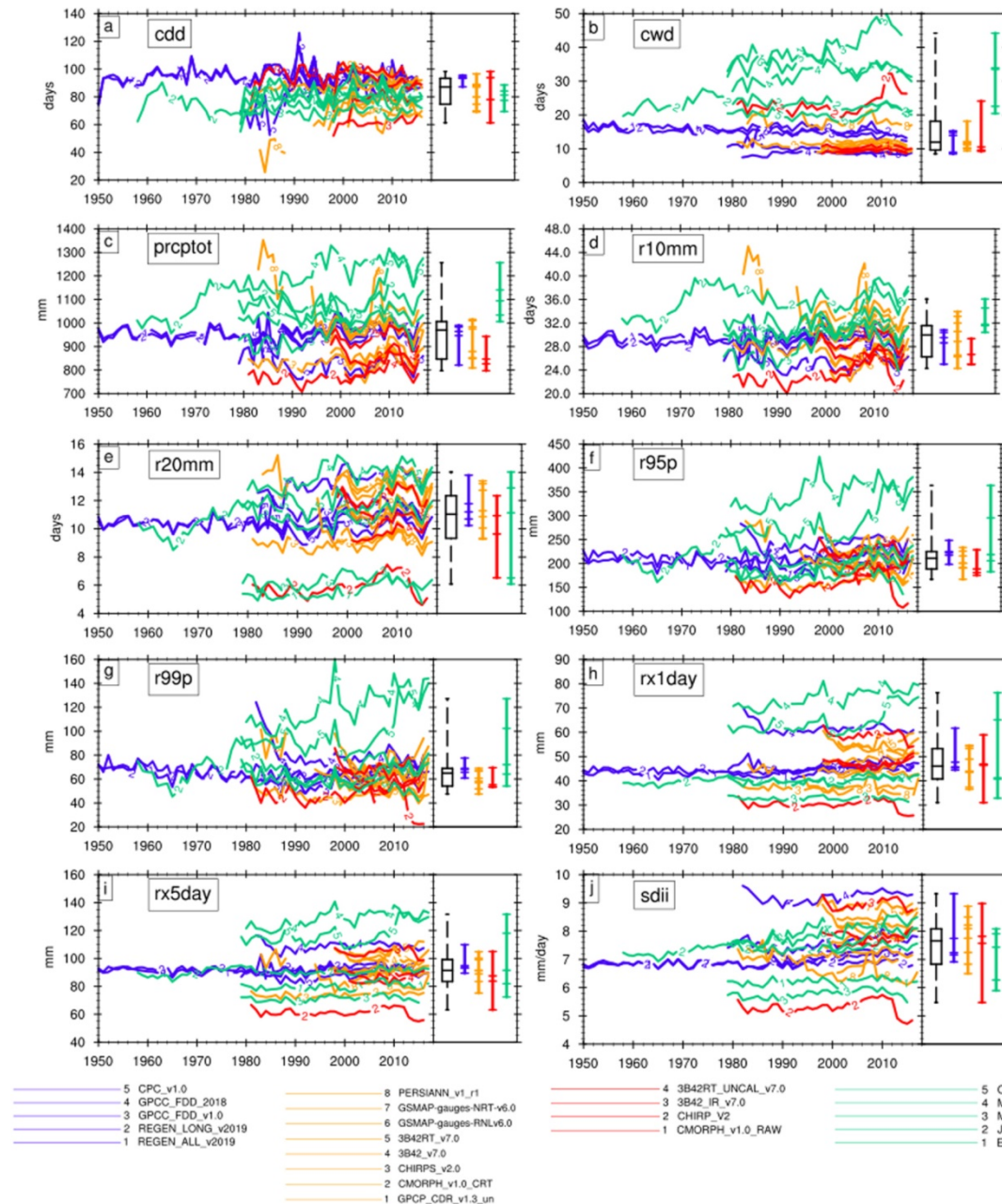
Figure 2.5.1. The time series of quasi-global land (50°S–50°N) averaged wettest day (Rx1day) for various gridded datasets. The spread of the various sub-ensemble of products is also shown on the right panel using a boxplot including all products (black boxplot). Adapted from Alexander et al., 2020

climate scale analyses of extremes as a complementary source to in situ gridded data while reanalysis should be used with caution.

Bador et al. (2020a) further indicates that better agreement on the space/time location of extremes is found among the products rather than on the actual magnitude of the extreme metrics. Donat et al. (2019) looked at the trends in extreme precipitation to reveal that precipitation totals and extremes have increased in humid regions since the mid-twentieth century. Conversely, despite showing tendencies to increase, no robust changes can be detected in the drier regions. Masunaga et al. (2019) performed a large number of product intercomparison and suggested that, for many of the satellite-based products, the uncertainty of

the climatology is shown to be a poor predictor of the uncertainty in the extreme of the distribution. Origins of the systematic bias depend qualitatively on precipitation regimes (climatology versus extremes, for instance) and may be traced back to uncertainties at fundamental levels of the satellite microwave algorithms (Sekaranom and Masunaga 2017, 2019). This underscores the need to focus on extreme and intense precipitation in the assessment and the intrinsic difficulty in exploring both totals and extreme precipitation. Focusing on a subset of products [PERSIANN-CDR, ERA-I, Water and global Change (WATCH) Forcing Data methodology applied to ERA-Interim data (WFDEI), National Centers for Environmental Prediction-Department of Energy Reanalysis 2 (NCEP2), and the Multi-Source Weighted-Ensemble Precipitation (MSWEP)] over the 1979–2017 period and GPCC as a reference, Chen et al. (2020) confirms the large discrepancies in the absolute magnitude of extremes intensity. The study further shows nuanced performances from the reanalysis and PERSIANN-CDR, highlighting a regional and seasonal variability in their capability to represent extremes compared to the reference. It is furthermore shown that performance can vary along the temporal record, adding uncertainty to trend analyses.

The previous generation of products were not well nor systematically assessed, but for the satellite-based products, studies revealed large spread among products (Herold et al. 2017; Aghakouchak et al. 2011, Sun et al., 2018). The current assessment suggests that the situation might have improved somewhat.

2.5.3. Global ocean

Conventional in situ data from networks of buoys (Wu and Wang, 2019), rain gauges over atolls in the tropics (Greene et al., 2008), radar measurements from islands (Henderson et al., 2017) or ship-based disdrometer observations (Klepp et al., 2018) are tentatively used to evaluate and characterize reanalyses and the satellite-based products. However, due to the scarcity of in situ precipitation observations (Serra, 2018), the assessment of the capabilities is usually very weak. It is even worse in the case of the extreme precipitation.

Figure 2.5.2 shows the probability of exceedance over the tropical ocean for various satellite-based products (De Meyer and Roca, 2021), exhibiting the large spread for threshold above ~75 mm/day. The analysis further reveals the disparity between the microwave constellation-based products and the IR or single microwave platform products (PERSIANN and GPCP). It also shows that two clusters of products emerge, one with a larger occurrence of "extreme" extremes (IMERG, GSMaP and HOAPS) than the other [CMORPH, Tropical Rainfall Measuring Mission (TRMM) Multi-satellite Precipitation Analysis (TMPA)]. MSWEP, as a simple combination of the two later products, is close to this cluster as well.

Burdanowitz et al. (2019) explore the scaling of ERA-5 extreme instantaneous precipitation at 30 km with SST over the global ocean and show significant departures from the OceanRAIN dataset. Masunaga et al. (2019) generally find a larger spread among the extremes of various products over the ocean compared to land (Masunaga et al., 2019).
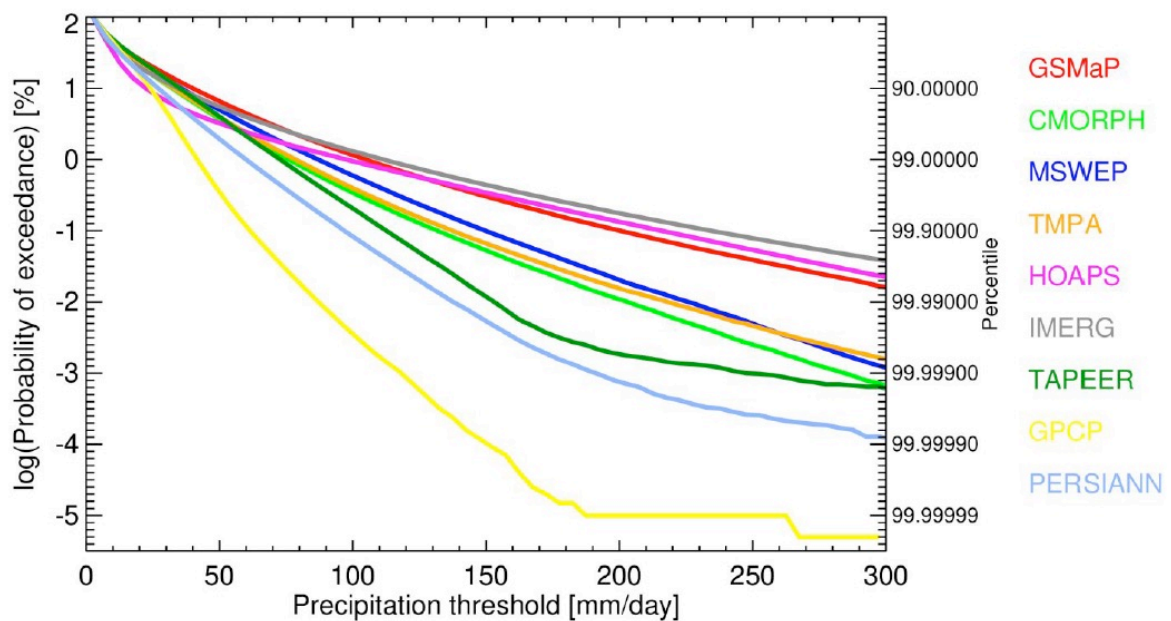
Figure 2.5.2. Probability of exceedance of daily 1°x1° accumulated precipitation over the tropical ocean (30°S–30°N) for the period 2017–2017 except for the TAPEER product where it is restricted to the 2012–2016 period.

2.5.4. Regional and process-oriented investigations

While a systematic exploration of all ongoing regional studies about precipitation extreme is out of the scope of the present chapter, we have selected only a few references that convey the main messages. These references can serve at a starting point for the interested reader.

2.5.4.1. Regional

2.5.4.1.1. *Asia*

Over the Tibetan Plateau, Wu et al. (2019) show that TRMM and CHIRPS overestimate extreme high precipitation. He et al. (2019) intercompared in situ, satellite and reanalysis gridded products over East mainland China (105°–140°E, 15°–35°N). Figure 2.5.3 shows the daily precipitation distribution for boreal summer together with the references rain-gauge network data.

The intercomparison confirms global results with reanalysis strongly underestimating the "extreme" extreme cases. The in situ gridded observations also seem to suffer from the same issue. PERSIANN, as already pointed out, is truncated and does not exhibit values above 120 mm/d. Only the 3B42 (TRMM) product seems to approach the reference datasets. In this region, extreme precipitation is distributed around two maximum centers, over the lower-middle reach of the Yangtze River basin and in South China. ERA-Interim, MERRA, and CFSR do not represent these regional features. The moist-season extreme precipitation in the Korean peninsula and Japan is often brought about by warm rain processes and hence may be difficult to properly capture in the satellite-based products relying partly on the microwave scattering by ice particles (Sohn et al., 2013). The same difficulty may be encountered for extremes in other regions beyond east Asia as well (Hamada et al., 2015).
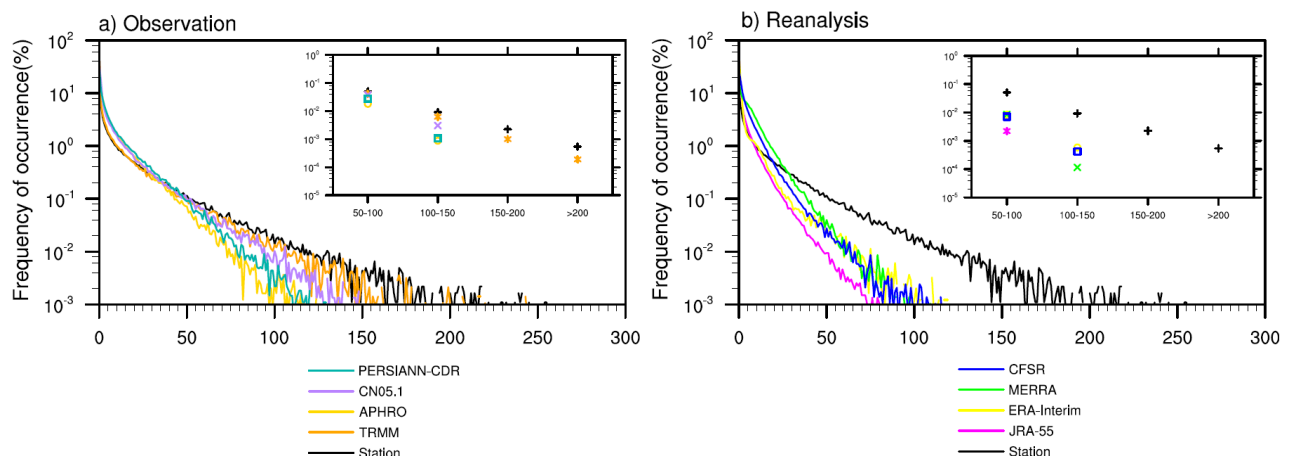
Figure 2.5.3. Frequency of occurrence of daily precipitation in mm/d for boreal summer. From He et al (2019). CN05.1 is based on the interpolation of data from 2400 observational stations in China (Wu and Gao, 2013). The Asian Precipitation–Highly Resolved Observational Data Integration Toward Evaluation of Water Resources (APHRODITE) dataset is based on rain gauge observation records over Asia.

2.5.4.1.2.   *Western and central Europe*

Using the European daily high-resolution Observational Gridded Dataset (E-OBS) as a reference, seven gridded products (one gauge-based, three satellite-based and two reanalysis-based products) were analyzed using temporally and spatially matched pairs of precipitation estimates with a focus on the detection of extreme events (Lockhoff et al., 2019). The occurrence of wet-day intensities is generally well reproduced by all products and deficiencies are noted in coastal regions and dry areas in the region. The performances show substantial scale dependence with skills showing up 3-day and 1.25° and above scale. This is confirming earlier results for GPCP daily that exhibits better performances at 3°/5 days (Lockhoff et al., 2014).

2.5.4.1.3.   *Over the continuous U.S.*

In an effort to identify robustness among various products, five in situ-based gridded products, three satellite-based datasets, two regional reanalyses and one regional climate model simulation have been intercompared in pairs using a Generalized Extreme Value (GEV) framework (Timmermans et al., 2019). The products are used at the 25 km, 5-day resolution. The results are in line with the European-based investigations with a strong scale dependence revealed by this consistency exploration. The inconsistency appears stronger over complex terrain in all products, and satellite-based products are characterized by seasonally varying performances.

2.5.4.1.4.   *Africa*

Harrison et al. (2019) investigate changing precipitation in Sub-Saharan Africa using rain gauge and satellite products. They show that satellite products struggle to correlate with the REGEN reference for the R1xday (wettest day) and Rx5day (consecutive 5-day maxima) extreme precipitation indices over the 1983–2013 period. They further compare a set of 12 satellite products and various rain gauge-based gridded products over a limited time span with a focus on the wet season (Figure 2.5.4). Their analysis concludes that sparse data indicates a positive trend in African rainfall extremes and that the satellite products were found useful to fill some space/time gaps in the conventional observational record.
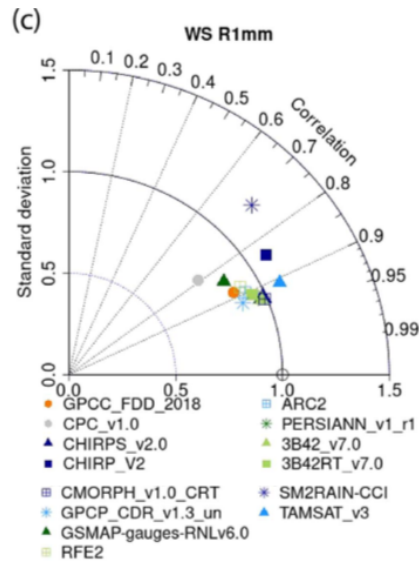
Figure 2.5.4. Taylor diagram for wet season indices, 1998–2013. Number of rain days (R1 mm). Diagrams show how gauge and satellite products compare to REGEN 1998–2013 data in terms of Pearson's correlation (azimuth angle), ratio of standard deviations (distance from black curve) and mean square error (distance from black circle on x-axis). Adapted from Harrison et al., 2019

While not directly an intercomparison or an assessment, the recent work of Le Coz and Van De Giesen (2020) offers some guidance for end-users about what satellite products to use for floods and extreme applications among others tailored for Africa, and is worth being mentioned as a useful entry point for this region.

2.5.4.1.5. *Australia*

Australia, like some other regions, has a very good ground-based network and associated gridded products [for example, the Australian Water Availability Project (AWAP, Jones et al., 2009) daily gridded 5 km x 5 km resolution dataset]. However, even then, in sparsely populated regions like the central and western parts of the country, very few in situ gauges exist and estimating extreme rainfall and/or trends in these regions is problematic (King et al., 2013). Contractor et al. (2015) intercompared daily precipitation values from AWAP with GPCP 1DD version 1.2 and TRMM 3B42 V7 over the period 1998–2013 and found that correlations were reasonably good, although were not better than 0.6 for Australia as a whole. The satellite products generally underestimated the most "extreme" extremes across the range of cities that Contractor et al. (2015) considered. It is worth noting, though, that an in-depth intercomparison of extreme precipitation in all products across whole the region has yet to be performed.

2.5.4.2. Process-oriented

2.5.4.2.1. *Atmospheric rivers*

Atmospheric rivers are associated with extreme precipitation. Focusing on the winter of 2017 on the Californian coast, Wen et al. (2018) showed that six major satellite estimates were able to report heavy precipitation during the atmospheric rivers. Yet while the ensemble mean was close to the rain gauge references, there was considerable spread characterized in the individual products. None of the products or the operational radar network accurately documented the peak extreme rain rate during the sequence of the events. Ramos et al. (2020) compared two cases of atmospheric rivers over California and Portugal in winter 2016 and evaluated more than 20 satellite, in situ and reanalysis gridded precipitation products. Similar

results were obtained for the satellite products. But unlike at the global scale, the reanalysis datasets were shown to outperform the satellite and gridded in situ products slightly with respect to this region and processes when compared with reference rain gauges (Wen et al., 2018).

2.5.4.2.2.   *Scaling of extreme precipitation with surface temperature*

The sensitivity of extreme precipitation to surface conditions (water vapor and temperature) has received considerable interest, and over the tropical land, earlier analysis raised questions about an otherwise physically-based theory based on thermodynamics that stipulates a ~6–7% K increase of the extreme with each surface degree of warming. By pooling data over land using a 10+ suite of satellite products, Roca et al. (2019) showed that the most recent, constellation-based, gridded daily products support the theory and do indeed exhibit a robust (low spread) Clausius-Clapeyron sensitivity. Over tropical oceans, the sensitivity of extremes for this generation of products is also in line with the theory and characterized by a small spread (De Meyer and Roca, 2021). The investigation further reveals that while the constellation-based products show robust scaling behavior, considerable uncertainty remains on the absolute magnitude of extreme precipitation as shown in Figure 2.5.5. It is not possible to identify which clusters might be the closest to truth.

In summary, the community has produced an extensive evaluation effort over various regions. The results are generally in line with the global studies. Yet we ought to take better advantage
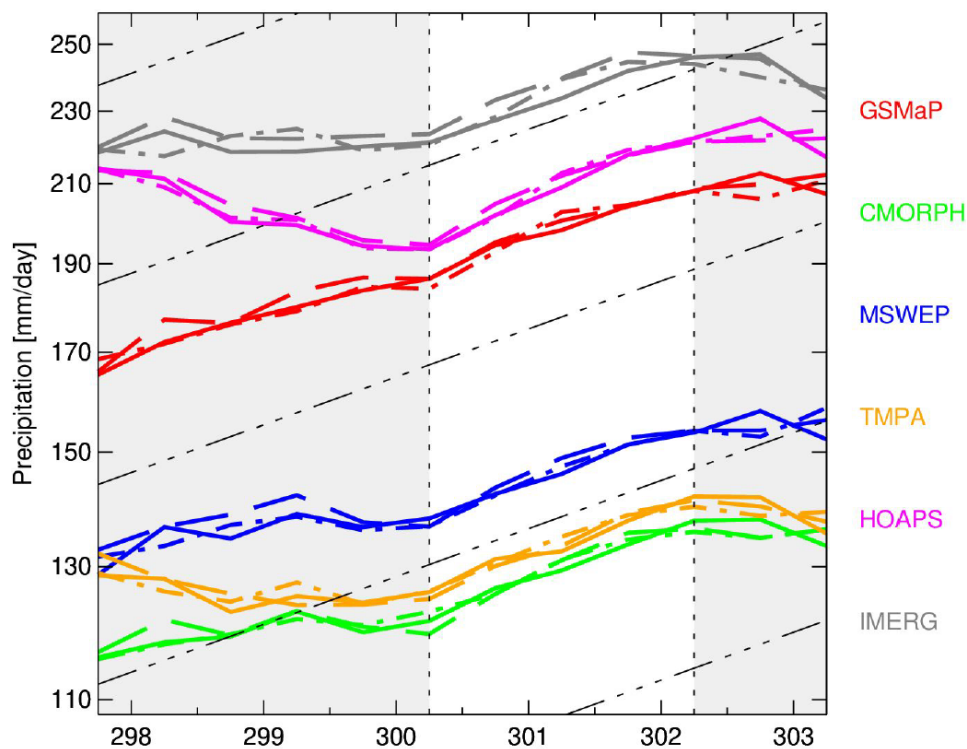
Figure 2.5.5. The value of the 99.9th percentile of the 1°x1° daily accumulated precipitation as a function of the SST lagged by 2 days. Each color corresponds to a precipitation product. Solid line for Operational SST and Sea Ice Analysis (OSTIA), dashed line for Optimally Interpolated Sea Surface Temperature (OISST) and dash-dotted lines for Optimally Interpolated Remote Sensing Systems Sea Surface Temperature (OIRSS). For the period 2007–2017. Regimes are separated by vertical dashed lines. Thegrey shaded areas indicate the non-robust cold regime between precipitation products (left) and the non-robust warm regime between SST products (right). Black dash-dotted lines correspond to the Clausius-Clapeyron 6%/K rate. From De Meyer and Roca, 2021

of these valuable studies in the assessment through new mechanisms to be proposed. The emergence of process-oriented multi-product assessments is encouraging to help end-users to navigate products.

2.5.5. Example applications

While assessment exercises tend to highlight the non-robust features of the assessed data, as it fuels dataset improvements, we have also highlighted some robust features that permit further scientific analysis. Indeed, the balance of evidence suggests we are now in an interesting position where some datasets are fit for some scientific applications while clearly not all the datasets are fit for all scientific investigations. While a guidance document would help navigate the situation, in the following paragraphs we showcase a sub-selection of studies that actually make use of the datasets to further advance our understanding of extremes within the water cycle.

2.5.5.1. Atmospheric physics

Using constellation-based satellite precipitation estimates from FROGS and the recent mesoscale convective system database Tracking Of Organized Convection Algorithm through a 3-DsegmentatioN (TOOCAN), based on homogeneous infrared observations from geostationary satellites (Fiolleau et al., 2020), the role of organized convection on the occurrence of extreme precipitation in the tropics has been investigated. The study shows that the long-lived systems are disproportionally responsible for extreme precipitation relative to their occurrence (Roca and Fiolleau, 2020).

2.5.5.2. Climate model evaluation of extremes

The sensitivity of climate model extremes to model resolution was investigated and assessed against the spread in the observational record (Bador et al., 2020b). It was shown that an increase in resolution, while improving the model's representation of intense precipitation, is unlikely to be enough to improve model performance significantly. This indicates that, in tandem to higher resolution, improvements in model physics and/or tuning is required to better improve model scores at simulating extremes. The use of the observational record for model evaluation of extremes is further considered in the framework of the emerging Department of Defense (DoD)-based and precipitation-centric model evaluation project (Pendergrass et al., 2020).

2.5.6. Summary

The observational estimation of extreme precipitation has benefited from the recent emergence of many new datasets, from in situ, reanalysis and satellite data. The current assessment effort falls short of addressing all of the concerns related to extreme precipitation. Among the identified gaps are extreme snowfall events over land and ocean and orographic intense precipitation. Nevertheless, this first assessment effort points towards a few sound conclusions.

Generally speaking, the new generation of satellite products can be used in support of scientific investigations along with the in situ-based gridded datasets. The current reanalysis datasets appear to suffer from larger uncertainties, making their fitness-for-purpose in extreme precipitation analysis more arguable.

More specifically, in the case of the satellite-based observations over land, the situation appears to have improved from the last decade and a number of salient features have

emerged. The new generation of satellite-based global datasets now appear to have the potential for climate scale analyses of extremes. For these products, uncertainties in climatology have been shown to be a poor predictor of the uncertainty in the extremes of the distribution. A very large number of regional investigations have been performed over various land areas, generally in line with the global assessment results, although such a number of studies is difficult to integrate.

Over the oceans, while a number of features are robust among the last generation of satellite constellation-based products, the large spread in the absolute magnitude of the extreme value remains to be addressed. Process-oriented evaluation has started to emerge in the literature and shows good promise to formulate further assessments.

As a consequence, a number of scientific investigations related to extreme precipitation have been supported by the datasets (scaling with SST, climate model evaluation, and so on), which is encouraging. Yet the various datasets may not all meet the requirements for some of the scientific investigations needed, prompting recommendations from agencies and product developers.

2.5.7. Recommendations

Based on this first and partial attempt to assess the ability of observational gridded precipitation products to document extreme precipitation, we are in a position to formulate some recommendations for the agencies and the community.

2.5.7.1. General considerations

  i.   Consolidate present findings; elaborate and refine the current set of diagnostics
  ii.   Improve the products, as the assessment has identified some non-robust features that deserve further attention. Feedback to dataset providers with specific details could be formulated in targeted workshops.
  iii. Fill the gaps in the assessment
  iv.   Communicate the robust dataset features to support further research using the datasets

2.5.7.2. Specific considerations

  i.   Explore further the process-oriented assessment
  ii.   A community effort is needed to clarify the magnitude of extreme precipitation over the ocean.
  iii. Better benefit from the scattered myriad of local and regional evaluation studies, possibly through an extensive regionally-oriented assessment with a common set of scores and metrics. GEWEX Regional Hydroclimate Projects and WCRP/Regional offices could play a role.
  iv.   The fact that some products are better fit for purpose than others requires a guidance document to help navigate the large suite of available datasets.
  v.   The products need to be assessed for the dry precipitation extremes (droughts) too.

2.5.8. Acknowledgments

2.5.9. References

Aghakouchak, A., A. Behrangi, S. Sorooshian, K. Hsu and E. Amitai, 2011: Evaluation of satellite-retrieved extreme precipitation rates across the central United States. *Journal of Geophysical Research: Atmospheres*, 116, 1–11, https://doi.org/10.1029/2010JD014741.

Alexander, L.V., M. Bador, R. Roca, S. Contractor, M.G. Donat, P.L. Nguyen, 2020: Intercomparison of annual precipitation indices and extremes over global land areas from in situ, space-based and reanalysis products. *Environmental Research Letters*, 15 (5), art. no. 055002.

Alexander, L.V., X. Zhang, G. Hegerl and S.I. Seneviratne, 2016: *Implementation plan for WCRP grand challenge on understanding and predicting weather and climate extremes*—the "Extremes Grand Challenge" Version, June 2016. Available at: https://www.wcrp-climate.org/images/documents/grand_challenges/WCRP_Grand_Challenge_Extremes_Implementation_Plan_v20160708.pdf.

Bador, M., L.V. Alexander, S. Contractor and R. Roca, 2020a: Diverse estimates of annual maxima daily precipitation in 22 state-of-the-art quasi-global land observation datasets. *Environmental Research Letters*, 15 (3), art. no. 035005.

Bador, M., J. Boé, L. Terray, L.V. Alexander, A. Baker, A. Bellucci, R. Haarsma, T. Koenigk, M.-P. Moine, K. Lohmann, D.A. Putrasahan, C. Roberts, M. Roberts, E. Scoccimarro, R. Schiemann, J. Seddon, R. Senan, S. Valcke and B. Vanniere, 2020b: Impact of higher spatial atmospheric resolution on precipitation extremes over land in global climate models. *Journal of Geophysical Research: Atmospheres*, 125, e2019JD032184, https://doi.org/10.1029/2019JD032184.

Burdanowitz, J., S.A. Buehler, S. Bakan and C. Klepp, 2019: On the sensitivity of oceanic precipitation to sea surface temperature. *Atmospheric Chemistry and Physics Discussions*, 1, 1–21, doi:10.5194/acp-2019-136.

Chen, S., B. Liu, X. Tan and Y. Wu, 2020: Inter-comparison of spatiotemporal features of precipitation extremes within six daily precipitation products. *Climate Dynamics*, **54**, 1057–1076, https://doi.org/10.1007/s00382-019-05045-z.

Contractor, S., L.V. Alexander, M.G. Donat and N. Herold, 2015: How Well Do Gridded Datasets of Observed Daily Precipitation Compare over Australia? *Advances in Meteorology*, art. no. 325718.

De Meyer, V., and R. Roca, 2021: Thermodynamic scaling of extreme daily precipitation over the tropical ocean from satellite observations. *Journal of the Meteorological Society of Japan*, 99, Special Edition on Global Precipitation Measurement (GPM): 5th Anniversary, https://doi.org/10.2151/jmsj.2021-020.

Donat, M.G., O. Angélil and A.M. Ukkola, 2019: Intensification of precipitation extremes in the world's humid and water-limited regions. *Environmental Research Letters*, 14 (6) (2019), Article 065003, 10.1088/1748-9326/ab1c8e.

Fiolleau, T., R. Roca, S. Cloche, D. Bouniol and P. Raberanto, 2020: Homogenization of Geostationary Infrared Imager Channels for Cold Cloud Studies Using Megha-Tropiques/ScaRaB. *IEEE Transactions on Geoscience and Remote Sensing*, 1–14, doi:10.1109/tgrs.2020.2978171.

Greene, J.S., M. Klatt, M. Morrissey and S. Postawko, 2008: The comprehensive pacific rainfall database. *Journal of Atmospheric and Oceanic Technology*, 25, 71–82, doi:10.1175/2007JTECHA904.1.

Hamada, A., Y. Takayabu, C. Liu and E.J. Zipser, 2015: Weak linkage between the heaviest rainfall and tallest storms. *Nature Communications*, 6, 6213, https://doi.org/10.1038/ncomms7213.

Harrison, L., C. Funk and P. Peterson, 2019: Identifying changing precipitation extremes in Sub-Saharan Africa with gauge and satellite products. *Environmental Research Letters*, 14, 085007.

He, S., J. Yang, Q. Bao, L. Wang and B. Wang, 2019: Fidelity of the observational/reanalysis datasets and global climate models in representation of extreme precipitation in East China. *Journal of Climate*, 32, 195–212, doi:10.1175/JCLI-D-18-0104.1.

Henderson, D.S., C.D. Kummerow, D.A. Marks and W. Berg, 2017: A regime-based evaluation of TRMM oceanic precipitation biases. *Journal of Atmospheric and Oceanic Technology*, 34, 2613–2635, doi:10.1175/JTECH-D-16-0244.1.

Herold, N., A. Behrangi and L.V. Alexander, 2017: Large uncertainties in observed daily precipitation extremes over land. *Journal of Geophysical Research*, 122, 668–681, https://doi.org/10.1002/2016JD025842.

Jones, D.A., W. Wang and R. Fawcett, 2009: High-quality spatial climate data-sets for Australia. *Australian Meteorological and Oceanographic Journal*, 58 (4), pp. 233–248.

King, A.D., L.V. Alexander and M.G. Donat, 2013. The efficacy of using gridded data to examine extreme rainfall characteristics: A case study for Australia. *International Journal of Climatology*, 33 (10), pp. 2376–2387.

Klepp, C., S. Michel, A. Protat, J. Burdanowitz, N. Albern, M. Kähnert, A. Dahl, V. Louf, S. Bakan and S.A. Buehler, 2018: OceanRAIN, a new in-situ shipboard global ocean surface-reference dataset of all water cycle components. *Scientific Data*, 5, 1–22, doi:10.1038/sdata.2018.122.

Le Coz, C., and N. Van De Giesen, 2020: Comparison of rainfall products over sub-saharan Africa. *Journal of Hydrometeorology*, 21, 553–596, doi:10.1175/JHM-D-18-0256.1.

Lockhoff, M., O. Zolina, C. Simmer and J. Schulz, 2014: Evaluation of satellite-retrieved extreme precipitation over Europe using gauge observations. *Journal of Climate*, 27, 607–623, doi:10.1175/JCLI-D-13-00194.1.

——, ——, —— and ——, 2019: Representation of precipitation characteristics and extremes in regional reanalyses and satellite-and gauge-based estimates over western and central Europe. *Journal of Hydrometeorology*, 20, 1123–1145, doi:10.1175/JHM-D-18-0200.1.

Masunaga, H., M. Schröder, F.A. Furuzawa, C. Kummerow, E. Rustemeier and U. Schneider, 2019a: Inter-product biases in global precipitation extremes. *Environmental Research Letters*, 14, 125016, doi:10.1088/1748-9326/ab5da9, http://dx.doi.org/10.1088/1748-9326/ab5da9.

Pendergrass, A.G., P.J. Gleckler, L.R. Leung and C. Jakob, 2020: Benchmarking Simulated Precipitation in Earth System Models. *Bulletin of the American Meteorological Society*, 101, E814–E816, doi:10.1175/bams-d-19-0318.1.

Ramos, A.M., R. Roca, P.M.M. Soares, A.M. Wilson, R.M. Trigo and F.M. Ralph, 2021: Uncertainty in different precipitation products in the case of two atmospheric river events. *Environmental Research Letters*, http://iopscience.iop.org/article/10.1088/1748-9326/abe25b.

Roca, R., and T. Fiolleau, 2020: Extreme precipitation in the tropics is closely associated with long-lived convective systems. *Communications Earth & Environment*, 1, 1–6, doi:10.1038/s43247-020-00015-4, http://dx.doi.org/10.1038/s43247-020-00015-4.

Roca, R., L.V. Alexander, G. Potter, M. Bador, R. Jucá, S. Contractor, M.G. Bosilovich and S. Cloché, 2019: FROGs: a daily 1x1 gridded precipitation database of rain gauge, satellite and reanalysis products. *Earth System Science Data*, 1017–1035, doi:10.5194/essd-11-1017-2019, https://www.earth-syst-sci-data-discuss.net/essd-2019-51/.

Sekaranom, A.B., and H. Masunaga, 2017: Comparison of TRMM-derived rainfall products for general and extreme rains over the Maritime Continent. *Journal of Applied Meteorology and Climatology*, 56, 1867–1881, doi:10.1175/JAMC-D-16-0272.1.

Sekaranom, A.B., and H. Masunaga, 2019: Origins of heavy precipitation biases in the TRMM PR and TMI products assessed with CloudSat and reanalysis data. *Journal of Applied Meteorology and Climatology*, 58, 37–54, doi:10.1175/JAMC-D-18-0011.1.

Serra, Y.L., 2018: Precipitation measurements from the Tropical Moored Array: A review and look ahead. *Quarterly Journal of the Royal Meteorological Society*, 144, 221–234, doi:10.1002/qj.3287.

Sohn, B.J., G.-H. Ryu, H.-J. Song and M.-L. Oh, 2013: Characteristic features of warm-type rain producing heavy rainfall over the Korean peninsula inferred from TRMM measurements. *Monthly Weather Review*, 141, 3873–3888, doi:10.1175/MWR-D-13-00075.1.

Sun, Q., C. Miao, Q. Duan, H. Ashouri, S. Sorooshian and K.L. Hsu, 2018: A Review of Global Precipitation Data Sets: Data Sources, Estimation, and Intercomparisons. *Reviews of Geophysics*, 56, 79–107, doi:10.1002/2017RG000574.

Timmermans, B., M. Wehner, D. Cooley, T. O'Brien and H. Krishnan, 2019: An evaluation of the consistency of extremes in gridded precipitation data sets. *Climate Dynamics*, 52, 6651–6670, doi:10.1007/s00382-018-4537-0, http://dx.doi.org/10.1007/s00382-018-4537-0.

Wen, Y., A. Behrangi, H. Chen and B. Lambrigtsen, 2018: How well were the early 2017 California Atmospheric River precipitation events captured by satellite products and ground-based radars? *Quarterly Journal of the Royal Meteorological Society*, 144, 344–359, doi:10.1002/qj.3253.

Wu, Q., and Y. Wang, 2019: Comparison of oceanic multisatellite precipitation data from tropical rainfall measurement mission and global precipitation measurement mission datasets with rain gauge data from ocean buoys. *Journal of Atmospheric and Oceanic Technology*, 36, 903–920, doi:10.1175/JTECH-D-18-0152.1.

Wu, Y., L. Guo, H. Zheng, B. Zhang and M. Li, 2019: Hydroclimate assessment of gridded precipitation products for the Tibetan Plateau. *Science of the Total Environment*, 660, 1555–1564, doi:10.1016/j.scitotenv.2019.01.119, https://doi.org/10.1016/j.scitotenv.2019.01.119.

Zhang, X., L. Alexander, G.C. Hegerl, P. Jones, A.K. Tank, T.C. Peterson, B. Trewin and F.W. Zwiers, 2011: Indices for monitoring changes in extremes based on daily temperature and precipitation data. *Wiley Interdisciplinary Reviews Climate Change*, 2(6), 851–870, doi:10.1002/wcc.147, 2011.

3. Emerging directions

3.1. Toward the new generation of products

George Huffman[1] and Pierre-Emmanuel Kirstetter[2]

[1] NASA Goddard Space Flight Center

[2] University of Oklahoma, Norman, OK

The fine time interval provided in modern precipitation products is only possible by combining estimates from many individual high-quality satellite sensors, and even then, additional approximations are needed to fill numerous gaps in the mosaic of short-interval segments from the various sensors. As such, the future directions of global observationally-based precipitation products involve improvements in the individual retrievals, improvements and operationalization of additional sensor estimates and innovations in assembling the merged products, including the intercalibration and homogenization of the data record. One major challenge is to both provide consistent estimates in any particular epoch of the constellation and to provide consistent estimates across generations of sensors with differing capabilities.

3.1.1. Passive microwave retrievals

3.1.1.1. Outstanding problems

Passive microwave (PMW) retrievals form the mainstay of modern global precipitation estimates. Improvements over 3+ decades of development have expanded their utility, but challenges remain, including orographic precipitation, snowfall and the performance of the estimates in specific weather regimes as discussed in Chapter 1. These topics critically impact detection and rate estimation (see Chapter 1), and are best addressed at the sensor level, as opposed to the merger process, because that allows detailed sensor information to be applied to the issues, in combination with ancillary data, such as atmospheric temperature and moisture profiles, generally drawn from numerical reanalyses/forecasts. The diversity of channels, resolutions and scanning patterns that sensors "see" considerably complicates efforts to make uniform retrievals as well.

3.1.1.2. Machine learning

Recent work on precipitation retrievals has focused on applying current concepts in machine learning algorithms. For example, recent work has shown encouraging results in applying machine learning approaches to PMW data (Adhikari et al., 2020). Importantly, machine learning techniques require quality training data. Uncertainties in satellite precipitation estimation often transfer from the calibration data set, for example, from PMW to Geostationary Earth Orbit Infrared (GEO-IR) estimates (Upadhyaya et al., 2020). A training precipitation set with properties improperly matching the capabilities of the satellite sensor and its observed information content can negatively impact precipitation detection and quantification retrievals and propagate systematic and random errors (Chapter 1.2).

3.1.1.3. Probabilistic QPE

The uncertainty structure of satellite-based quantitative precipitation estimation (QPE) is largely unknown at fine spatio-temporal scales and requires more than just one deterministic "best precipitation estimate" to adequately cope with the intermittent, highly skewed distribution that characterizes precipitation. Because satellite retrievals are underdetermined, uncertainty

should be an integral part of QPE (Kirstetter et al., 2018; Chapter 1.2). Precipitation probability mapping has been shown to outperform deterministic estimates by mitigating systematic biases in the deterministic retrievals, quantifying uncertainty and advancing the monitoring of precipitation extremes.

3.1.1.4. Surface-based calibrators

While satellite retrievals have almost exclusively been calibrated by precipitation gauges, the installed base of surface radars in the U.S., Europe, Australia, Japan and elsewhere seems to invite use if questions of quality control, access and archive record can be overcome (Chapter 1.2). The proliferation of communications microwave link-base precipitation estimates holds similar promise as well (Leijnse et al., 2007; Messer et al., 2006), with the same caveats.

3.1.2. Other estimates

Besides PMW retrievals, a number of other satellite sensor families provide precipitation estimates. In the grand tradition of precipitation estimation, none of these sensors provides totally new data band, but (except for GEO-IR), little or no use has been made of them.

3.1.2.1. GEO

GEO-IR estimates pre-date the start of PMW data, and present the interesting dilemma that they are plentiful, but tend to be of lower quality due to reliance on relating cloud-top structure to surface precipitation. As such, these data are used as backup information in multi-satellite products that depend on PMW data. Nonetheless, this use is a key and ongoing need, meaning continued advancement is important. Following on the discussion of machine learning approaches above, researchers are specifically applying machine learning to GEO-IR data (including Tao et al., 2018). Research has already demonstrated that using multi-channel GEO data can provide improved precipitation estimates, including Precipitation Estimation from Remotely Sensed Information using Artificial Neural Networks–Multispectral Analysis (PERSIANN-MSA; Behrangi et al., 2009). Machine learning techniques should be beneficial here as well, but a primary barrier to operational use of multiple channels is the need to access the global collection of the requisite channels, and in some cases handling the differences among similar channels on different sensors. At present, only the GEO-IR is available in an archived and current source of uniformly formatted global datasets, including the CPC Global 4-km Merged IR dataset (CPC, 2020) and the Gridded Satellite (GridSat) collection (Knapp et al., 2011). The long-term (and current) record of GEO precipitation estimates would be significantly improved by creating global datasets for the GEO-Visible and GEO-Water Vapor channels as companions to the GEO-IR.

Succeeding generations of GEO satellites carry progressively more-capable sensors, exemplified by NOAA's Advanced Baseline Imager (ABI) sensor on board the latest Geostationary Operational Environmental Satellites (GOES-R Series). ABI provides three times more spectral channels, four times the resolution and five times faster scanning when compared to its predecessor imager on board previous-generation GOES (Schmit et al., 2017). The GOES-R series also carries a lightning sensor that potentially provides additional input for estimating precipitation. This new generation of GEO sensors opens new opportunities in quantifying precipitation rates, and makes it imperative to provide easy, analysis-ready access to the multiple channels provided across the various satellites, including developing analysis schemes that account for the different channel frequencies. One clear requirement is that the precipitation research community needs to demonstrate the skill of multi-channel GEO versus single-channel GEO-IR versus PMW, all using modern algorithms, to determine the cost-

benefit analysis of the three-channel (and even-more-channel) GEO retrievals against the development effort and expense for the requisite input datasets.

3.1.2.2. Advanced Very High Resolution Radiometer (AVHRR)

One limitation to GEO observations is that the footprints are sufficiently distorted above the 60° latitude circle in both hemispheres that the data are not used at higher latitudes, as exemplified by the CPC Global 4-km Merged IR dataset covering the latitude band 60°N-S. In addition, current GEO-IR schemes tend to confuse surface ice and snow with cloudiness, leading to low skill in polar regions. Recently, Xie et al. (2019) introduced the use of AVHRR IR data for precipitation estimates. These sensors have a history back to 1979 on the NOAA-series polar orbiters, are uniformly processed and include cloudiness estimates that allow the (approximate) separation of surface snow and ice from clouds. Ehsani et al. (2020) provide another example of this concept. Despite flying on only a few polar orbiters, the convergence of orbital swaths near the poles allows relatively frequent observations of any given location. Going forward, the Visible Infrared Imaging Radiometer Suite (VIIRS) sensor will provide equivalent data.

3.1.2.3. Cloud volume

The series of the old Television-Infrared Operational Sounder (TIROS) Operational Vertical Sounder (TOVS), current Advanced Infrared Sounder (AIRS) and relatively new Cross-track Infrared Sounder (CrIS) instruments have been used to provide precipitation estimates based on cloud volume parameters [and the same could be done with the Infrared Atmospheric Sounding Interferometer (IASI)]. Even though the original (Susskind and Pfaendtner, 1989; Susskind et al., 1997) estimates are fairly approximate, they have proved useful as a basis for providing high-latitude estimates for most of the GPCP Versions 1, 2, and 3 products (Huffman et al., 2001; Adler et al., 2018; Huffman et al., 2020a). Improvements with the Smith and Barnet (2019) Version 7 products are expected to refine the AIRS and CrIS estimates, and the advent of an equivalently-long timeseries of AVHRR/CrIS implies that the two approaches should be evaluated for use together at the high latitudes for both GPCP and other multi-satellite products. The MODIS instruments on Terra and Aqua have 16 IR "cloud" channels that might be used in a similar way, but are not presently.

3.1.2.4. Assimilation/forecast

An additional data source that warrants consideration is numerical assimilation/model estimates of precipitation. While not "observational", many end-users are less concerned about the origin of the estimates and more about having the "best" estimates. Most numerical schemes have known problems in "convective" weather regimes, which typifies much of the tropics and sub-tropics. However, it has long been the case that numerical products prove better than observations in "stratiform" weather regimes that typify higher latitudes (Ebert et al., 2007). These considerations suggest that the merged products should have data fields that incorporate such numerical assimilation/forecast estimates in locations/times for which they are competitive with the observational estimates. Such a combination can naturally incorporate improvements in both retrievals and assimilations as enhanced versions are released. This discussion raises the point that the relative performance of each is a worthy research topic on an ongoing basis, and of considerable interest to end-users.

3.1.2.5. Soil moisture

Another approach to estimating precipitation is to work backwards from satellite estimates of soil moisture. In summary, given local soil, vegetation and previous rainfall conditions, changes in soil moisture sensed by satellites can be approximately related to current rainfall. The Soil

Moisture Analysis Rainfall Tool (SMART; Crow et al., 2011) and Soil Moisture to Rain (SM2Rain; Brocca et al., 2014) are examples, with the former focusing on creating adjusted satellite datasets to obtain the timeseries of rainfall that is most consistent with the record of soil moisture changes. The relatively infrequent soil moisture observations make operational use a challenge that is a matter of current research.

3.1.3. Merged products

3.1.3.1. Outstanding problems

Most users focus on merged precipitation data products, as noted previously, and Chapter 1 has discussed known issues intrinsic to the merger schemes. First, it is helpful to recall that some merged datasets prioritize homogeneity in the data record, usually by severely down-selecting the choice of input data. These are said to follow Climate Data Record (CDR) standards, and include GPCP (Adler et al., 2018) and Precipitation Estimation from Remotely Sensed Information using Artificial Neural Networks–Climate Data Record (PERSIANN-CDR). High-Resolution Precipitation Products (HRPP), on the other hand, try to enforce homogeneity, but include "all possible" data. These include CMORPH (Joyce et al., 2004), GSMaP (Kubota et al., 2007), and IMERG (Huffman et al., 2020b), among others. All of these datasets choose some intercalibration, with CDRs usually picking a PMW standard, and HRPPs tending to use a calibrator that incorporates spaceborne radar. Homogeneity for the calibrator across sensors is key, and one main reason that continued access to a reasonably wide-swath spaceborne radar in future missions is considered a high priority. A second outstanding issue is how best to fill the numerous gaps that exist when PMW data are segmented to a short-interval time grid (typically 30–60 minutes), discussed in Chapter 1 as "revist-gap mitigation." As a first approximation, the "morphing" concept pioneered in Joyce et al. (2004) is used in CMORPH, GSMaP and IMERG. The best choice for how to compute the propagation vectors is a matter of current research, and the IMERG team plans to introduce the Scheme for Histogram Adjustment of Ranked Precipitation Estimates in the Neighborhood (SHARPEN; Tan et al., 2020) to counteract some of the averaging effects implicit in morphing. The grand challenge is to develop and operationalize a better "storm development" algorithm that estimates the lifecycle stages of precipitation systems. For example, Rain Estimation Using Forward-Adjusted Advection of Microwave Estimates (REFAME; Behrangi et al., 2010) uses time series of local GEO-IR brightness temperatures to better track the evolution of the precipitation between PMW overpasses.

3.1.3.2. Short-interval combinations with surface data

One modification to satellite-only merged products that seems attractive is to use submonthly precipitation gauge data to adjust multi-satellite estimates, since gauges are generally considered the gold standard for actual amounts. It would be nice to do this at the finest-possible time interval, but even daily gauges tend to be representative of relatively small regions (i.e., short correlation distances), meaning rather dense gauge networks are required. Clearly, oceans and many land areas lack the necessary station coverage. Xie and Xiong (2011) developed a scheme that used probability density functions (PDFs) of dense gauge data to both bias-correct CMORPH and create a combination with the de-biased CMORPH. The University of California Santa Barbara/Climate Hazards Center generates gauge-enhanced 0.05°x0.5° precipitation estimates by blending Global Telecommunication Systems station observations with bias-corrected cold cloud duration imagery in GEO-IR (Funk et al., 2015). The time interval is chosen to provide gauge estimates that are representative of larger regions than the typical daily gauge reports. The same research group is considering applying this approach to IMERG.

Other candidate surface-based precipitation datasets for possible merger with or routine calibration of merged datasets includes surface radar networks, microwave links for telecommunications, lightning-detection networks and citizen science data, such as from the Global Learning and Observations to Benefit the Environment (GLOBE) program (https://www.globe.gov/). All of these sources present challenges in terms of availability in real or post-real time, accessible archives of both the Level 1 (that is, sensor) and Level 2 (product) data and quality control. Note well that the potential for using surface data should not obscure the fact that many regions lack adequate surface data for routine use in merged products, or even for confident validation.

3.1.3.3. Weighted merger

As quasi-global precipitation products have proliferated, Beck et al. (2017) took advantage of the diversity of estimates to develop regionally-varying weights for each dataset to build a "best" average global dataset, MSWEP. This approach should score better than any individual estimate, but it depends critically on what the standard is for choosing the weights, and paradoxically only maintains a strong, stable advantage as long as the individual datasets continue to be produced and included. Additionally, the weighting should be recomputed any time any of the inputs is upgraded to a new version, although it could be a matter of judgment whether any particular change requires the effort of computing new weights.

3.1.4. Uncertainty estimates

A final unmet need is for precipitation datasets to provide estimates of uncertainty, starting with the individual sensors, and carrying through to the merged products (Chapter 1). While Chapter 1 contains a discussion of sources of uncertainty, here, the future development work is to turn these concepts into gridbox-by-gridbox estimates. The focus has to be on using globally available inputs for this error computation, which excludes detailed use of surface data, except where those data are being merged into the product.

One potential approach is for the individual sensor estimates to provide probabilistic QPE, as described in Chapters 1.1.4 and 3.1.1, and then carry that entire set of information through the merged datasets. It is an open question whether specifying a set of quantiles or giving coefficients of a fitted function is best. There is also a critical need for methods to aggregate the gridbox-level uncertainties to larger space/time data averaging, such as daily and/or 1°x1°. At these scales, the work of the Megha-Tropiques team has paved the way for a more systematic evaluation of the uncertainty associated with sampling (Roca et al., 2018; Chambon et al., 2012). Whatever form these "expert" error estimates take, it is important that the merged datasets provide a "simple" error statement for non-expert users. For example, the IMERG team has prototyped a "Quality Index" that maps from a quantitative estimate of correlation to a simple "stoplight" chart (Huffman et al., 2020b), but much research remains. Regardless of the approach, it is a best practice that the simple error index should be traceable to a quantitative error statement. Chapter 3.2 addresses this topic in more detail.

3.1.5. Recommendations

i. Address orographic and snowfall regimes at the single-sensor level.
ii. Match training datasets for machine learning to the satellite sensor capabilities.
iii. Pursue scientific, technical and administrative issues to unlock the promise that surface-based datasets such as radar and communication microwave links hold as calibration and validation information.

iv. Assemble analysis-ready multi-channel GEO datasets; IR, visible and water vapor cover the long record, while more channels, as well as lightning data, are available in recent years.

v. Pursue retrievals from AVHRR, VIIRS, TOVS, AIRS, CrIS and IASI to provide useful estimates at high latitudes.

vi. Upgrade merged products to provide data fields that incorporate numerical assimilation/forecast estimates where they are useful, and provide routine reports on the relative skill of retrievals and assimilations/forecasts.

vii. Pursue the use of soil moisture observations in satellite precipitation estimates.

viii. Address the grand challenge of making detailed observational estimates of storm lifecycle development for use in merged products.

ix. Pursue incorporating short-interval surface data, including gauges, radar, telecommunications microwave links, lightning-detection networks and citizen science, recognizing that deficiencies in data coverage are severe limitations on global application.

x. Continue to develop skill-weighted mergers of datasets.

xi. Prioritze advancing uncertainty estimates at the gridbox level, and developing a methodology for aggregating these estimates to larger time/space scales.

3.1.6. References

Adhikari, A., M.R. Ehsani, Y. Song and A. Behrangi, 2020: Comparative Assessment of Snowfall Retrieval from Microwave Humidity Sounders Using Machine Learning Methods. *Earth and Space Science*, early release e2020EA001357, 65 pp., doi:10.1029/2020ea001357.

Adler, R.F., M. Sapiano, G.J. Huffman, J.-J. Wang, G. Gu, D.T. Bolvin, L. Chiu, U. Schneider, A. Becker, E.J. Nelkin, P. Xie, R. Ferraro and D.-B. Shin, 2018: The Global Precipitation Climatology Project (GPCP) Monthly Analysis (New Version 2.3) and a Review of 2017 Global Precipitation. *Atmosphere*, 9, 14 pp., doi:10.3390/atmos9040138.

Beck, H.E., N. Vergopolan, M. Pan, V. Levizzani, A.I.J.M. van Dijk, G. Weedon, L. Brocca, F. Pappenberger, G.J. Huffman and E.F. Wood, 2017: Global-Scale Evaluation of 22 Precipitation Datasets Using Gauge Observations and Hydrological Modeling. *Hydrology and Earth System Sciences*, 21(12), 6201–6217, doi:10.5194/hess-21-6201-2017.

Behrangi, A., K.-L. Hsu, B. Imam, S. Sorooshian, G.J. Huffman and R.J. Kuligowski, 2009: PERSIANN-MSA: A Precipitation Estimation Method from Satellite-Based Multispectral Analysis. *Journal of Hydrometeorology*, 10, 1414–1429, doi:10.1175/2009JHM1139.1.

Behrangi, A., B. Imam, K. Hsu, S. Sorooshian, T.J. Bellerby and G.J. Huffman, 2010: REFAME: Rain Estimation Using Forward Adjusted-Advection of Microwave Estimates. *Journal of Hydrometeorology,* 11, 1305–1321, doi:10.1175/2010JHM1248.1.

Brocca, L., L. Ciabatta, C. Massari, T. Moramarco, S. Hahn, S. Hasenauer, R. Kidd, W. Dorigo, W. Wagner and V. Levizzani, 2014: Soil as a Natural Rain Gauge: Estimating Global Rainfall from Satellite Soil Moisture Data. *Journal of Geophysical Research: Atmospheres*, 119, 5128–5141, doi:10.1002/2014JD021489.

Chambon, P., I. Jobard, R. Roca, and N. Viltard, 2012: An Investigation of the Error Budget of Tropical Rainfall Accumulation Derived from Merged Passive Microwave and Infrared Satellite Measurements. *Quarterly Journal of the Royal Meteorological Society*, 139, 879–893, doi:10.1002/qj.1907.

CPC, 2020: CPC Global 4-km Merged IR dataset. Posted at
https://catalog.data.gov/dataset/climate-prediction-center-ir-4km-dataset and archived at
https://disc.gsfc.nasa.gov/datasets/GPM_MERGIR_1/summary?keywords=cpc%20ir.

Crow, W.T., M.J. van den Berg, G.J. Huffman and T. Pellarin, 2011: Correcting Rainfall Using
Satellite-Based Surface Soil Moisture Retrievals: The Soil Moisture Analysis Rainfall Tool
(SMART). *Water Resources Research*, 47, W08521, doi:10.1029/2011WR010576.

Ebert, E.E., J.E. Janowiak and C. Kidd, 2007: Comparison of Near-Real-Time Precipitation
Estimates from Satellite Observations and Numerical Models. *Bulletin of the American
Meteorological Society*, 88, 47–64, doi:10.1175/BAMS-88-1-47.

Ehsani, M.R., A. Behrangi, A. Adhikari, Y. Song, G.J. Huffman and D.T. Bolvin, 2020:
Assessment of the Advanced Very High-Resolution Radiometer for Snowfall Retrieval in High
Latitudes Utilizing CloudSat and Machine Learning. *Journal of Hydrometeorology*, in review.

Funk, C., P. Peterson, M. Landsfeld, D. Pedreros, J. Verdin, S. Shukla, G. Husak, J. Rowland,
L. Harrison, A. Hoell and Michaelsen, 2015: The Climate Hazards Infrared Precipitation with
Stations—a New Environmental Record for Monitoring Extremes. *Science Data*, 2, 150066,
doi:10.1038/sdata.2015.66.

Huffman, G.J., R.F. Adler, M. Morrissey, D.T. Bolvin, S. Curtis, R. Joyce, B. McGavock, J.
Susskind, 2001: Global Precipitation at One-Degree Daily Resolution from Multi-Satellite
Observations. *Journal of Hydrometeorology*, 2, 36–50, doi:10.1175/1525-
7541(2001)002<0036:GPAODD>2.0.CO;2.

Huffman, G.J., R.F. Adler, A. Behrangi, D.T. Bolvin, E.J. Nelkin and Y. Song, 2020a: Algorithm
Theoretical Basis Document (ATBD) for Global Precipitation Climatology Project Version 3.1
Precipitation Data, 31 pp,
https://docserver.gesdisc.eosdis.nasa.gov/public/project/MEaSUREs/GPCP/GPCP_ATBD_V3.1.pdf.

Huffman, G.J., D.T. Bolvin, D. Braithwaite, K. Hsu, R. Joyce, C. Kidd, E.J. Nelkin, S.
Sorooshian, E.F. Stocker, J. Tan, D.B. Wolff and P. Xie, 2020b: Integrated Multi-satellitE
Retrievals for the Global Precipitation Measurement (GPM) mission (IMERG). In: Advances in
Global Change Research, Vol. 67, *Satellite Precipitation Measurement* (V. Levizzani, C. Kidd,
D. Kirschbaum, C. Kummerow, K. Nakamura, F.J. Turk, eds.). Springer Nature, Dordrecht,
ISBN 978-3-030-24567-2 / 978-3-030-24568-9 (eBook), 343–353, doi:10.1007/978-3-030-
24568-9_19.

Joyce, R.J., J.E. Janowiak, P.A. Arkin and P. Xie, 2004: CMORPH: A method that produces
global precipitation estimates from passive microwave and infrared data at high spatial and
temporal resolution. *Journal of Hydrometeorology*, 5, 487–503, https://doi.org/10.1175/1525-
7541(2004)005<0487%3ACAMTPG>2.0.CO%3B2.

Kirstetter, P.-E., N. Karbalaee, K. Hsu and Y. Hong, 2018: Probabilistic Precipitation Rate
Estimates with Space-Based Infrared Sensors. *Quarterly Journal of the Royal Meteorological
Society*, 144, 191–205, doi:10.1002/qj.3243.

Knapp, K.R., S. Ansari, C.L. Bain, M.A. Bourassa, M.J. Dickinson, C. Funk, C.N. Helms, C.C.
Hennon, C.D. Holmes, G.J. Huffman, J.P. Kossin, H.-T. Lee, A. Loew and G. Magnusdottir,
2011: Globally Gridded Satellite Observations for Climate Studies. *Bulletin of the American
Meteorology Society*, 92, 893–907, doi:10.1175/2011BAMS3039.1.

Kubota, T., S. Shige, H. Hashizume, K. Aonashi, N. Takahashi, S. Seto, M. Hirose, Y.N. Takayabu, K. Nakagawa, K. Iwanami, T. Ushio, M. Kachi and K. Okamoto, 2007: Global precipitation map using satellite-borne microwave radiometers by the GSMaP project: Production and validation. *IEEE Transactions on Geoscience and Remote Sensing*, 45, 2259–2275, https://doi.org/10.1109/TGRS.2007.895337.

Leijnse, H., R. Uijlenhoet and J.N.M. Stricker, 2007: Rainfall Measurement Using Radio Links from Cellular Communication Networks. *Water Resources Research*, 43, W03201, 6 pp., doi:10.1029/2006WR005631.

Messer, H., A. Zinevich and P. Alpert, 2006: Environmental Monitoring by Wireless Communication Networks. *Science*, 312, 713, doi:10.1126/science.1120034.

Roca, R., N. Taburet, E. Lorant, P. Chambon, M. Alcoba, H. Brogniez, S. Cloché, C. Dufour, M. Gosset and C. Guilloteau, 2018: Quantifying the Contribution of the Megha-Tropiques Mission to the Estimation of Daily Accumulated Rainfall in the Tropics. *Quarterly Journal of the Royal Meteorological Society*, 144, 49–63, doi:10.1002/qj.3327.

Schmit, T.J., P. Griffith, M.M. Gunshor, J.M. Daniels, S.J. Goodman and W.J. Lebair, 2017: A Closer Look at the ABI on the GOES-R Series. *Bulletin of the American Meteorological Society*, 98, 4. 681–698, doi:10.1175/BAMS-D-15-00230.1.

Smith, N., and C.D. Barnet, 2019: Uncertainty Characterization and Propagation in the Community Long-Term Infrared Microwave Combined Atmospheric Product System (CLIMCAPS). *Remote Sensing*, 11, 1227, 25 pp, doi:10.3390/rs11101227.

Susskind, J., and J. Pfaendtner, 1989: Impact of interactive physical retrievals on NWP. *Report on the Joint ECMWF/EUMETSAT Workshop on the Use of Satellite Data in Operational Weather Prediction: 1989–1993*, Vol. 1, (T. Hollingsworth, ed.). ECMWF, Shinfield Park, Reading RG2 9AV, U.K., 245–270.

Susskind, J., P. Piraino, L. Rokke, L. Iredell and A. Mehta, 1997: Characteristics of the TOVS Pathfinder Path A Dataset. *Bulletin of the American Meteorological Society*, 78, 1449–1472, doi:10.1175/1520-0477(1997)078<1449:COTTPP>2.0.CO;2.

Tan, J., G.J. Huffman, D.T. Bolvin, E.J. Nelkin and M. Rajagopal, 2020: SHARPEN: A Scheme to Restore the Distribution of Averaged Precipitation Fields. *Journal of Hydrometeorology*, submitted.

Tao, Y., K.L. Hsu, A. Ihler, X.G. Gao and S. Sorooshian, 2018: A Two-Stage Deep Neural Network Framework for Precipitation Estimation from Bispectral Satellite Information. *Journal of Hydrometeorology*, 19, 393–408, doi:10.1175/JHM-D-17-0077.1.

Upadhyaya, S.A., P.-E. Kirstetter, J.J. Gourley and R.J. Kuligowski, 2020: On the Propagation of Satellite Precipitation Estimation Errors: From Passive Microwave to Infrared Estimates. *Journal of Hydrometeorolgy*, 21, 1367–1381, doi:10.1175/JHM-D-19-0293.1.

Xie, P., R. Joyce, S. Wu, L. Ren and B. Katz, 2019: *A Preliminary Examination of the Second Generation CMORPH Satellite Precipitation Estimates*. 44th NOAA Annual Climate Diagnostics and Prediction Workshop, held in Durham, NC, USA, 22–24 October 2019.

Xie, P., and A.-Y. Xiong, 2011: A Conceptual Model for Constructing High-Resolution Gauge-Satellite Merged Precipitation Analyses. *Journal of Geophysical Research: Atmospheres*, 116, 14 pp., doi:10.1029/2011JD016118.

3.2. Directions in error modeling

Viviana Maggioni[1] and Christian Massari[2]

[1] Sid and Reva Dewberry Department of Civil, Environmental, and Infrastructure Engineering, George Mason University, Fairfax, VA, USA. E-mail: vmaggion@gmu.edu

[2] Research Institute for Geo-Hydrological Protection, National Research Council (CNR)

3.2.1. Introduction

Past validation studies highlighted a myriad of factors, such as retrieval techniques, sensor types, topography, spatial and temporal sampling and algorithms, that contribute to uncertainties associated with satellite precipitation products. All these factors result in errors in precipitation products, whose estimation is fundamental for hydrological modeling, land data assimilation systems, water resources management and climate studies. The ability to model errors in precipitation is paramount for not only obtaining information about satellite products' accuracy and precision in regions and during periods in which in situ measurements are not available, but also to perturb input precipitation to force land surface and hydrologic models. Despite the importance of error models, there is a clear imbalance between research efforts dedicated to the assessment of the performance of satellite precipitation products (as highlighted in Chapter 1.2) and those related to the development of precipitation error modeling.

Nevertheless, in the recent past, several models have been developed to estimate errors and uncertainties in satellite precipitation datasets. Some rely on a reference, some focus on the uncertainty component alone and do not require a reference, some are based on an additive approach and others use a multiplicative error assumption. Error models highly depend on the product temporal and spatial resolution, on precipitation rates and products, and on a priori error model structure. Thus, error models are unlikely to be universal. This section reviews the most common techniques, discusses their limitations and provides recommendations for the agencies and the scientific community.

3.2.2. Results

Two main types of error models are commonly used to assess errors and uncertainties in precipitation data: additive and multiplicative. The multiplicative error model was found superior to the additive approach thanks to its ability to separate the systematic and random components of the error; its applicability to the large range of variability in daily precipitation; and its predictive skills (Tian et al., 2013). Most methods require a benchmark dataset to estimate such errors and uncertainties. However, Adler et al. (2009) proposed a framework, later expanded by Tian and Peters-Lidard (2010), to assess uncertainties in global satellite precipitation datasets using the spread of coincidental and co-located estimates from an ensemble of six different products. Nevertheless, this approach only provides a relative analysis and some of the products in the ensemble are not completely independent.

One of the first error models was proposed by Huffman et al. (1997) and applied to the GPCP analysis (Adler et al., 2003; Huffman et al., 2009) and the Tropical Rainfall Measuring Mission (TRMM) Multi-satellite Precipitation Analysis (TMPA; Huffman et al., 2007). This model provides root mean square random error estimates for each grid box and at each time step (i.e., monthly and daily). Once again, the limitation of this approach is that the error estimates depend on the samples being functionally independent, which may not be the case when considering finer temporal resolution.

Several studies focused on the estimation of the sampling error and modeled its standard deviation using a power law (e.g., Bell et al., 1990; Gebremichael and Krajewski, 2004; Steiner et al., 2003; Hong et al., 2006). For instance, Gebregiorgis and Hossain (2013, 2014) proposed estimating the variance of daily satellite precipitation error using information such as rain rate and geophysical features. However, these techniques assume that: i) precipitation errors can be modeled with a lognormal distribution, which, at high rain rates, can be unrealistic (Gebremichael and Krajewski, 2005); and ii) the variance is an appropriate estimator of the satellite precipitation error. The Gebregiorgis and Hossain (2013, 2014) approach was shown to perform better when the false alarm and the hit components of the error are dominant, but the performance degraded when the missed precipitation represents a large component of the total error.

Solutions have been proposed to characterize uncertainties and errors associated with global high-resolution satellite precipitation datasets. For instance, Hossain and Anagnostou (2006) introduced the two-dimensional satellite rainfall error model (SREM2D), a stochastic model that estimates the joint probability of successful delineation of rainy and non-rainy areas. SREM2D has been successfully applied in hydrologic modeling for streamflow simulations and debris flow predictions (Maggioni et al., 2013; Falck et al., 2015; Nikolopoulos et al., 2017). An example of the SREM2D performance in adjusting a satellite precipitation product (Hydro Estimator, HYDRO-E), used as input to a hydrological model in the Tocantins-Araguaia basin in Brazil, is presented in Figure 3.2.1.
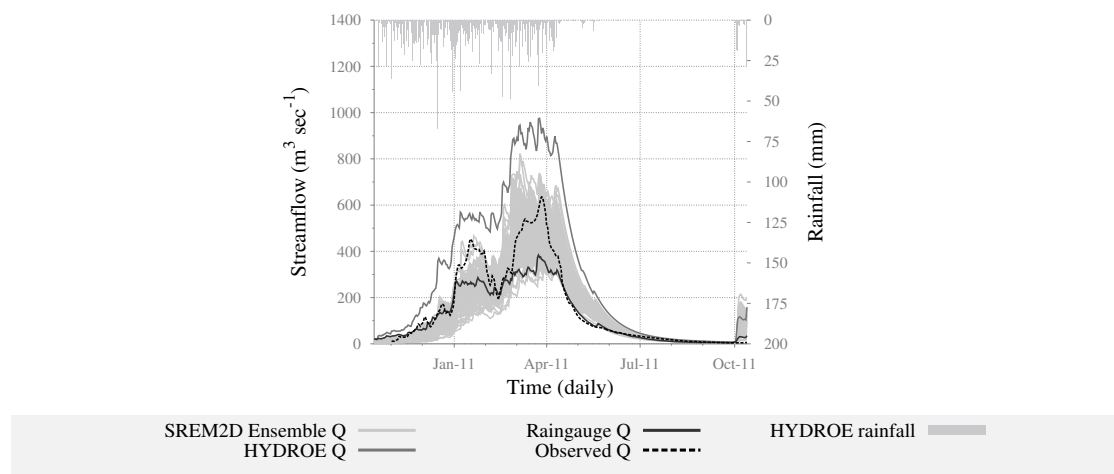
Figure 3.2.1. Streamflow simulations in a sub-basin of Tocantins-Araguaia watershed in Brazil during October 15, 2010–October 14, 2011 using input precipitation from different sources: i) the satellite-based HYDRO-E product, ii) rain gauges and iii) HYDRO-E perturbed using the SREM2D error model (ensemble). This figure shows how SREM2D was able to push the satellite product closer to both ground obversions of streamflow (black dashed line) and the simulation that uses reference rain gauges as input (black solid line).

Bellerby and Sun (2005) designed a methodology to quantify the uncertainty of high-resolution satellite precipitation products by generating probabilistic and ensemble representations of the measured precipitation field. Teo and Grimes (2007) presented a model for uncertainty estimation of satellite rainfall values based on a stochastic ensemble generation of rainfall. Many of these methods use a Monte Carlo approach to generate spatially correlated random fields and ensembles of precipitation error. However, describing the spatial dependence of precipitation fields is not straightforward, as different rainfall intensities are characterized by different correlation structures (that is, when observed values are low, they tend to be scattered

and intermittent with poor spatial dependence, while when the rainfall intensity is high, it tends to be more temporally spatially dependent; Bárdossy and Pegram, 2009).

Gebremichael et al. (2011) proposed a non-parametric method to estimate errors and uncertainties at fine resolutions (3-hourly/25 km), based on conditional density functions of satellite precipitation at each grid box, calibrated using a ground reference. Maggioni et al. (2014) introduced the Precipitation Uncertainties for Satellite Hydrology (PUSH) framework, which models errors as a combination of a random and a systematic component and considers missed precipitation cases, false alarms and hit biases. PUSH was later modified by Oliveira et al. (2018) to account for factors like seasonality and surface type and has been proven to have potential when estimating satellite precipitation errors on a global scale (Khan and Maggioni, 2020). On a similar note, Wright et al. (2017) proposed a simpler approach, based on a shifted gamma distribution, to characterize precipitation and produce a "best guess" distribution of the true precipitation by also considering hits, misses and false alarms. They were the first to explore the potential benefit of incorporating atmospheric variables such as humidity and precipitation from numerical weather models (specifically, atmospheric reanalysis) in a satellite precipitation error model.

As noted above, the complexity in error model formulation varies quite largely, from methods that estimate the variance of a precipitation product to others that also evaluate false alarms and missed cases. Very simple or more complex bias correction methods can significantly reduce errors in streamflow simulated by a hydrological model (Serrat-Capdevila et al., 2014). For instance, simple long-term bias correction was shown by Beck et al. (2017) to yield reasonable streamflow performance over tropical regions. However, such correction may not be appropriate anywhere and anytime, given the non-stationary nature of precipitation biases, or for any kind of application (Ciabatta et al., 2016; Bitew and Gebremichael, 2011).

3.2.3. Summary

Although in the recent past numerous attempts have been made to develop error models of satellite precipitation products, several issues limit their use in applications. First off, the majority of these approaches is based on assumptions regarding the distribution of precipitation (and/or associated errors). Second, simple error models may be preferable for some applications, but more complex solutions may be more appropriate for others. For instance, hydrological models used to simulate floods should be particularly sensitive to extreme precipitation events and the ability of detecting such events. Thus, an error model that accounts for missed precipitation cases and false alarms would be preferable. Third, precipitation errors and uncertainties depend on the product's temporal and spatial resolution, seasonality, rain rate and geophysical features. Thus, the same error model would unlikely perform similarly everywhere in the world (for example, oceans versus land, complex topography versus plains, tropics versus high latitudes), at any time (for example, winters versus summers), for any precipitation event (for example, solid versus liquid precipitation, convective versus stratiform systems) and for any application (drought versus flood monitoring).

3.2.4. Recommendations

Based on this first and partial attempt to assess the current status of satellite precipitation error modeling, here are some recommendations for the agencies and the community:

- Encourage the use of satellite precipitation error models in applications;
- Elaborate on the limitations and capabilities of current error models;

- Investigate possible reference datasets for calibrating error model parameters (such as distribution parameters, missed precipitation fraction and false alarm rates), especially in those regions of the world where no dense ground observation networks exist;
- Communicate such limitations to support further research using these models;
- Incorporate ancillary information (for example, topography, land surface characteristics, climate variables) within model precipitation errors;
- Consolidate current modeling approaches targeting different applications (different applications may have different needs, and the "one fits all" model may not be the appropriate solution); and
- Assess the performance of error models of different complexity across regions characterized by a variety of land uses, topography and climatologies.

3.2.5. Acknowledgments

The authors would like to thank Dr. Sana Khan for her contribution to this assessment and a better depiction of the status of satellite precipitation error modeling.

3.2.6. References

Adler, R.F., G.J. Huffman, A. Chang, R. Ferraro, P.-P. Xie, J. Janowiak, B. Rudolf, U. Schneider, S. Curtis, D. Bolvin, A. Gruber, J. Susskind, P. Arkin and E. Nelkin, 2003: The version-2 global precipitation climatology project (GPCP) monthly precipitation analysis (1979–present). *Journal of Hydrometeorology*, 4, 1147–1167, doi:10.1175/1525-7541(2003)004,1147:TVGPCP.2.0.CO;2.

Adler, R.F., J.-J. Wang, G. Gu and G.J. Huffman, 2009: A ten-year tropical rainfall climatology based on a composite of TRMM products. *Journal of the Meteorological Society of Japan*, 87, 281–293, https://doi.org/10.2151/jmsj.87A.281.

Bárdossy, A., and G.G.S. Pegram, 2009. Copula based multisite model for daily precipitation simulation. *Hydrology & Earth System Sciences*, 13(12).

Beck, H.E., A.I. van Dijk, V. Levizzani, J. Schellekens, D.G. Miralles, B. Martens and A. de Roo, 2017: MSWEP: 3-hourly 0.25 global gridded precipitation (1979–2015) by merging gauge, satellite, and reanalysis data. *Hydrology and Earth System Sciences*, 21 (1), 589.

Bell, T.L., A. Abdullah, R.L. Martin and G.R. North, 1990: Sampling errors for satellite-derived tropical rainfall: Monte Carlo study using a space–time stochastic model. *Geophysical Research Letters*, 95, 2195–2205, doi:10.1029/JD095iD03p02195.

Bellerby, T.J., and J. Sun, 2005. Probabilistic and ensemble representations of the uncertainty in an IR/microwave satellite precipitation product. *Journal of Hydrometeorology*, 6(6), pp.1032–1044.

Bitew, M.M., and M. Gebremichael, 2011: Assessment of satellite rainfall products for streamflow simulation in medium watersheds of the Ethiopian highlands. *Hydrology and Earth System Sciences*, 15, 1147–1155.

Ciabatta, L., L. Brocca, C. Massari, T. Moramarco, S. Gabellani, S. Puca and W. Wagner, 2016: Rainfall-runoff modelling by using SM2RAIN-derived and state-of-the-art satellite rainfall products over Italy. *International Journal of Applied Earth Observation and Geoinformation*, 48, 163–173.

Falck, A., V. Maggioni, J. Tomasella, D. Vila and F. Diniz, 2015: Propagation of satellite precipitation uncertainties through a distributed hydrologic model: a case study in the Tocantins-Araguaia basin in Brazil. *Journal of Hydrology*, 527, pp. 943–957.

Gebregiorgis, A.S., and F. Hossain, 2013: Understanding the dependency of satellite rainfall uncertainty on topography and climate for hydrologic model simulation. *IEEE Transactions on Geoscience and Remote Sensing*, 51, 704–718, doi:10.1109/TGRS.2012.2196282.

Gebregiorgis, A.S., and F. Hossain, 2014: Estimation of satellite rainfall error variance using readily available geophysical features. *IEEE Transactions on Geoscience and Remote Sensing*, 52, 288–304, doi:10.1109/TGRS.2013.2238636.

Gebremichael, M., and W.F. Krajewski, 2004: Characterization of the temporal sampling error in space-time-averaged rainfall estimates from satellites. *Geophysical Research Letters*, 109, D11110, doi:10.1029/2004JD004509.

Gebremichael, M., and W.F. Krajewski, 2005: Modeling distribution of temporal sampling errors in area-time-averaged rainfall estimates. *Atmospheric Research*, 73, 243–259, doi: 10.1016/j.atmosres.2004.11.004.

Gebremichael, M., G.-Y. Liao and J. Yan, 2011: Nonparametric error model for a high resolution satellite rainfall product. *Water Resources Research*, 47, W07504, doi:10.1029/2010WR009667.

Hong, Y., K.-L. Hsu, H. Moradkhani and S. Sorooshian, 2006: Uncertainty quantification of satellite precipitation estimation and Monte Carlo assessment of the error propagation into hydrologic response. *Water Resources Research*, 42, W08421, doi:10.1029/ 2005WR004398.

Hossain, F., and E.N. Anagnostou, 2006: Assessment of a multi-dimensional satellite rainfall error model for ensemble generation of satellite rainfall data. *IEEE Geoscience and Remote Sensing Letters*, 3, 419–423, doi:10.1109/ LGRS.2006.873686.

Huffman, G.J., 1997: Estimates of root-mean-square random error for finite samples of estimated precipitation. *Journal of Applied Meteorology and Climatology*, 36, 1191–1201, doi:10.1175/1520-0450(1997)036,1191:EORMSR.2.0.CO;2.

Huffman, G. J., D.T. Bolvin, E.J. Nelkin, D.B. Wolff, R.F. Adler, G. Gu, Y. Hong, K.P. Bowman and E.F. Stocker, 2007: The TRMM Multisatellite Precipitation Analysis (TMPA): Quasi-global, multiyear, combined-sensor precipitation estimates at fine scales. *Journal of Hydrometeorology*, 8, 38–55, doi:10.1175/JHM560.1.

Huffman, G.J., R.F. Adler, D.T. Bolvin and G. Gu, 2009: Improving the global precipitation record: GPCP version 2.1. *Geophysical Research Letters*, 36, L17808, doi:10.1029/2009GL040000.

Khan, S., and V. Maggioni, 2020: Evaluating the Applicability of the PUSH Framework to Quasi-Global Infrared Precipitation Retrievals at 0.5°/Daily Spatial/Temporal Resolution. *Asia-Pacific Journal of Atmospheric Sciences*, 10.1007/s13143-020-00185-3.

Maggioni V., H. Vergara, E. Anagnostou, J. Gourley, Y. Hong and D. Stampoulis, 2013: Investigating the applicability of error correction ensembles of satellite rainfall products in river flow simulations. *Journal of Hydrometeorology*, 14(4), pp. 1194–1211.

Maggioni, V., M.R.P. Sapiano, R.F. Adler, Y. Tian, and G.J. Huffman, 2014: An error model for uncertainty quantification in high-time-resolution precipitation products. *Journal of Hydro-meteorology,* 15, 1274–1292, https://doi.org/10.1175/JHM-D-13-0112.1.

Nikolopoulos, E., E. Destro, V. Maggioni, F. Marra and M. Borga, 2017: Satellite-rainfall estimates for debris flow prediction: An evaluation based on rainfall depth-duration thresholds. *Journal of Hydrometeorology*, 18(8), pp. 2207–2214.

Oliveira, R., V. Maggioni, D. Vila and L. Porcacchia, 2018: Using satellite error modeling to improve GPM-level 3 rainfall estimates over the Central Amazon region. *Remote Sensing*, 10, 336, https://doi.org/10.3390/rs10020336.

Serrat-Capdevila, A., J.B. Valdes, E. Stakhiv, 2014: Water management applications for satellite precipitation products: synthesis and recommendations. *Journal of the American Water Resources Association*, 50, 509–525, https://doi.org/10.1111/jawr.12140.

Steiner, M., T.L. Bell, Y. Zhang and E.F. Wood, 2003: Comparison of two methods for estimating the sampling-related uncertainty of satellite rainfall averages based on a large radar dataset. *Journal of Climate*, 16, 3759–3778, doi:10.1175/1520-0442(2003)016,3759: COTMFE.2.0.CO;2.

Teo, C.K., and D.I. Grimes, 2007: Stochastic modelling of rainfall from satellite data. *Journal of Hydrology*, 346(1–2), pp.33–50.

Tian, Y., and C.D. Peters-Lidard, 2010: A global map of uncertainties in satellite-based precipitation measurements. *Geophysical Research Letters*, 37, L24407, https://doi.org/10.1029/2010GL046008.

Tian, Y., G.J. Huffman, R.F. Adler, L. Tang, M. Sapiano, V. Maggioni and H. Wu, 2013: Modeling errors in daily precipitation measurements: Additive or multiplicative? *Geophysical Research Letters*, 40, 2060–2065, https://doi.org/10.1002/grl.50320.

Wright, D.B., D.B, Kirschbaum and S. Yatheendradas, 2017: Satellite precipitation characterization, error modeling, and error correction using censored shifted gamma distributions. *Journal of Hydrometeorology*, 18(10), pp. 2801–2815.

3.3. Emerging techniques for precipitation assessment and consistency studies

Ali Behrangi

University of Arizona

3.3.1. Introduction

Accurate precipitation estimation is critical to study the Earth and advance science and applications. Towards this goal, observations from satellite, ground radar and in situ instruments are used, either individually or in combination, to better capture spatiotemporal sampling and accuracy of precipitation. Despite their overall merits, ground radars and in situ observations provide limited coverage for global precipitation estimation. In certain conditions, in situ data also face major uncertainties (for example, to measure snowfall due to gauge undercatch problems) (Yang et al., 2005; Behrangi et al., 2018). Recognizing their spatiotemporal coverage, various space-borne sensors and missions have been utilized for precipitation retrieval. Some of them have precipitation studies and estimation as their main objective (for example, the TRMM and GPM missions) and several others are used because they are capable of providing the information needed for precipitation retrieval. Besides adding to precipitation sampling, the new sensors often contribute by filling remaining gaps in one or more areas. For example, with TRMM, major advancement in estimating near-surface and profile of moderate and intense precipitation was obtained over the tropics ($\sim 35^{\circ}$S/N); CloudSat enabled detection and estimation of snowfall and light rain with unprecedented sensitivity (~ -28 dBZ using the 94 GHz Cloud Profiling Radar observations) within $\sim 81^{\circ}$S/N; and GPM extended TRMM capabilities and offered potentials for snowfall retrievals within $\sim 65^{\circ}$S/N using its dual-polarization radar and passive microwave measurements at higher frequencies. Combination of such complementary datasets has made it possible to make new estimates for precipitation amount and distribution that can be used to guide and assess other precipitation products (for examples, see Behrangi et al., 2014; Olson et al., 2018). Besides those sensors that provide valuable information with direct application in precipitation retrieval, new opportunities have also become available through other instruments developed to better monitor and study the Earth system. If independent from typical methods used for precipitation retrieval, they may provide unique information for a consistency check or independent assessment. An example is the use of the Gravity Recovery and Climate Experiment (GRACE) mission (Tapley et al., 2004) to add insights on snowfall accumulation by monitoring mass variations. Here we discuss a few of such opportunities.

3.3.2. Mass change observations

In high latitudes and cold regions, satellite and ground measurements face large uncertainties. Unknown or variable surface emissivity over snow and ice surfaces and the dominance of light rain and snowfall in high latitudes and cold regions have made it difficult for both microwave and infrared techniques to retrieve snowfall. Rain gauges also face large snowfall undercatch that might exceed 100%, making it difficult to estimate snowfall and quantify its accumulation. It has been shown that using a completely independent observational technique (that is, gravimetry versus radiometry), it is possible to estimate snowfall accumulation by monitoring mass variations over sufficiently large areas. Using ten years of GRACE observations and through the mass balance method, where and when no surface melting occurs for at least a month, Behrangi et al. (2018) calculated monthly and seasonal snowfall accumulation and utilized them to assess other precipitation products (that is, GPCC and GPCP) as well as two common gauge-undercatch correction factors (CFs). In their study, evapotranspiration and

sublimation were quantified from reanalysis, but it was found that they only slightly contribute to the mass balance equation. The study was limited to grids with near surface temperature below 1°C for at least a month, so runoff could be negligible within the mass balance equation. GRACE and evapotranspiration observations were also used in large endorheic basins in High Mountain Asia to estimate monthly accumulated precipitation (Behrangi et al., 2017). An endorheic system is a closed drainage system that retains water and allows no outflow to other external bodies of water; therefore there is no need for streamflow observations to close the mass budget equation. The results were compared with satellite and in situ-based precipitation products, and it was found that most of the products agree well with each other and GRACE analysis in summer, but capture about or less than 50% of the total precipitation estimated using GRACE in winter. Similarly, GRACE observations were used to study the recent increase in lake volumes of the Tibetan Plateau's endorheic basins, and it was found that increased net precipitation contributes the majority of water supply for the lake volume increase (Zhang et al., 2017).

3.3.3. Mass change and streamflow observations

With streamflow observations at basins outlets, there is no need to limit the mass balance analysis to endorheic basins or grids that are cold enough to not generate runoff from snowmelt. Studies using streamflow and GRACE observations have shown great applications for precipitation assessment over the arctic basins. In a recent study, observations of streamflow and storage (mass) change from GRACE, together with estimates of evapotranspiration and sublimation, were used to close the mass budget equation over six arctic basins and investigate monthly time series and multiyear precipitation rates over the studied basins (Behrangi et al., 2019). These analyses were then used to assess two popular CFs: the Legates climatology (CF-L) utilized in GPCP and the Fuchs dynamic correction model (CF-F) used in GPCC monitoring product. The results over the study basins suggested that, based on GRACE and streamflow observations, the CF-F is preferred. GPCP uses CF-L to correct GPCC before merging with satellite data. This study suggests that more efforts are needed to assess which CF method (or combination of methods) should be used for global implementation in GPCP. In lack of other in situ observations, the use of mass change observations seems to provide valuable insights, even at coarse spatial resolution.
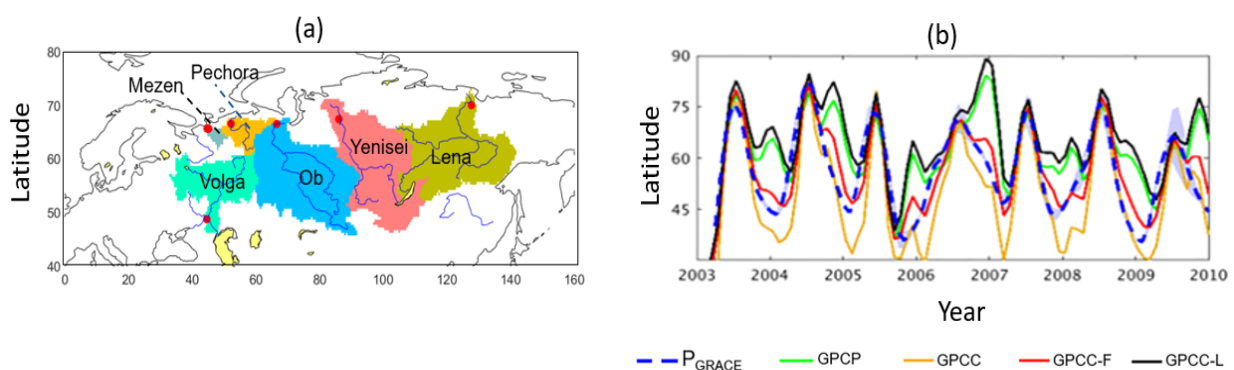
Figure 3.3.1. Times series of monthly mean precipitation rates from GPCC, GPCP, GPCC-L, GPCC-F, and GRACE over the Volga basin. Figures from Behrangi et al. (2019), with modifications. The red dots in panel (a) show the location of the outlet of the basins.

3.3.4. Mass change and ice discharge observations

Precipitation estimation over ice sheets (for example, Antarctica) is challenging because in addition to difficulties that snow and ice surface bring to precipitation estimation from radiometers, estimating snowfall accumulation over Antarctic ice sheets is complicated by ice

divergence, the continual export of mass from the interior to the oceans via ice flow (Rignot et al., 2011). In other words, it is not possible to perform mass balance analysis (for example, using GRACE) over Antarctic grids or basins without accounting for ice discharge that can be as much as 2000 Gt per year (Gardner et al., 2018). However, efforts have made it possible to reconstruct ice discharge and changes in ice discharge over the Antarctic ice sheet by merging a comprehensive record of changes in Antarctic-wide ice flow, calculated by feature tracking of hundreds of thousands of Landsat image and mapping of surface velocity (Rignot et al., 2011; Gardner et al., 2018). Using mass change observations from GRACE and observational-based estimates of ice discharge values and their uncertainties over several Arctic basins, Behrangi et al. (2020) calculated annual snowfall accumulation over seven large Antarctic basins and compared the outcomes with several satellite and reanalysis products (Fig. 3.2.2). Their mass balance estimated snowfall accumulation using ice discharge and storage change observations were bounded by CloudSat snowfall estimates, presumably the most viable satellite-based snowfall product, with and without adjustment for the unmeasured near surface. Similar to Grazioli et al. (2017), the adjustment factor was calculated by dividing the cumulative precipitation at near-surface by precipitation accumulation at 1.2 km above the surface using the ECMWF Integrated Forecast System (ECMWF IFS). Such analyses provide an independent assessment of current satellite-based snowfall estimates over Antarctic and similar ice sheets (for example, part of Greenland where rainfall is not frequent), especially as GRACE-Follow On (GRACE-FO) continues to provide mass change observations.
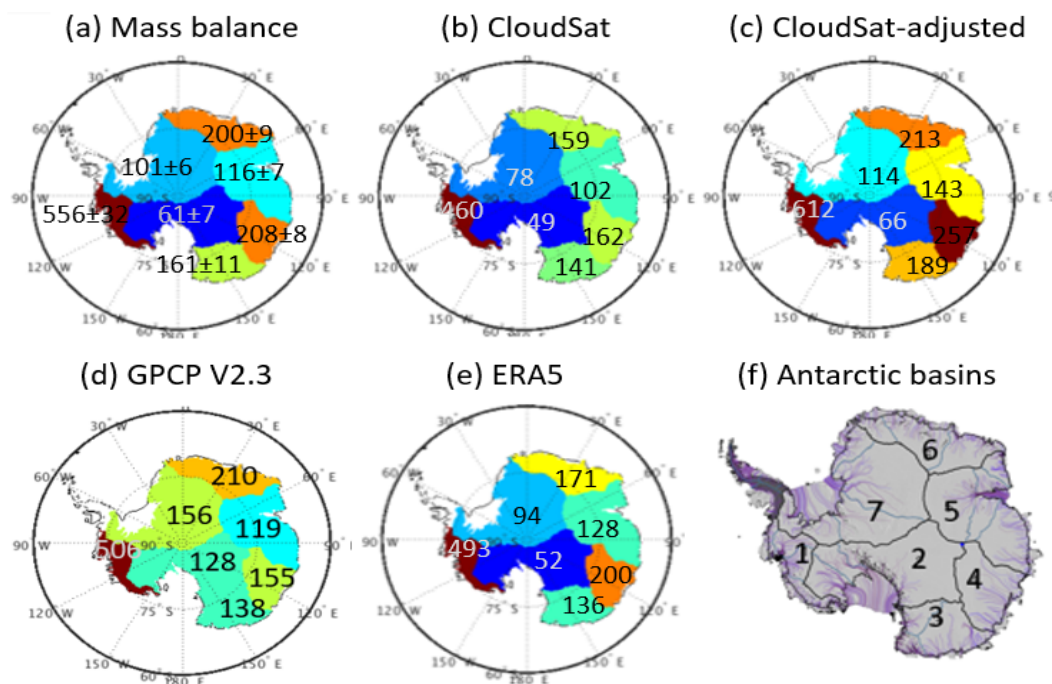
Figure 3.3.2. Annual snowfall rate estimated from various products for each of the seven basins [shown in panel (f)]. The errors shown for mass budget estimates represent combined errors from GRACE, ice discharge and basal melt estimates with details discussed in Gardner et al. (2018). The figure is based on Behrangi et al. (2020) with some modifications.

3.3.5. Snow depth observations

Observation of snow depth can provide an estimate of the net precipitation accumulation after accounting for snow density, sublimation, redistribution due to wind and melt losses between the two survey dates. By calculating snow water equivalent (SWE) from snow depth observations, it is possible to directly compare snowfall accumulation with changes in SWE.

Through the selection of a major snowfall event with a large accumulation signal, one can also maximize the snowfall accumulation signal and minimize the losses during the short period. Using spatially-complete SWE products from the Airborne Snow Observatory (ASO, Painter et al., 2016), Behrangi et al. (2018) used changes in SWE observations to quantify snow accumulation in cold mountain environments in the western U.S. and compared the outcomes to six satellite-based precipitation products, a ground-based radar, and three in situ snow pillows. They also assessed the bias-scaling relationship (that is, point versus areal estimates) that is often not considered when point measurements are used in evaluating gridded products. By focusing on snowfall over snow accumulation period in CONUS, Panahi and Behrangi (2020) used changes in SWE based on a gridded in situ observation product (University of Arizona snow water estimate, UA-SWE) together with mass change observations from GRACE to assess snowfall estimates of several precipitation products as well as to investigate the gauge undercatch correction methods. While expanding such analysis to other regions using satellite-based SWE observation is possible (for example, Tian et al., 2014), the quality of SWE products determines the extent of these assessment methods.

Snow depth observations are also available over sea ice and can be used for an independent assessment of snowfall accumulation. Almost no reference precipitation data sets exists over sea ice and the current precipitation products are highly uncertain. Studies have shown that using an ultra-wideband radar system on NASA's Operation IceBridge (OIB) airplane, snow depth on sea ice can be measured and used to determine uncertainties in other satellite-derived snow depth products (Brucker and Markus, 2013). By using a proper snow density value, snow depth measurements on sea ice have been used to assess snowfall accumulation from satellite (Song et al., 2020) or reanalysis (Boisvert et al., 2018; Blanchard-Wrigglesworth et al., 2018) products over sea ice. Efforts are underway to use satellite altimetry to produce spatially and temporally more-complete observations of snow depth on sea ice than that offered by OIB. Launched in September 2018, the Ice, Cloud and land Elevation Satellite (ICESat-2) together with CryoSat-2 should enable extending snow depth estimations over the entire arctic sea ice using differences in freeboard heights observed by the two instruments (e.g., Kwok et al., 2020). Upon retrieving quality snow depth estimates, the outcomes can potentially provide unique opportunities for the assessment of precipitation products over sea ice.

3.3.6. Complementary radar observations

Over ocean where in situ observations are generally lacking and precipitation products have large spread (Adler et al. 2012), using complementary observations from the best-known satellite products could provide a reference to assess other satellite products. Recognizing the complementary observations from CloudSat (for example, for drizzle, light precipitation and snowfall estimation) and TRMM (for moderate and intense precipitation), Behrangi et al. (2014; 2012) developed a Merged CloudSat, TRMM and Advanced Microwave Scanning Radiometer (AMSR) (MCTA) product and used that to determine the zonal distribution of precipitation over the ocean. AMSR coincides with CloudSat, and is used where and when CloudSat faces signal saturation problems under intense precipitation events. A comparison of MCTA with GPCP V2.2 showed that GPCP may underestimate oceanic precipitation by about 5%. This number agreed well with what Rodell et al. (2015) found through water budget analysis. The launch and operation of GPM enables us to extend the estimate of moderate and intense precipitation from the tropics to the extratropics (that is, from $35^oS/N$ to $65^oS/N$). Accordingly, a new product was developed by Behrangi and Song (2020) that provides seasonal maps of the Merged CloudSat, TRMM, and GPM (MCTG) precipitation rates. MCTG provides additional insights on zonal and regional magnitude and distribution of precipitation rate over the ocean, and it was recently used to assess and revise GPCP over the oceans together with the Tropical Composite Climatology (TCC) (Adler et al., 2009; Wang et al., 2014). The revised GPCP product (V3.1)

(Huffman et al., 2020) shows major differences compared to its previous version (V2.3), especially over the Southern Oceans (Fig. 3.3.3), and suggests an increase of about 6% in global oceanic precipitation. This is another example of how recent sensors can be used to guide precipitation assessments where and when accurate or sufficient in situ data are generally lacking.
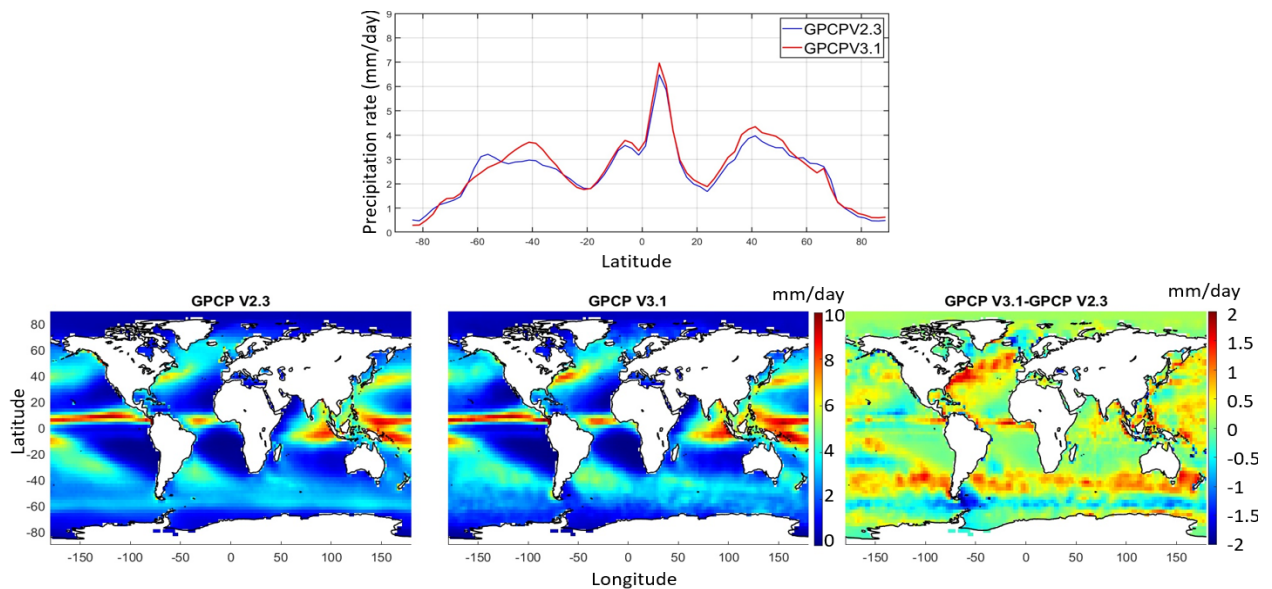

Figure 3.3.3. (Top row) Comparison of the zonal distribution of precipitation from GPCP V2.3 and GPCP V3.1. Annual maps of mean precipitation from of GPCP V2.3, GPCP V3.1, and their difference (GPCP V3.1 minus GPCP V2.3) are shown in the bottom left panel, the bottom middle panel and the bottom right panel, respectively. The plots are constructed based on average precipitation calculated from 36 years (1983–2018) of data.

3.3.7. Concluding remarks

Here we provided examples of a few opportunities that can add insights to precipitation assessment, especially over regions and periods where current precipitation products face large uncertainties. These were mainly based on observation of some properties of precipitation (that is, mass change from GRACE and GRACE-FO, SWE from ASO, snow depth from OIB, etc.) together with other types of observations such as streamflow and ice discharge. The value of complementary observations from radars over the ocean was also discussed.

The use of complementary or independent observations to assess precipitation products seems valuable and is likely not limited to those presented here. With the emergence of new generation of sensors to better study the Earth system, it is important to keep an eye on their potential for guiding current precipitation products and consistency checks across the variables of the water cycle. Nonetheless, the extent that such observations can be useful depends on how they might contribute to filling existing gaps, their quality and associated uncertainties.

3.3.8. References

Adler, R.F., J.-J. Wang, G. Gu and G.J. Huffman, 2009: A Ten-Year Tropical Rainfall Climatology Based on a Composite of TRMM Products. *Journal of the Meteorological Society of Japan*, 87A, 281–293.

Adler, R.F., G. Gu and G.J. Huffman, 2012: Estimating Climatological Bias Errors for the Global Precipitation Climatology Project (GPCP). *Journal of Applied Meteorology and Climatology*, 51(1), 84–99, doi: 10.1175/jamc-d-11-052.1.

Behrangi, A., M. Lebsock, S. Wong and B. Lambrigtsen, 2012: On the quantification of oceanic rainfall using spaceborne sensors. *Journal of Geophysical Research: Atmospheres*, 117(D20), doi: 10.1029/2012jd017979.

Behrangi, A., G. Stephens, R.F. Adler, G.J. Huffman, B. Lambrigtsen and M. Lebsock, 2014: An Update on the Oceanic Precipitation Rate and Its Zonal Distribution in Light of Advanced Observations from Space. *Journal of Climate*, 27(11), 3957-3965, doi: 10.1175/jcli-d-13-00679.1.

Behrangi, A., A.S. Gardner, J.T. Reager and J.B. Fisher, 2017: Using GRACE to constrain precipitation amount over cold mountainous basins. *Geophysical Research Letters*, 44(1), 219–227, doi: 10.1002/2016gl071832.

Behrangi, A., A. Gardner, J.T. Reager, J.B. Fisher, D. Yang, G.J. Huffman and R.F. Adler, 2018: Using GRACE to Estimate Snowfall Accumulation and Assess Gauge Undercatch Corrections in High Latitudes. *Journal of Climate*, 31(21), 8689-8704, doi: 10.1175/jcli-d-18-0163.1.

Behrangi, A., A. Singh, Y. Song and M. Panahi, 2019: Assessing Gauge Undercatch Correction in Arctic Basins in Light of GRACE Observations. *Geophysical Research Letters*, 46(20), 11358-11366, doi: 10.1029/2019gl084221.

Behrangi, A., A.S. Gardner and D.N. Wiese, 2020: Comparative analysis of snowfall accumulation over Antarctica in light of ice discharge and gravity observations from space. *Environmental Research Letters*, https://doi.org/10.1088/1748-9326/ab9926.

Behrangi, A., and Y. Song, 2020: A new estimate for oceanic precipitation amount and distribution using complementary precipitation observations from space and comparison with GPCP. *Environmental Research Letters*, 15(12), 124042, doi: 10.1088/1748-9326/abc6d1.

Blanchard-Wrigglesworth, E., M.A. Webster, S.L. Farrell and C.M. Bitz, 2018: Reconstruction of Snow on Arctic Sea Ice. *Journal of Geophysical Research: Oceans*, 123(5), 3588–3602, doi:10.1002/2017JC013364.

Boisvert, L.N., M.A. Webster, A.A. Petty, T. Markus, D.H. Bromwich and R.I. Cullather, 2018: Intercomparison of Precipitation Estimates over the Arctic Ocean and Its Peripheral Seas from Reanalyses. *Journal of Climate*, 31(20), 8441–8462, doi: 10.1175/jcli-d-18-0125.1.

Brucker, L., and T. Markus, 2013: Arctic-scale assessment of satellite passive microwave derived snow depth on sea ice using Operation IceBridge airborne data. *Journal of Geophysical Research: Oceans*, 118(6), 2892–2905, https://doi.org/10.1002/jgrc.20228.

Gardner, A.S., G. Moholdt, T. Scambos, M. Fahnstock, S. Ligtenberg, M. van den Broeke and J. Nilsson, 2018: Increased West Antarctic and unchanged East Antarctic ice discharge over the last 7 years. *The Cryosphere*, 12(2), 521–547, doi: 10.5194/tc-12-521-2018.

Grazioli, J., J.B. Madeleine, H. Gallee, R.M. Forbes, C. Genthon, G. Krinner and A. Berne, 2017: Katabatic winds diminish precipitation contribution to the Antarctic ice mass balance.

Proceedings of the National Academy of Sciences of the United States of America, 114(41), 10858–10863, doi: 10.1073/pnas.1707633114.

Huffman, G.J., A. Behrangi, R.F. Adler, D.T. Bolvin, E.J. Nelkin, G. Gu, J.J. Wang and Y. Song, 2020: Introduction to the New Version 3 GPCP Monthly Global Precipitation Analysis, in preparation.

Kwok, R., S. Kacimi, M.A. Webster, N.T. Kurtz and A.A. Petty, 2020: Arctic Snow Depth and Sea Ice Thickness From ICESat-2 and CryoSat-2 Freeboards: A First Examination. *Journal of Geophysical Research: Oceans*, 125(3), e2019JC016008, doi: 10.1029/2019jc016008.

Olson, W.S., and the GPM Combined Radar-Radiometer Algorithm Team, 2018: GPM Combined Radar-Radiometer Precipitation ATBD (Version 5), https://pps.gsfc.nasa.gov/Documents/Combined_algorithm_ATBD.V05.pdf.

Painter, T.H., D.F. Berisford, J.W. Boardman, K.J. Bormann, J.S. Deems, F. Gehrke, A. Hedrick, M. Joyce, R. Laidlaw, D. Marks, C. Mattmann, B. McGurk, P. Ramirez, M. Richardson, S.M. Skiles, F.C. Seidel and A. Winstral, 2016: The Airborne Snow Observatory: Fusion of scanning lidar, imaging spectrometer, and physically-based modeling for mapping snow water equivalent and snow albedo. *Remote Sensing of Environment*, 184, 139–152, https://doi.org/10.1016/j.rse.2016.06.018.

Panahi, M., and A. Behrangi, 2020: Comparative Analysis of Snowfall Accumulation and Gauge Undercatch Correction Factors from Diverse Data Sets: In Situ, Satellite, and Reanalysis. *Asia-Pacific Journal of Atmospheric Sciences*, doi: 10.1007/s13143-019-00161-6.

Rignot, E., J. Mouginot and B. Scheuchl, 2011: Ice Flow of the Antarctic Ice Sheet. *Science*, 333(6048), 1427–1430, doi: 10.1126/science.1208336.

Rodell, M., H.K. Beaudoing, T.S. L'Ecuyer, W.S. Olson, J.S. Famiglietti, P.R. Houser, R. Adler, M.G. Bosilovich, C.A. Clayson, D. Chambers, E. Clark, E.J. Fetzer, X. Gao, G. Gu, K. Hilburn, G.J. Huffman, D.P. Lettenmaier, W.T. Liu, F.R. Robertson, C.A. Schlosser, J. Sheffield and E.F. Wood, 2015: The Observed State of the Water Cycle in the Early Twenty-First Century. *Journal of Climate*, 28.21, 8289–8318, https://doi.org/10.1175/JCLI-D-14-00555.1.

Song, Y., A. Behrangi and E. Blanchard-Wrigglesworth, 2020: Assessment of Satellite and Reanalysis Cold Season Snowfall Estimates over Arctic Sea Ice. *Geophysical Research Letters*, e2020GL088970, doi: 10.1029/2020gl088970.

Tapley, B.D., S. Bettadpur, J.C. Ries, P.F. Thompson and M.M. Watkins, 2004: GRACE Measurements of Mass Variability in the Earth System. *Science*, 305(5683), 503–505, doi: 10.1126/science.1099192.

Tian, Y., Y. Liu, K.R. Arsenault and A. Behrangi, 2014: A new approach to satellite-based estimation of precipitation over snow cover. *International Journal of Remote Sensing*, 35(13), 4940–4951, doi: 10.1080/01431161.2014.930208.

Wang, J.-J., R.F. Adler, G.J. Huffman and D.F. Bolvin, 2014: An Updated TRMM Composite Climatology of Tropical Rainfall and Its Validation. *Journal of Climate*, 27, 273–284. doi:10.1175/JCLI-D-13-00331.1.

Yang, D., D. Kane, Z. Zhang, D. Legates and B. Goodison, 2005: Bias corrections of long-term (1973–2004) daily precipitation data over the northern regions. *Geophysical Research Letters*, 32(19), doi:10.1029/2005gl024057.

Zhang, G., T. Yao, C.K. Shum, S. Yi, K. Yang, H. Xie, W. Feng, T. Bolch, L. Wang, A. Behrangi, H. Zhang, W. Wang, Y. Xiang and J. Yu, 2017: Lake volume and groundwater storage variations in Tibetan Plateau's endorheic basin. *Geophysical Research Letters*, 44(11), 5550–5560, doi: 10.1002/2017gl073773.

3.4. Requirements for a constellation of precipitation sensors

Chris Kidd

Earth System Science Interdisciplinary Center, University of Maryland, College Park, USA and NASA/Goddard Space Flight Center, Greenbelt, USA

A fundamental requirement for the accurate measurement and representation of any parameter is that the observations made must be commensurate with, or finer than, the variable being measured. This is challenging for satellite-based observations due to the physical and engineering constraints imposed upon the characteristics of the observations being made. Measuring precipitation from spaceborne sensors is no exception.

3.4.1. A constellation for precipitation

For the measurement of precipitation, several key factors must be considered:

Precipitation characteristics: precipitation is temporally very variable with changes occurring over timescales of a few seconds, but which also impact the longer-term accumulations. Furthermore, precipitation varies greatly spatially, from a few tens of metres in intense storms, to over tens of kilometres in synoptic systems. Scale is a key driver of the characteristics of precipitation: at the instantaneous scale, precipitation intensity is heavily skewed towards the normal – zero, although coarser spatial and temporal scales results in more normally-distributed values.

Observing capabilities: Given the variability of precipitation, frequent and regular observations are key to providing representative measurements. However, frequent and regular observations (with reasonable resolution) are only available from GEO VIS/IR sensors, which do not observe precipitation per se but infer it from the cloud tops. Despite many schemes to derive precipitation from multi-spectral VIS/IR observations (some simple, some complex), the fact is that these still rely upon the cloud top properties. Such schemes will not improve upon schemes utilizing PMW data at the time of the PMW observation: however, VIS/IR observations have an essential role in providing information on precipitation when no PMW data is available.

Engineering and physical aspects: The use of PMW observations is key to providing good precipitation estimates. However, there are physical limitations to the engineering achievable and the range of channels that can be usefully employed. In particular, the resolution of PMW sensors is limited by the size of the antenna and the frequencies used. Although it may be possible to utilize higher frequencies to provide finer spatial resolutions, such higher frequencies are less direct to surface precipitation.

User requirements: Ultimately, precipitation is measured for the benefit of the user community, which has a vast range of requirements: spatially from metres through kilometres, temporally from seconds to annual and latency from minutes through seasonal (GEO 2010). Matching the fundamental characteristics of precipitation with the observational and engineering limitations effectively sets the boundaries within which the user community must operate.

Observations from PMW radiometers are therefore seen as *the* sensor for global precipitation measurements from satellites. These sensors, initially developed in the 1970s, have evolved into the suite of sensors that are available to the community today: these now form a constellation of about 10–12 precipitation-capable sensors available at any particular time. A broad range of science and user communities are now dependent upon the precipitation products provided by these sensors for a range of applications, from climate monitoring to

disease early warning. The current precipitation constellation consists of both conically scanning and cross-track multi-channel instruments, many of which are beyond their operational and design lifetime, but continue to operate through the cooperation of the responsible agencies. The Group on Earth Observations (GEO) and subsequent discussions by the Coordinating Group for Meteorological Satellites (CGMS) have raised the issue of how a robust future precipitation constellation should be constructed. The key factors to be considered can be summarized as:

i. sufficiently fine spatial resolutions necessary to capture precipitation-scale systems and reduce the non-linearity ("beam-filling effect") of the observations;
ii. wide channel diversity for each sensor necessary to cover the range of precipitation types, characteristics and intensities that are observed across the globe;
iii. an observation interval that provides temporal sampling commensurate with the variability of precipitation; and
iv. precipitation radars within the constellation to provide a consistent calibration source across the globe, as demonstrated by the impact of the first two spaceborne radars on the Tropical Rainfall Measuring Mission (TRMM) and Global Precipitation Measurement (GPM) Core Observatory (CO).

These issues are critical in determining the direction of future constellation requirements, while preserving the continuity of the existing constellation necessary for long-term climate-scale studies.

The current precipitation constellation, as epitomized by the GPM mission, includes 10 or more precipitation-capable missions from several international agencies, including CNES, ESA, the European Organisation for the Exploitation of Meteorological Satellites (EUMETSAT), ISRO, JAXA, NASA, NOAA and the U.S. DoD. Additional operational precipitation-capable PMW missions exist, but data access/usage arrangements limit their widespread exploitation. The multi-agency aspect affects the coordination of each mission's orbital crossing times. To ensure consistent overpass times, the operational EUMETSAT Meteorological Operational satellite (MetOp)-B and -C, and NOAA Suomi National Polar-orbiting Partnership (SNPP) and NOAA-20 orbits are rigorously maintained, but in doing so, each pair essentially gathers observations at the same time. The overpass times of other missions drift over the course of 14–15 years between the extremes of ca.13:30 to 22:30 (ascending) while the precessing orbits of GPM and Megha-Tropiques provide overpasses across all times over the period of a few months (albeit with highly intermittent sampling). Due to the irregular nature of the PMW observations, the frequent and regular observations made by the GEO satellite sensors are crucial in providing continuous precipitation estimated through the use of merged precipitation retrieval schemes.

Despite the case for the utilization of satellite-based PMW sensors, satellites within the current precipitation constellation are old, with many missions beyond their designed operational lifetime: at present, their average age is just under 10 years old. It is therefore crucial that there is a concerted program of new satellites/sensors to ensure continuity in satellite-based precipitation measurements that meets the needs of the user community. The majority of the sensors in the current precipitation constellation are cross-track scanning sounding instruments, not designed for precipitation retrievals, and this is also reflected in the precipitation-capable sensors proposed in the near future (see below). The gain or loss of these sensors to/from the constellation directly impacts the temporal sampling of the observations together with the ability to accurately retrieve the precipitation. The oft-cited "3-hour" repeat observation time quoted for the GPM mission should be seen as an idealized (statistical) mean revisit time: in reality, there are significant regional temporal gaps of 4 hours or more in global sampling.

Several precipitation-capable missions are currently being planned for launch over the next decade. These include:

3.4.1.1. EUMETSAT: European Polar-orbiting System, Second Generation (EPS SG)

These satellites and sensors will provide continuity to the current MetOp series of satellites, with similar orbital characteristics to current missions. The Second Generation A (SG-A) satellites will carry the cross-track MicroWave Sounder (MWS), while the SG-B satellites will carry the conically-scanning MicroWave Imager (MWI) and the Ice Cloud Imager (ICI).

3.4.1.2. NOAA: Joint Polar System Satellite

The first in the JPSS series (JPSS-1, a.k.a. NOAA-20) is operational and will be joined by JPSS-2/-3/-4, with each satellite carrying an ATMS sounding instrument.

3.4.1.3. U.S. Department of Defense: Weather Satellite Follow-on–Microwave (WSF-M)

The U.S. DoD has two SSMIS/GMI-like sensors as part of their WSF-M with a contractual launch date of October 2023.

3.4.1.4. JAXA: Advanced Microwave Scanning Radiometer-3

JAXA is currently building the third generation AMSR sensor to be flown on their Global Observations SATellite for Greenhouse gases and Water Cycle satellite 3 (GOSAT-3). The sensor will build upon the heritage of the AMSR sensors with addition of high-frequency channels.

3.4.1.5. NASA: Time-Resolved Observation of Precipitation structure and storm Intensity with a Constellation of small Satellites (TROPICS)

The TROPICS mission will provide a total of seven cubesats, one pathfinder to be launched June 2021 in a polar orbit, to be followed by six in a low-inclination orbit to look at the evolution of weather systems across the Tropics.

3.4.1.6. NASA: Aerosols, Clouds, Convection and Precipitation (ACCP) mission

NASA is currently finalizing the ACCP mission architecture with a goal of observing precipitation processes.

3.4.1.7. China Meteorological Administration (CMA)/National Remote Sensing Center of China (NRSCC): Rain mapping missions

The Chinese rain mapping missions are scheduled to be flown from 2023 onwards as FY-3G and FY-3J. Both missions would include PMW and AMW sensors with similar characteristics to the current GPM mission.

The collection of sufficient observations for generating precipitation estimates with reasonable confidence is very precarious, even with the current constellation. The precipitation community has been very adept at exploiting data from a range of satellite missions and sensors not necessarily design for the retrieval of precipitation. A number of strategies needs to be

considered to ensure a continuation of adequate precipitation measurements from satellite systems:

i. New missions: These are the largest driver for maintaining the capabilities of the precipitation constellation. However, this requires long-term planning since missions (even cube-/small-sats) take a decade (or more) from formulation to operation. Crucially, there are few dedicated precipitation-specific missions planned, particularly in terms of mapping capabilities, channel selection, orbital characteristics and data latency. Coordination between the satellite agencies is crucial to ensure an optimal sampling strategy.

ii. Redundancy: larger satellite systems tend to provide a better degree of redundancy, allowing multi-decadal records of observations to be collected. The long-term reliability of (precipitation-capable) cubesats has yet to be fully evaluated, but their orbital characteristics are likely to be a main driver of their mission lifetime. While the MetOp and NOAA polar-orbiting missions typically have on-orbit backup satellites, use of their backup missions in the precipitation constellation is limited, since their observations generally cover the same space/time domains of the primary missions.

iii. Extended mission lifetimes: many missions operate beyond their designed operational lifetime, yet within the end-of-life disposal requirements. The utilization of such missions is essential to maintain the number of available satellite sensors. To date, missions such as TRMM and Megha-Tropiques have had extended mission lives, together with post-operation missions such as MetOp-A. The extension of mission lifetimes has been possible for medium to large satellite systems that often carry additional fuel: cubesats do not have this same capability.

iv. Retrieval scheme resilience: retrieval schemes rely upon a set of sensor-specific channels to generate a precipitation estimate. Unfortunately, most schemes will not provide an estimate if one channel is not usable, despite valid data from the other channels. In reality, a single channel loss on diverse-channel sensors (that is, SSMIS/AMSR-type) only degrades the retrieved precipitation very marginally. The flexibility of the retrieval schemes is therefore vital to deal with data loss from one or more input channels or sources. Further, new techniques should be investigated and developed that merge observational data before the retrieval stage, rather than merge precipitation estimates post-retrieval: it is possible to envisage a scenario where two satellites in very similar orbits, both experiencing channel degradation, could between them provide the capabilities of a single sensor.

3.4.1.8. ESA Copernicus Imaging Microwave Radiometer (CIMR)

The Copernicus Imaging Microwave Radiometer (CIMR) is currently being developed by ESA to provide fine resolution observations over frequencies from 1.4 to 37 GHz using a deployable 7m antenna. The anticipated launch date is post-2028.

3.4.1.9. ESA Arctic Weather Satellite (AWS)

The Arctic Weather Satellite (AWS) mission currently under development will provide frequent coverage of Earth for improved nowcasting and numerical weather prediction, carrying a cross-track microwave sounder.

3.4.2. Recommendations

i. Reaffirmation of a commitment and support for current and planned precipitation-capable missions

ii. Development a long-term strategy for a viable constellation of precipitation-capable sensors that meet the necessary scientific and user requirements. Specifically,
   a) PMW sensors with diverse channels covering the primary precipitation-sensitive frequencies with good spatial resolution, exemplified by the AMSR/GMI class of sensors, and
   b) operational AMW capabilities in a non-Sun-synchronous orbit for cross-calibration of all PMW (and IR) precipitation estimates, exemplified by the PR/DPR sensors.
iii) Support for the continuation of precipitation-capable missions beyond their nominal mission lifetime, subject to the limitations imposed by deorbiting/sensor degradation considerations
iv) Exploit new technologies, such as cubesats, where these meet the necessary scientific and user requirements
v) Implement mitigation strategies within the precipitation retrieval schemes to maximize the utilization of sub-optimal observations to help ensure continuity in adequate sampling.

Annex 1 - Acronyms

1D-VAR	One-dimensional variational
4D	Four-dimensional
ABI	Advanced Baseline Imager sensor
ACCP	Aerosols, Clouds, Convection and Precipitation mission
AIP	Algorithm Intercomparison Programme
AIRS	Advanced Infrared Sounder
AMeDAS	Automated Meteorological Data Acquisition System
AMO	Atlantic Multidecadal Oscillation
AMSR	Advanced Microwave Scanning Radiometer
AMSR-2	Advanced Microwave Scanning Radiometer version 2
APHRODITE	Asian Precipitation–Highly Resolved Observational Data Integration Toward Evaluation of Water Resources dataset
AR5	Intergovernmental Panel on Climate Change Fifth Assessment Report
ASO	Airborne Snow Observatory
ATBD	Algorithm Theoretical Basis Document
ATMS	Advanced Technology Microwave Sounder
AVHRR	Advanced Very High Resolution Radiometer
AWAP	Australian Water Availability Project
AWS	Arctic Weather Satellite
CDR	Climate Data Record
CERES EBAF	Clouds and the Earth's Radiant Energy System (CERES) Energy Balanced and Filled (EBAF)
CF	Correction factor
CF-F	Fuchs dynamic correction model
CF-L	Legates climatology correction factor
CFSR	Climate Forecast System Reanalysis
CHIRPS v2.0	Climate Hazards Group InfraRed Precipitation with Station version 2 data archive
CHUVA	Cloud Processes of the Main Precipitation Systems in Brazil: A Contribution to Cloud-Resolving Modeling and to the Global Precipitation Measurement (GPM)
CIMR	Copernicus Imaging Microwave Radiometer
CMA	China Meteorological Administration
CMIP	Coupled Model Intercomparison Project (phases 1–6)
CMORPH	NOAA Climate Prediction Center Morphing Technique
CNES	French Centre National d'Etudes Spatiales
CONUS	Continental United States
CORDEX	Coordinated Regional Climate Downscaling Experiment
CORRA	Combined Ku Radar-Radiometer Algorithm
CPC	National Weather Service Climate Prediction Center retrospective analysis
CPC 2020	Climate Prediction Center (CPC) Global 4-km Merged Infrared dataset
CPI	Convective Percent Index
CrIS	Cross-track Infrared Sounder
CRM	Cloud resolving models
CRU	The University of East Anglia's Climatic Research Unit's global climate dataset
CSH	Goddard Convective-Stratiform Heating algorithm
DoD	U.S. Department of Defense
DPR	Dual-Frequency Precipitation Radar

ECMWF	European Centre for Medium-Range Weather Forecasts
ECMWF IFS	European Centre for Medium-Range Weather Forecasts (ECMWF) Integrated Forecast System
ENSEMBLES	Ensemble-based Predictions of Climate Changes and their Impacts project
ENSO	El Niño Southern Oscillation
E-OBS	European daily high-resolution Observational Gridded Dataset
EOBS	Ensemble-based Predictions of Climate Changes and their Impacts (ENSEMBLES) Observation dataset
EPC	Emissivity principal components
EPS SG	European Polar-orbiting System, Second Generation
ERA5	European Centre for Medium-Range Weather Forecasts Reanalysis version 5 dataset
ERA-Interim	European Centre for Medium-Range Weather Forecasts Re-Analysis dataset
ETCCDI	Expert Team on Climate Change Detection and Indices
EUMETSAT	European Organisation for the Exploitation of Meteorological Satellites
EURO-CORDEX	European Coordinated Regional Downscaling Experiment
FAR	False alarm ratio
FEWS NET	Famine Early Warning Systems Network
FOV	Field of view
FROGS	Frequent Rainfall Observations on GridS
GCE	Goddard Cumulus Ensemble model
GCM	General circulation model
GCMS	Coordinating Group for Meteorological Satellites
G-CRM	Global cloud-resolving model
GEO	Group on Earth Observations
GEO-IR	Geostationary Earth Orbit Infrared
GEV	Generalized Extreme Value framework
GEWEX	Global Energy and Water Exchanges project
GLOBE	Global Learning and Observations to Benefit the Environment program
GMI	Global Precipitation Measurement (GPM) Microwave Imager
GOES-R	Geostationary Operational Environmental Satellites
GOSAT-3	Global Observations SATellite for Greenhouse gasses and Water Cycle satellite 3
GPCC	Global Precipitation Climatology Centre
GPCP	Global Precipitation Climatology Project
GPM	Global Precipitation Measurement
GPM CO	Global Precipitation Measurement Core Observatory
GPROF	Goddard profiling algorithm
GRACE	Gravity Recovery and Climate Experiment
GRACE-FO	Gravity Recovery and Climate Experiment (GRACE)-Follow On
GridSat	Gridded Satellite
GSMaP	Global Satellite Mapping of Precipitation
GV	Ground validation
GV-MRMS	Ground Validation Multi-Radar/Multi-Sensor
HH	Hydrometeor Heating algorithm
HOAPS	Hamburg Ocean Atmosphere Parameters and Fluxes from Satellite Data
HRPP	High-Resolution Precipitation Products
HSS	Heidke Skill Scores
IASI	Infrared Atmospheric Sounding Interferometer
ICESat-2	Ice, cloud and land elevation satellite

ICI	Ice Cloud Imager
IMERG	Integrated Multi-Satellite Retrievals for Global Precipitation Measurement (GPM)
IMERG-T	Test mode for the Integrated Multi-Satellite Retrievals for Global Precipitation Measurement (GPM)
IOD	Indian Ocean Dipole
IPCC	Intergovernmental Panel on Climate Change
IPHEx	Integrated Precipitation and Hydrology Experiment
IPWG	International Precipitation Working Group
IR	Infrared
ISO	International Organization for Standardization
ISRO	Indian Space Research Organization
ITCZ	Intertropical Convergence Zone
JAXA	Japanese Aerospace Exploration Agency
JRA25	Japanese 25-year ReAnalysis
LEO	Low Earth Orbit
LH	Latent heat
MCTA	Merged precipitation estimate from the CloudSat, Tropical Rainfall Measuring Mission (TRMM) and Aqua platforms
MCTG	Merged precipitation estimate from the CloudSat, Tropical Rainfall Measuring Mission (TRMM) and Global Precipitation Measurement (GPM) platforms
MERRA-2	Second Modern-Era Retrospective analysis for Research and Applications
MetOp	Meteorological Operational satellites (MetOp-A, MetOp-B and MetOp-C)
MHS	Microwave Humidity Sounder
MJO	Madden-Julian Oscillation
MODIS	Moderate resolution Imaging Spectroradiometer
MRMS	Multi-radar multi-sensor
MS	Matched Scan
MSWEP	Multi-Source Weighted-Ensemble Precipitation dataset
M-T	Megha-Tropiques
MW	Microwave
MWI	MicroWave Imager
MWS	MicroWave Sounder
NASA	National Aeronautics and Space Administration
NCEP2	National Centers for Environmental Prediction-Department of Energy Reanalysis 2
NEWS	National Aeronautics and Space Administration's Energy and Water cycle Study
NOAA	National Oceanic and Atmospheric Administration
NOAA-20	Satellite of the Joint Polar Satellite System constellation
NRL	Naval Research Laboratory
NRL-Blend	Naval Research Laboratory (NRL) blended satellite
NRSCC	National Remote Sensing Center of China
NS	Normal Scan
NSCE	Nash–Sutcliffe coefficient of efficiency
OIB	Operation IceBridge
OISST	Optimum Interpolation Sea Surface Temperature
OLR	Outgoing longwave radiation
OLYMPEX	Olympic Mountain Experiment
OSTIA	Operational Sea Surface Temperature (SST) and Sea Ice Analysis
PERSIANN	Precipitation Estimation from Remotely Sensed Information using Artificial

	Neural Networks
PERSIANN-CCS	Precipitation Estimation from Remotely Sensed Information using Artificial Neural Networks-Cloud Classification System
PERSIANN-CDR	Precipitation Estimation from Remotely Sensed Information using Artificial Neural Networks-Climate Data Record
PERSIANN-MSA	Precipitation Estimation from Remotely Sensed Information using Artificial Neural Networks–Multispectral Analysis
PDF	Probability density function
PDO	Pacific Decadal Oscillation
PIP	Precipitation Intercomparison Projects
PMW	Passive microwave
POD	Probability of detection
PR	Precipitation Radar
PRH	Precipitation Radar Heating algorithm
PRPS	Precipitation Retrieval and Processing Scheme
PRUDENCE	Prediction of Regional scenarios and Uncertainties for Defining European Climate change risks and Effects project
PUSH	Precipitation Uncertainties for Satellite Hydrology
Q_1	Apparent heat source Q_1
QA	Quality Assurance
QC	Quality Control
QPE	Quantitative precipitation estimation
RAMS	Regional Atmospheric Modeling System
RCM	Regional climate model
REFAME	Rain Estimation Using Forward-Adjusted Advection of Microwave Estimates
REGEN	Rainfall Estimates on a Gridded Network dataset
RMS	Root mean square
SBM	Spectral bin microphysics
SCaMPR	Self-Calibrating Multivariate Precipitation Retrieval
SF	SeaFlux
SG-A	MetOp Second Generation group A satellites
SHARPEN	Scheme for Histogram Adjustment of Ranked Precipitation Estimates in the Neighborhood
SLH	Spectral Latent Heating algorithm
SMART	Soil Moisture Analysis Rainfall Tool
SNPP	Suomi National Polar-orbiting Partnership
SREM2D	Two-Dimensional Satellite Rainfall Error Model
SSMIS	Special Sensor Microwave Imager/Sounder
SST	Sea surface temperature
SWE	Snow water equivalent
TAPEER	Tropical Amount of Rainfall with Estimation of Errors algorithm
TB	Brightness temperature
TIROS	Television-Infrared Operational Sounder
TMPA	Tropical Rainfall Measuring Mission (TRMM) Multi-satellite Precipitation Analysis
TOOCAN	Tracking Of Organized Convection Algorithm through a 3-D segmentation
TOVS	Television-Infrared Operational Sounder (TIROS) Operational Vertical Sounder
TRAIN	Goddard Trained Radiometer algorithm
TRMM	Tropical Rainfall Measuring Mission

TRMM 3B42 V7	Tropical Rainfall Measuring Mission (TRMM) Precipitation L3 1 day 0.25 degree x 0.25 degree V7
TROPICS	Time-Resolved Observation of Precipitation structure and storm Intensity with a Constellation of small Satellites
UA-SWE	University of Arizona snow water estimate
UDEL	Data from Willmott, Matsuura and collaborators at the University of Delaware
VIIRS	Visible Infrared Imaging Radiometer Suite
VIS	Visible
WATCH	Water and global Change
WCRP	World Climate Research Programme
WFDEI	Water and global Change (WATCH) Forcing Data methodology applied to ERA-Interim data
WSF-M	Weather Satellite Follow-on–Microwave
WSR-88D	Weather Surveillance Radar, 1988, Doppler

The
World Climate Research Programme (WCRP)
facilitates analysis and prediction of Earth system change for use in a range of practical applications of direct relevance, benefit and value to society.

WCRP
World Climate Research Programme